The role of bone marrow extracellular matrix proteins on platelet biogenesis and function

***

Die Rolle der extrazellulären Matrixproteine des Knochenmarks auf die Thrombozytenbiogenese und -funktion

Doctoral thesis for a doctoral degree

at the Graduate School of Life Sciences,

Julius Maximilians-Universität Würzburg,

Institute of Experimental Biomedicine I

submitted by

Daniela Semeniak

from Eberswalde, Germany

Würzburg, 2017

Chairperson: Prof. Dr. Manfred Gessler

Members of the *Promotionskomitee*:   Prof. Dr. Harald Schulze

                                                         Prof. Dr. Katrin Heinze

                                                         Prof. Dr. Thomas Dandekar

Summary

Platelets, small anucleated blood cells responsible for hemostasis, interact at sights of injury with several exposed extracellular matrix (ECM) proteins through specific receptors. Ligand binding leads to activation, adhesion and aggregation of platelets. Already megakaryocytes (MKs), the immediate precursor cells in bone marrow (BM), are in constant contact to these ECM proteins (ECMP). The interaction of ECMP with MKs is, in contrast to platelets, less well understood. It is therefore important to study how MKs interact with sinusoids via the underlying ECMP. This thesis addresses three major topics to elucidate these interactions and their role in platelet biogenesis.

First, we studied the topology of ECMP within BM and their impact on proplatelet formation (PPF) *in vitro*. By establishing a four-color immunofluorescence microscopy we localized collagens and other ECMP and determined their degree of contact towards vessels and megakaryocytes (MKs). In *in vitro* assays we could demonstrate that Col I mediates increased MK adhesion, but inhibits PPF by collagen receptor GPVI. By immunoblot analyses we identified that the signaling events underlying this inhibition are different from those in platelet activation at the Src family kinase level.

Second, we determined the degree of MK-ECM interaction in situ using confocal laser scanning microscopy of four-color IF-stained femora and spleen sections. In transgenic mouse models lacking either of the two major collagen receptors we could show that these mice have an impaired association of MKs to collagens in the BM, while the MK count in spleen increased threefold. This might contribute to the overall unaltered platelet counts in collagen receptor-deficient mice.

In a third approach, we studied how the equilibrium of ECMP within BM is altered after irradiation. Collagen type IV and laminin-α5 subunits were selectively degraded at the sinusoids, while the matrix degrading protease MMP9 was upregulated in MKs. Platelet numbers decreased and platelets became hyporesponsive towards agonists, especially those for GPVI activation.

Taken together, the results indicate that MK-ECM interaction differs substantially from the well-known platelet-ECM signaling. Future work should further elucidate how ECMP can be targeted to ameliorate the platelet production and function defects, especially in patients after BM irradiation.

Zusammenfassung

Thrombozyten, kleine kernlose Zellen, die für die Hämostase verantwortlich sind, interagieren an verletzten Gefäßwänden mit exponierten extrazellulären Matrixproteinen (EZMP) durch Oberflächenrezeptoren. Durch die Ligandenbindung werden die Thrombozyten aktiviert, adhärieren und aggregieren schlussendlich. Schon Megakaryozyten (MKs), die unmittelbaren Vorläuferzellen im Knochenmark (KM), stehen ebenfalls mit EZMP im ständigen Kontakt. Im Gegensatz zur Thrombozyteninteraktion ist die Interaktion der MKs mit EZMP jedoch nicht sehr gut untersucht. Aus diesem Grund ist es wichtig zu verstehen wie MKs mit Sinusoiden durch die darunterliegenden EZMP interagieren. Diese Doktorarbeit beleuchtet dazu drei Hauptthemen, die zu einem besseren Verständnis dieser Interaktion und dessen Rolle in der Thrombozytenbildung beitragen.

In einem ersten Themenblock klärten wir die Topologie verschiedener EZMP des Knochenmarks und deren Rolle bei der Proplättchenbildung auf. Durch die Etablierung einer Vierfarben-Immunfluoreszenzmikroskopie, lokalisierten wir verschiedene Kollagene und andere EZMP im KM und bestimmten deren Kontakt zu Gefäßen und MKs. In *in vitro*-Ansätzen konnten wir demonstrieren, dass Kollagen Typ I eine erhöhte Adhäsion von MKs vermittelt, aber die Proplättchenbildung durch den Kollagenrezeptor GPVI inhibiert. Mittels Immunoblotanalysen identifizierten wir eine Signalkaskade, die von der Thrombozytenaktivierung auf der Ebene der *Src family* Kinasen abweicht.

In einem zweiten Themenkomplex bestimmten wir in situ den Grad an Interaktion von MKs mit EZMP mittels konfokaler Laserscanning-Mikroskopie von vierfach immunfluoreszenzgefärbten Femora- und Milzschnitten. In transgenen Mäusen, denen einer der zwei Hauptkollagenrezeptoren fehlen, konnten wir zeigen, dass MKs dieser Mäuse eine veränderte Assoziation zu Kollagenen im Knochenmark aufweisen, während die MK-Anzahl in der Milz um das Dreifache anstieg. Dies könnte insgesamt zur unbeeinflussten Thrombozytenzahl in diesen Mäusen beitragen.

In einem dritten Themenkomplex untersuchten wir wie das Gleichgewicht im Knochenmark nach Bestrahlung beeinflusst ist. Spezifisch Kollagen Typ IV und laminin-α5 waren an den Sinusoiden degradiert, während die Expression der matrixabbauenden Protease MMP-9 in MKs hochreguliert war. Die Thrombozytenzahl

sank und sie wurden hyporesponsiv auf Agonisten, speziell auf diejenigen für die GPVI-Aktivierung.

Zusammengefasst zeigen die Ergebnisse, dass die Interaktion von MKs mit EZMP sich substantiell von der Thrombozyten-EZMP vermittelten Signaltransduktion unterscheidet. Zukünftige Untersuchungen sollen weiter beleuchten wie EZMP gezielt beeinflusst werden können um Defekte in der Thrombozytenproduktion und –funktion abzumildern, besonders in Patienten nach Bestrahlung.

Contents

Contents

1 Introduction

1.1 Hematopoiesis

Every day approximately $6x10^{11}$ to $7x10^{11}$ blood cells are generated in humans. They are all derived from hematopoietic stem cells (HSCs), representing a cell population of 0.1% of cells residing in the bone marrow (BM). These HSCs own the potential for self-renewal and to differentiate into all cells of the myeloid and lymphoid lineage. During the last years, many variations in the concept of the hierarchical differentiation process were proposed (Nishiki, Kurita and Chiba 2017, Akashi *et al.,* 2000), nonetheless the understanding of hematopoiesis remains enigmatic (Fig. 1).
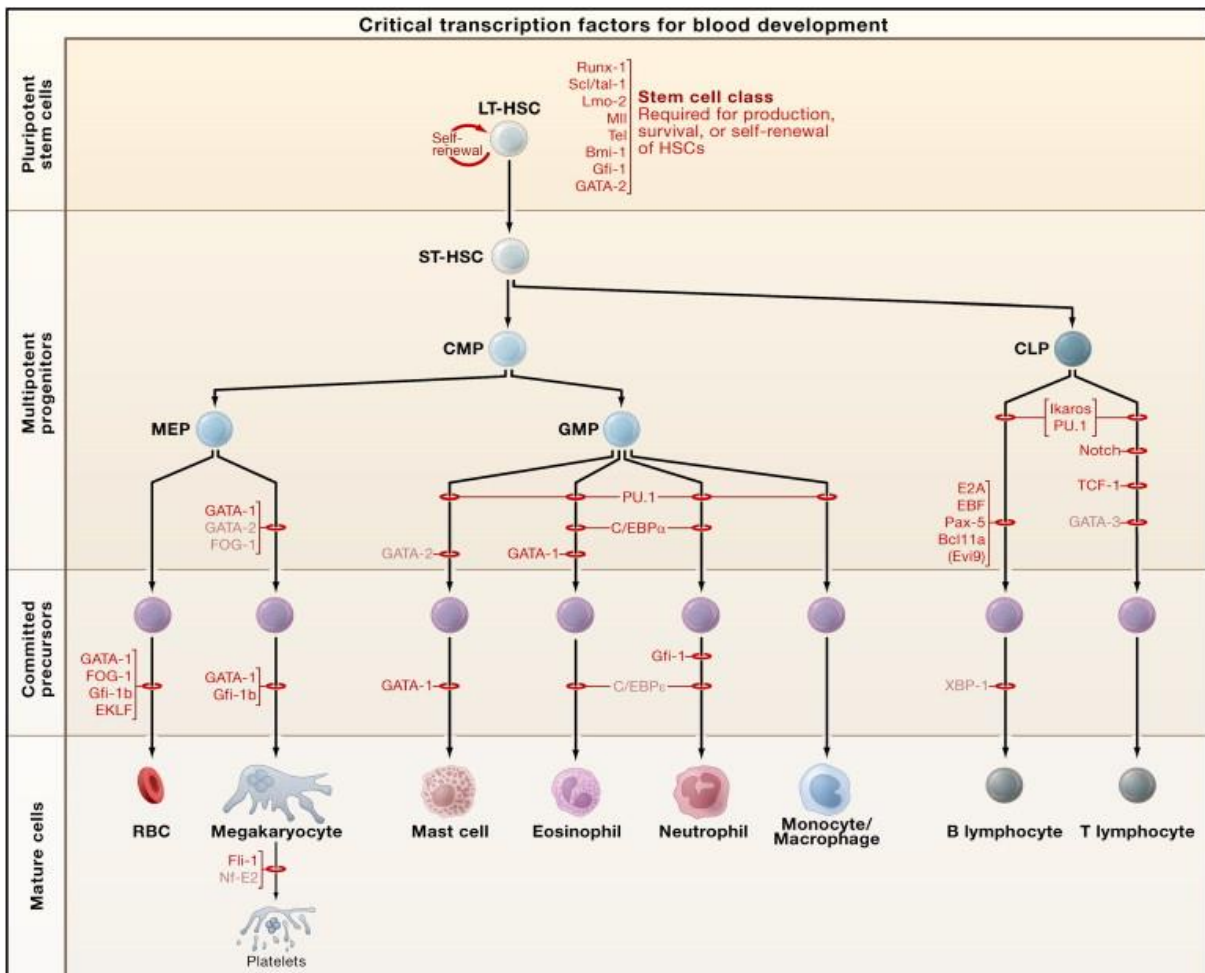
Fig. 1: Hierarchical hematopoietic system. HSCs possess the potential for self-renewal and differentiation into all cells of the myeloid and lymphoid lineages. Differentiation into mature cells is dependent on transcription factor regulation and cytokines. LT-HSC = long term hematopoietic stem cell; ST-HSC = short term hematipoietich stem cell; CLP = common lymphoid progenitor; CMP = common myeloid progenitor; MEP = megakaryocyte erythroid progenitor; GMP = granulocyte macrophage progenitor; RBC = red blood cell (Image taken from Orkin and Zon, 2008).

Hematopoiesis is dependent on a multiplicity of cytokines that promote survival, proliferation, and differentiation of HSCs and progenitor cells (Metcalf, 1993). One of the most important cytokines is *stem cell factor* (SCF), which promotes the maintenance of stem cell survival and self-renewal but has little influence on cell division (Miura *et al.*, 1993). Only the combination with other regulative factors such as *interleukin-3* (IL-3) leads to a proliferation of stem and progenitor cells (Metcalf, 1993). It has been shown that the absence of SCF or its receptor c-kit leads to embryonic lethality, emphasizing its importance in hematopoiesis (Russell, 1979). Besides the BM also the spleen as a part of the reticuloendothelial system can act as a hematopoietic organ, designated as extramedullary hematopoiesis. However, this type of hematopoiesis is rather found in disease-conditions like beta-thalassemia or myelofibrosis, in which BM cells are forced to migrate outside the marrow to other organs due to space limitations (Galanello and Origa, 2010; Pizzi *et al.*, 2016). Usually the spleen is responsible for the removal of old or activated cells from the circulation.

During fetal development, hematopoiesis initially takes place in the yolk sac and then switches to the liver (Fig. 2). In the yolk sac first hematopoietic- and also endothelial-precursor cells develop from the hemangioblast. These primitive HSCs transmigrate to the liver at week 10 of gestation (Bleyer *et al.,* 1971), where they form the first megakaryocytic cells.
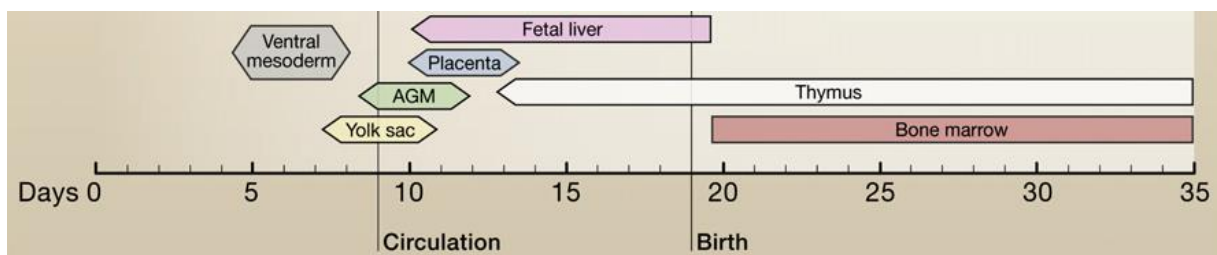
Fig. 2: Hematopoietic tissues in murine embryogenesis and neonates. Hematopoiesis takes place in different organs during embryogenesis: first in the yolk sac, after 10 days in the fetal liver (10 weeks in humans) and finally in the BM. AGM = aorta-gonad mesonephros (Image taken from Orkin and Zon, 2008).

Platelets, derived from these MKs, appear to be bigger than adult platelets and achieve the capability to adhere to each other not before 12 to 15 weeks of gestation (Fruhling *et al.*, 1949). These observations already indicated that fetal hematopoiesis is different from adult hematopoiesis (Andres, Schulze and Speer, 2015). However, only in 2003 the first evidence for developmental differences between preterm infants/neonates and adults in platelet function were shown in a study, where Israels and colleagues could

demonstrate a hyporesponsiveness of platelets in aggregation and activation, due to a decreased expression of platelet surface receptors.

1.2 Megakaryopoiesis

Among all hematopoietic cells derived from HSCs, MKs are the largest cells in the BM. During differentiation, they progressively grow in size and undergo several DNA replication steps without cytokinesis, designated endomitosis. Hence, MKs are polyploid cells and their chromosomal set can range from 2N to 128N. The amplification of the chromosomal set is indispensable for the formation of proteins and granules, which are fundamental for the later generated platelets (Raslova, 2003). MKs develop an internal demarcation membrane system (DMS) by invagination, serving as a reservoir for 1000 to 2000 platelets that can be released by a single MK.

Although MK development stages are defined to some degree, it is still difficult to outline a specific, mature MK. The first stage of differentiation is defined as megakaryoblast (Stage I), possessing positivity for acetylcholinesterase and later showing a high nuclear to cytoplasmatic ratio (Long *et al.,* 1982; Long and Williams 1981). Due to the large number of ribosomes, megakaryoblasts appear basophilic by Romanovsky-staining. In contrast, the promegakaryocyte, representing the second stage of development (Stage II), is less basophilic and contains alpha- and dense-granules. Despite the increase in size and ploidy, one cannot simply outline a mature MK as the largest cell with the highest ploidy level. Also smaller MKs with lower ploidy than 128N are able to generate platelets.

Usually, surface receptors that are up- and down-regulated during differentiation serve as markers for certain developmental stages. In *in vitro* studies, Smith and colleagues (2017) could show by flow cytometric analyses that expression levels of surface receptors like α2β1, GPVI, GPIbα and αIIbβ3 increase simultaneously during MK development, whereas LAIR-1 and CD34 expression decrease. Thus, surface receptor expression is not suitable to evaluate the fine-tuned maturation stages during MK development. Recently, an assay to distinguish MK maturation stages by the polarization of the DMS was established (Antkowiak *et al.*, 2016), but is discussed controversially. Until now it remains difficult to define a mature MK as long as it does not form proplatelets.

However, one promising target to evaluate the late stage of MK maturation seems to be the transcription factor (TF) NF-E2, consisting of the two subunits p45 and p18. The lack of the subunit p45 leads to a profound thrombocytopenia with increased MK numbers (Shivdasani *et al.*, 1995). Although p45-null MKs have a polyploid nucleus and a disorganized DMS, they fail to form proplatelets, indicating a role of this TF exclusively in platelet formation (Lecine *et al.,* 1998). Also β1-tubulin, one transcriptional target of NF-E2 is only expressed during the last stages of MK maturation. The expression of this tissue-specific tubulin isoform is completely abolished in mice lacking NF-E2. In concordance, in murine p45 *NF-E2$^{-/-}$* cells, transduced with a retrovirus containing p45 NF-E2 cDNA, proplatelet formation (PPF) *in vitro* could fully be restored (Lecine *et al.*, 2000).

Thrombopoietin (TPO) is the most important cytokine driving megakaryopoiesis. TPO is mainly produced in the liver and signal transduction occurs via its receptor c-Mpl, which is expressed earliest on hemangioblasts and HSCs and further on MKs and platelets. TPO was first described in 1958 as a humoral factor able to elevate the platelet count in response to thrombocytopenic stimuli (Kaushansky and Drachmann 2002). First efforts to biochemically purify TPO, e. g. from plasma or serum in the 1980s, failed (McDonald *et al.*, 1989; Vannucchi *et al.*, 1988). In 1994, several groups succeeded to purify or clone TPO for the first time (Kaushansky *et al.*, Wendling *et al.*, Lok *et al.*, Sauvage *et al.*, 1994). The TPO plasma level is typically inversely linked to platelet numbers in the circulation, implying that TPO levels increase in case of reduced platelet numbers and *vice versa*. The lack of TPO or its receptor leads to a decrease in platelet and MK numbers up to 85% (Gurney *et al.,* 1994; de Sauvage *et al.*, 1996). Interestingly, TPO was shown to be dispensable for the late stage of platelet biogenesis (Ito *et al.*, 1996).

A second pivotal regulator of megakaryopoiesis is the chemokine *stromal derived factor 1* (SDF-1), also designated as CXCL12. Up to this day, SDF-1 is thought to be involved in the migration of MKs towards vessels along an SDF1-gradient in the BM (Palotta *et al.*, 2011). However, recently this model is challenged by the spatial limitation of MK migration due to the dense vessel network within the BM (Stegner & van Eeuwijk *et al.,* 2017).

1.3 Platelet biogenesis and function

The mechanism of how MKs generate platelets has been studied for over 100 years. Over the time, two different models were mainly described. The first model that describes the bursting of MKs into thousands of platelets has lost support over the last years (Kosaki, 2008). The second hypothesis illustrating the process of proplatelet formation is now overall accepted (Wright, 1906; Becker and DeBruyn, 1976).

Once a MK is mature and in close contact on with vessel sinusoids, long protrusions start to evaginate through the endothelial lining in a unidirectional way into the vessel lumen. Those protrusions consist of a cytoplasmic shaft with numerous platelet-sized swellings. Due to the shear forces, this pseudopod-like extensions further fragment in the blood stream into preplatelets and finally into platelets (Fig. 3) (Junt *et al.*, 2007). However, the rupture of MKs was observed in cases of acute platelet needs, indicating relevance of both models but with different functions (Nieswandt & Stritt, 2015). The high dynamic process of platelet biogenesis in MKs is driven by the main cytoskeletal proteins actin and tubulin. PPF and elongation is provided by microtubules composed of the MK- and platelet-specific β1-tubulin isoform that lines the shafts in a bipolar arrangement (Lecine *et al.*, 2000). Along with their role in proplatelet elongation, microtubules transport organelles and granules into proplatelets until they are captured by the proplatelet tip (Richardson *et al.,* 2005). In contrast, F-actin is the crucial polymer for proplatelet branching. It is present throughout proplatelets and forms the assembly points (Italiano *et al.*, 1999).

Interestingly, in contrats to murine fetal liver-derived MKs, BM-derived MKs hardly form proplatelets *in vitro*, indicating that additional, still unknown factors present in the BM play a crucial role for PPF. Only by the addition of hirudin, an anticoagulant which acts through its inhibitory function on thrombin, PPF can be increased *in vitro* (Strassel *et al.,* 2012). However, the underlying mechanism is still unknown. In contrast, up to half of all mature, fetal liver-derived MKs can produce proplatelets simultaneously. This allows the investigation of platelet biogenesis *in vitro,* although these MKs form proplatelets omnidirectional and the released platelets are hyporesponsive upon stimulation with various agonists (Israels *et al.*, 2003).
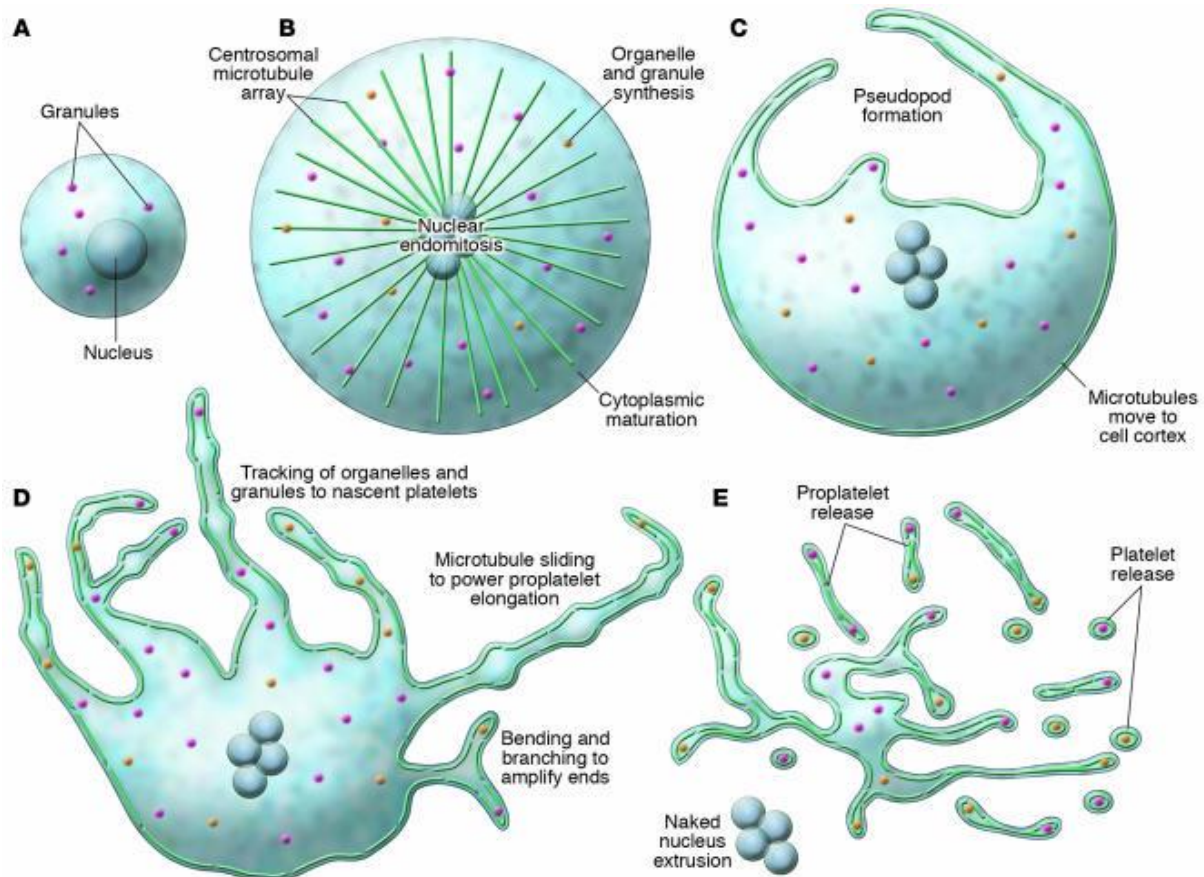
Fig. 3: Platelet production by a MK. To release a platelet **(A)** a MK **(B)** has to undergo nuclear endomitosis. Further microtubules translocate to the cell cortex **(C)** and drive the proplatelet elongation **(D)**. Preplatelets are finally fragmented into platelets and the naked MK nucleus remains in the end **(E)** (Image taken from Patel, Hartwig and Italiano 2005).

The anucleated cell fragments released from MKs, designated platelets, are the key players in hemostasis. Their main function is to prevent blood loss upon vessel injuries through the formation of an occlusive aggregate. In humans, platelet counts typically range from 150,000 to 450,000/µl, whereas mice have a platelet count of approximately 1,000,000/µl. While murine platelets circulate in the peripheral blood for 5 days, the lifespan of a human platelet is up to 10 days (Fox *et al*, 2007; Harker *et al.*, 2000). Platelets are limited in their *de novo* protein synthesis since they lack a nucleus. Newly generated platelets (reticulated platelets) still carry ribosomal and messenger RNA, which decrease within the first 24 h (Angénieux *et al.*, 2016). This feature can technically be exploited to determine the fraction of newly generated platelets by measuring the degree of thiazole orange (TO) binding to platelets.

Platelets contain organelles including mitochondria, a dense tubular system and three types of granules: α-granules, dense granules (δ-granules) and lysosomes. The most prominent organelles, δ- and α-granules, are unique to platelets and carry high

concentrations of bioactive cargos (Flaumenhaft, 2003). While δ-granules contain mainly non-proteinaceous compounds (e.g. Serotonin, ADP, Ca^{2+}) that support platelet aggregation, α-granules store a broad variety of different proteins (e.g. Factor V, Factor XI, Factor XIII, fibrinogen) involved in coagulation and adhesion (Maynard *et al.*, 2007, Flaumenhaft and Koseoglu, 2017).

The formation of an occlusive aggregate is a process dependent on a multiplicity of factors and can be divided into three major steps. First, platelets recognize and bind the glyco-protein complex GPIb-V-IX *von Willebrand factor* (vWF) that is immobilized on collagen fibers and becomes only accessible upon vessel injury. This leads to tethering, rolling and subsequently to the deceleration of platelets, which allows further interactions of other platelet receptors with subendothelial proteins. In the second step, the platelet specific glyco-protein VI (GPVI) recognizes glycine-proline-hydroxyproline (GPO)-motifs within the collagen filament and platelet activation takes place via the non-covalently associated Fc receptor (FcR) γ-chain. This receptor has a cytoplasmic *immunoreceptor tyrosine based activation motif* (ITAM). Collagen binding mediates the dimerization of GPVI and leads to the phosphorylation of two tyrosine residues in the ITAM-motif by the *Src family kinases* (SFKs) Fyn and Lyn (Nieswandt & Watson, 2003).

Subsequent activation steps include the tyrosine phosphorylation of *spleen tyrosine kinase* (Syk), the *linker of activated T-cells* (LAT) and phospholipase Cγ2 (PLCγ2) culminates in the production of 1,4,5-triphosphate (IP_3) and diacylglycerol (DAG) by hydrolysis of phosphatidylinositol-4,5-bisphosphate (PIP_2). The resulting elevation of intracellular free calcium ions causes the release of second mediators like ADP and thromboxane A_2 (TxA_2) by granule secretion and also leads to integrin activation. Together with thrombin (generated from the coagulation cascade) these second wave mediators enhance platelet activation via G-protein-coupled receptors (GPCRs).

Signaling events downstream of GPVI and GPCRs converge in a conformational change of integrins from a low affinity state to a high affinity state, which allows outside-in signaling and rearrangement of the cytoskeleton. This third activation step leads to stable platelet-platelet interaction and finally to aggregation and thrombus formation to seal the injured vessel (Fig. 4) (Varga-Szabo, Pleines & Nieswandt, 2008).
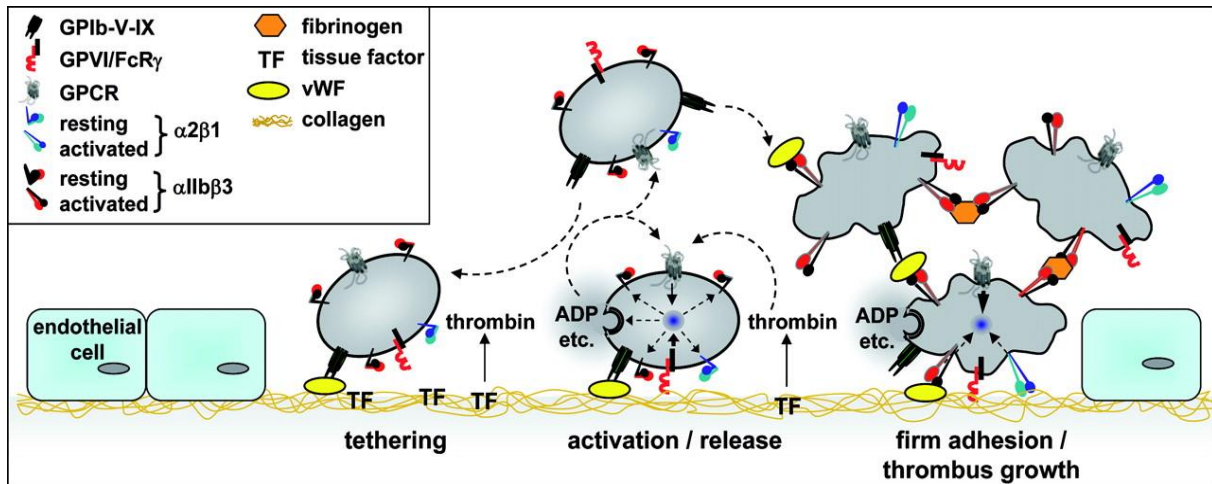
Fig. 4: Platelet activation, adhesion and aggregation upon vessel injury. Exposed vWF upon vessel injury binds to GPIb-V-IX, leading to rolling and tethering of platelets. Subsequent GPVI binding to collagen fibers results in platelet activation and aggregation.

Under pathological circumstances, platelets can form aggregates in an uncontrolled manner, which might lead to occlusion of vessels. These thrombi might embolize, resulting in stroke or myocardial infarction. Up to this day, those events form the basis of the leading causes of morbidity and mortality worldwide (Naghavi *et al.*, 2015).

1.4 Bone and bone marrow

The human body contains 270 bones at birth, which reduces to 206 during adulthood due to bone fusions. The skeleton consists of two parts, the axial and the appendicular skeleton. The axial skeleton, composed of skull, vertebral column and ribs, maintains the upright posture. The appendicular skeleton is formed by the pectoral girdles, the upper limbs, the pelvic girdle and the lower limbs and serves as protection for the organs and enables movement.

1.4.1 Bone structure and composition

Bones do not only have obvious functions as a sustaining and protecting organ, but some are also sites of hematopoiesis. Bone is a tissue of heterogeneous composition. It consists of a mineral phase composed of hydroxylapatite, an organic phase and water. 90% of the organic phase is made of collagen type I, 5% are noncollagenous proteins, including osteocalcin, osteopontin, or fibronectin, and 2% are biochemically lipids (Thews, Mutschler and Vaupel, 1999). Macroscopically the bone can be devided into compact and spongy bone. The compact bone, composed of osteons, is more resistant to mechanical forces than the spongy bone, which contains a network of

trabecula that is arranged along the directions of action to prevent workload due to its elasticity (Buckwalter *et al.*, 1995).
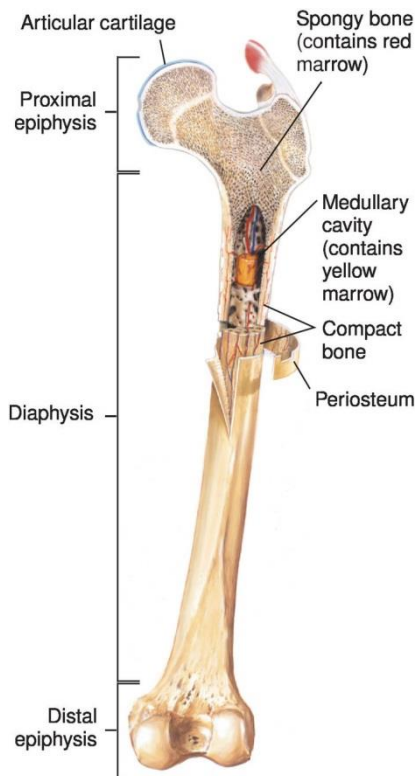
Fig. 5: Structure of a human femur. The femur consists of three major parts, the proximal and distal epiphyses at the ends and the central diaphysis. The compact bone cortex covers the BM that functions as the hematopoietic tissue.
Image taken from:http://medical-dictionary.the freedictionary.com

Hematopoiesis in adults takes place mainly in the long bones, like femora and tibiae, as well as in certain flat bones like skull or ribs. The femora, the favored bone to study hematopoietic processes in mice, can be divided into three major parts: the proximal and distal epiphyses as well as the diaphysis (Fig. 5). The epiphyses mainly consist of spongy bone, whereas the diaphysis contains the marrow surrounded by compact bone. Blood vessels including arterioles and sinusoids are present throughout the whole BM and the hematopoietic cells are located in the areas between these vessels. The fenestrated endothelium of the sinusoids, allows the egress of mature blood cells into the circulation. Furthermore, extracellular matrix (ECM) proteins represent a major part of the BM.

1.4.2 Extracellular matrix proteins

The extracellular matrix proteins like collagens, laminins and fibronectin form a three-dimensional network within the BM, thereby defining the microenvironment and forming functionally distinct niches which allow the orientation and migration of cells. The first niche concept was postulated by Schofield in 1978. According to that model,

an osteoblastic niche is situated near the bone cortex at the endosteum with hypoxic conditions and habits quiescent HSCs (Wilson and Trumpp, 2006). Hematopoietic progenitors migrate from this niche towards the vessels near the vascular niche, while differentiating into mature blood cells. This migration and maturation is enabled by gradients of oxygen, interstitial pressure, or different chemokines like CXCL12 (SDF-1α) (Aguilar *et al.*, 2017; Thon 2014). Recently, the concept of an "architectural" niche is discussed. Several observations were made that at least partially disprove such a model: HSCs can be found within the whole BM and thus mature MKs are equally distributed at both "niches" (Stegner and van Eeuwijk *et al.*, 2017). However, it cannot be denied that there are gradients of CXCL12, oxygen or other factors that might support the directed release of mature blood cells into the circulation.

Collagens are the most abundant ECM proteins within the BM and constitute almost 25% of the total protein content in animals. They are the major components of several connective tissues like skin, tendons, ligaments, cartilage, bone, basement membrane and blood vessels, but differ in their composition. In tendons, collagen forms a long rope-like structure, whereas in bone the interstitial space between the molecules is calcified, thus leading to a rigid structure. In vertebrates, at least 28 different collagen types have been identified so far. Collagen consists of three α-chains with a characteristic triplet sequence of glycine, followed by two proline residues (Kielty and Grant, 2002). The second proline serves as a substrate for a proline hydroxylase that forms the amino acid hydroxyproline (single letter code "O") posttranslationally.

This GPO-motif comprises up to 10% of all amino acids in type I and III collagens. The three left-handed polypeptide helices are held together by interchain-hydrogen bonds. While collagen I (Col I) often accompanies collagen III (Col III), specifically Col I is present at the bone cortex. Collagen IV (Col IV) has a specific characteristic of up to 26 interruptions in the triplet sequence, making it more flexible and allowing cell binding and interchain-crosslinking (Vandenberg *et al.,* 1991).

Due to limited solubility of collagens in physiological buffers, artificial collagen related peptides (CRP) have been synthesized for several areas of research. Those CRPs concentrate the GPO-motif by cross linking. Whereas the motif GKO-(GPO)$_{10}$-GKOG is often used to mimic Col I and III, the polypeptide GFOGER is used to mimic Col IV.

MKs and platelets express several collagen receptors on their surface. The major receptors GPVI and α2β1 integrin are expressed on MKs and platelets. In contrast, the *leukocyte associated immunoglobulin receptor-1* (LAIR-1) and the *discoidin domain receptor 1* (DDR1), that are only found in very early stages during megakaryopoiesis, are absent from platelets. They are thought to transmit inhibitory signals (Abbonante *et al.*, 2013; Smith *et al.*, 2017), while GPVI and α2β1 integrin transduce activatory signals.

Laminins define a second group of ECM proteins within BM are crucial components of the basement membrane, typically found in the subendothelial layer. Laminins form heterotrimers, comprising one each out of five α-, three β- and three γ-chains. So far, 18 out of 45 theoretically possible chain combinations are known (Yousif, Russo and Sorokin, 2013). Laminins form cross-shaped molecules, linked by disulphide bonds with one long helical arm and three short arms, which harbor various binding sites for Col IV and other proteoglycans. The long arm mediates cell binding via integrins, including MK binding through its receptor α6β1 integrin. Most of the laminins are detected during embryogenesis and only laminins with the isoforms –α4 or –α5 can be detected later within the BM (Yousif, Russo and Sorokin, 2013).

Existing mouse models, lacking either *Lama4* or *Lama5,* emphasize the importance of both isoforms. *Lama5$^{-/-}$* mice are embryonic lethal and protein function can only be investigated in conditional knockout models (Miner, Cunningham and Sanes, 1998). In contrast, *Lama4$^{-/-}$* mice are viable, but show an impaired microvasculature and have severe bleedings already during embryogenesis and the postnatal period, due to a massively reduced platelet count of up to 50% (Thyboll *et al.*, 2002). In these mice, the laminin-α5 isoform is overall upregulated at blood vessels and an increased extravasation of T-lymphocytes is shown, indicating that laminin-α5 provides a stop signal for T-lymphocyte extravasation through laminin-α4 (Wu *et al.*, 2009; Kenne *et al.*, 2010).

However, the lack of the main laminin receptor, the α6β1 integrin, leads to a marked reduction in arterial thrombosis, whereas the hemostatic function was unaltered (Schaff *et al.,* 2013). Recently, it was shown that the fibronectin receptor α5β1 integrin and the vitronectin receptor αvβ1 can also bind to laminin-α5 (Sasaki and Timpl, 2001). Furthermore, Nigatu and colleagues described in 2006 that MKs are able to synthesize

laminin-α5, which can be secreted by activated platelets, promoting the adhesion of platelets via the α6β1 integrin.

Fibronectin (FN) is a dimeric protein of two similar subunits, linked by disulphide bonds. Several splicing isoforms, have been described and can be divided into soluble fibronectin, present in the blood plasma, and cellular fibronectin, that can be found within BM. Fibronectin can bind to MKs via its receptor α5β1 integrin and has additional binding sites for heparin, collagens or fibrin (Nègre *et al.,* 1994). FN is reported to play roles in megakaryocytic proliferation, differentiation and platelet release (Han, Guo and Story, 2002). Another member of the nectin family is vitronectin, showing structural similarities to FN. It is found in blood plasma as well as in the BM.

1.5 Matrix remodeling

The BM matrix is subjected to a tight regulation by formation and degradation of proteins. The matrix metalloproteinases (MMPs) compose a family of proteinases that are crucial for morphogenesis, tissue repair, development and remodeling and their dysregulation can lead to disorders like fibrosis, arthritis or cancer (Visse and Nagase, 2003). The 23 MMPs, that have been identified so far, consist of a pro-domain, a catalytic domain including a zinc finger, a hinge region and a hemopexin region (Fig. 6) and show a rather negligible activity under steady-state conditions. However, MMP-9 activity increases during inflammatory conditions, cell migration, or apoptosis. MMP activity was first found and described in tails of tadpoles, undergoing metamorphosis (Gross and Lapière 1962).

All MMPs are identified by their sequence homology to MMP-1, the zinc-binding motif HEXGHXXGXXH in their catalytic domain and the existence of the cysteine switch motif PRCGXPD. This sequence is located within the domain which maintains the MMPs as inactive zymogen (proMMP).
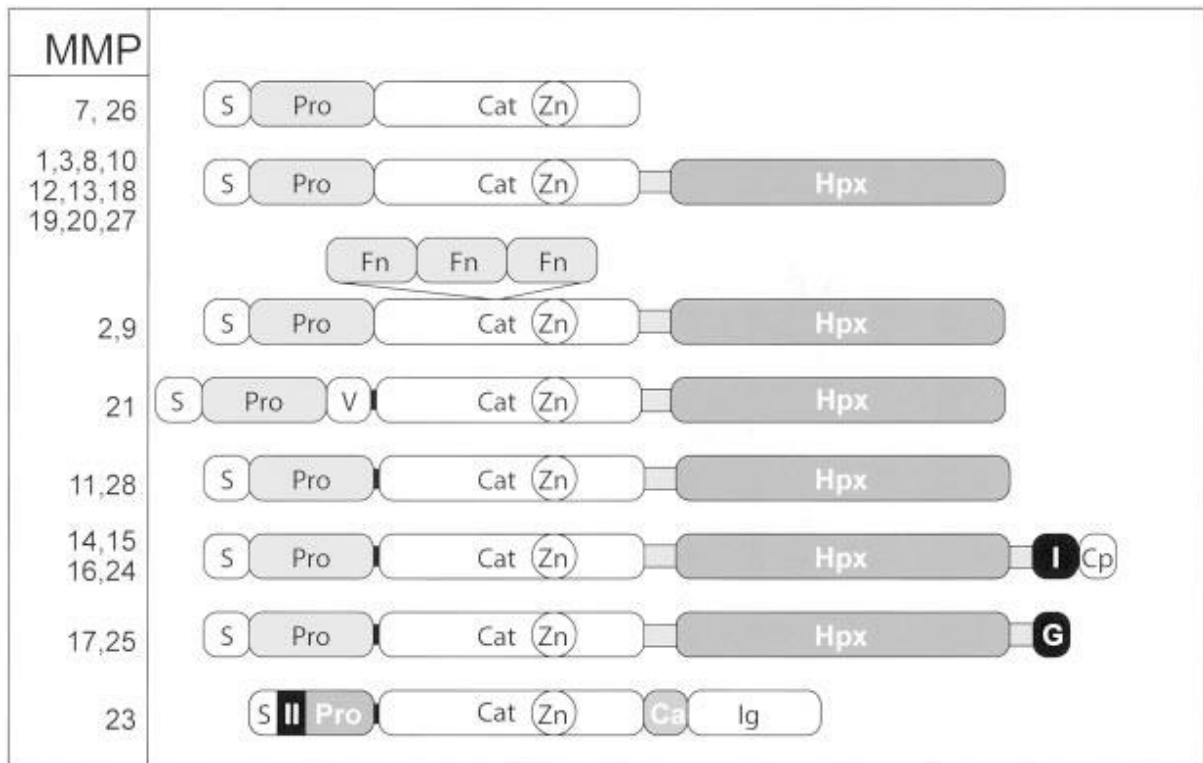
Fig. 6: Domain structure of MMPs. MMPs consist of a signal peptide (S), a propeptide (Pro), a catalytic domain (Cat), containing a zinc finger motif (Zn). The hemopexin domain (Hpx), the fibronectin (Fn) domain, the vitronectin insert (V), the type I transmembrane domain I and II (I, II), the GPI anchor (GPI), the cytoplasmic domain (Cp), the cysteine array region (Ca) and the IgG-like domain (Ig) are specific for the different MMPs. The furin cleavage site is depicted in a black band (Image taken from Vissel and Nagase 2003).

MMPs are either secreted from cells or are anchored to the plasma membrane and can be divided into six groups based on their sequence homology, substrate specificity and domain organization: collagenases, gelatinases, stromelysins, matrilysins, membrane-type MMPs and others. Only two MMPs are mainly responsible for the degradation of collagen and referred to as gelatinases: MMP-2 (gelatinase A) and MMP-9 (gelatinase B). Both enzymes are characterized by three repeats of a type II fibronectin domain, located in the catalytic domain. This domain binds to gelatin, collagens and also laminins (O´Reilly *et al.*, 1999). While MMP-2 digests Col I, II and III, MMP-9 degrades mainly Col IV, V, XI, and XIV, vitronectin and laminins (Aimes and Quigley 1995; Van den Steen *et al.*, 2002). MMP activation is a multi-step process: first, the signal peptide is cleaved posttranslationally. The generated pro-MMPs can then be activated through enzymatic cleavage of the pro-domain (Nagase *et al.*, 1990). While mice lacking *Mmp2* show no obvious abnormalities, mutations in the human *Mmp2* lead to multicentric osteolysis (Itoh *et al.*, 1997; Martignetti *et al.*, 2001). However, the lack of *Mmp9* in mice causes a shortened femur, but has no other

apparent effects, while human gene variations are causative for metaphysal anadysplasia (Lausch *et al.*, 2009).

Endogenous MMP inhibitors comprise the group of *tissue inhibitors of matrix metalloproteinases* (TIMPs). The four known TIMPs (1-4) in vertebrates bind MMPs in a 1:1 stoichiometry (Patterson *et al.*, 2001) and their expression is regulated during development and tissue remodeling. Indeed, TIMPs act as inhibitors for all MMPs but TIMP-3 seems to shows a higher affinity to *a disintegrin and metalloproteinase domain-containing protein 10 and 17* (ADAM-10 and ADAM-17). This indicates inhibition of rather those enzymes than of MMPs (Amour *et al.*, 1998 and 2000). Moreover, by specifically downregulating MMP-2 and MMP-9 levels, RECK, a glycosylphosphatidylinositol (GPI)-anchored protein, can inhibit the proteolytic activity of MMP-2 and -9 (Takahashi *et al.*, 1998).

1.6 Irradiation of the hematopoietic compartment

As a consequence of the atomic bomb dropping and the reactive fallout in Japan, a new research area was initiated to investigate how humans can be protected from irradiation. Scientists explored that the hematopoietic system is the most radiation-sensitive tissue and in 1949, Jacobson and colleagues could show that mice survive an otherwise lethal dose of radiation when the spleen was exteriorized and protected from radiation (Jacobson *et al.*, 1949). In the 1950s, engraftment of donor-derived BM cells in lethally irradiated mice and dogs was reported (Ford *et al.,* 1956; Ferrebee *et al.*, 1958). The first successful BM transplantation was performed by Dr. E. Donnall Thomas in Cooperstown, New York in 1956. He transplanted BM cells of a healthy twin in a lethally irradiated man, who had leukemia (Thomas *et al.*, 1957). This was the starting point for the research of BM transplantations.

Leukemias and lymphomas as malignant diseases are restricted in their treatment. The favored and mostly exclusive treatment for those diseases is an HSC- or BM-transplantation (Kassim and Savani 2017; Kondo, 2016). The recipient has to be prepared for transplantation in a way that the own malignant cells are eradicated and niche space for new, donor-derived HSCs is provided within BM. This is achieved by total body irradiation (TBI) at a lethal dosage. After the eradication an allogeneic HSC-transplantation (HSCT) or BM-transplantation (BMT) is performed by intravenous injection of these cells. The transplanted cells typically engraft into the BM of the

recipient and adopt the function of the complete hematopoietic system. However, how these cells can find the BM as their destination (so called "homing") is still partly unclear.

In cancer therapy, two types of transplantations can be performed. For allogeneic HSCT donor and recipient have to be matched for their major histocompatibility complex (MHC) proteins, the *human leukocyte antigen* (HLA) system. In many cases the HLA-system of a sibling might be suitable (Sureda *et al.*, 2015). Conversely, sometimes also an autologous donation can be conducted for certain tumor entities, and typically performed when patients are in remission. Both types of transplantation bear risks for the recipients. After an allogeneic transplantation, the T-cells of the donor can cause the *graft-versus-host disease* (GvHD), where symptoms like skin lesions, liver damage or defects in the gastrointestinal tract bear a high mortality risk (Korngold and Sprent, 1987). In contrast, dornor T-cells can also mediate a beneficial anti-tumor effect, designated as *graft-versus leukemia* (GvL) (Bleakley and Riddell, 2004). The aim is to balance both immune reactions in a way that the beneficial GvL predominates over the GvHD. Autologous transplantation harbors the risk that single malignant cells might be present in the stored cells that are then again amongst the transplanted cells. A situation of a "complete chimerism" is achieved, when the BM transplantation was successful and the donor cells were able to generate a new hematopoietic system.

Also, for some non-malignant diseases BM transplantation can currently be the only curative therapy. For congenital diseases (beta-thalassemia), autoimmune diseases (Wiskott-Aldrich-syndrome) or metabolic disorders (adrenoleukodystrophy) it is essential to create enough space for healthy donor-derived HSCs (Klaihmon *et al.*, 2017; Yildiran *et al.*, 2017; Miller *et al.*, 2011). To achieve this, a sublethal dosage of radiation is sufficient. After engraftment of donor cells, these adopt the function as the hematopoietic system and can thus compensate for defective recipient cells. Due to the partial co-existence of recipient cells next to new donor-derived cells this is referred to as "incomplete chimerism".

The sources for stem cells used for transplantations are diverse. Along the BM, stem cells can be isolated from umbilical cord blood (UC) or from G-CSF-mobilized peripheral blood (PBSC). The decision, which source is used for the HSC isolation depends on the age of the donor and recipient, clinical comorbidities as well as the severity of the disease (Smith and Wagner, 2009).

Besides the mentioned side effects like GvHD, also other complications can occur after HSCT or BMT. Several studies describe mild to life threatening bleeding episodes, due to the long lasting thrombocytopenia after transplantation (Labrador *et al.*, 2015; Holler *et al.,* 2009). Compared to other cells of the hematopoietic system, platelet recovery appears to be delayed after irradiation and subsequent HSCT/BMT (Isoyama *et al.*, 2010). Some studies report on transient vasodilatation (Olson *et al.*, 2013), but it remains unclear why specifically MKs and platelets show such a delayed engraftment.

1.7 Aim of this study

Upon vessel injury ECM proteins like collagens, fibronectin or laminins are exposed to platelets, thereby activating them, which subsequently leads to the occlusion of the injured vessel by thrombus formation. In the BM, these ECM proteins form a dense network that provides niche space for MKs, the immediate precursor cells of platelets. The molecular mechanisms mediating the migration of MKs towards the vessel niche followed by the directed formation of proplatelets are not well understood.

Therefore, the aim of this study was to investigate the role of different ECM proteins and their receptors on platelet biogenesis with a focus on collagens. In a first approach we examined the behavior of MKs towards distinct collagen types and also other ECM proteins concerning their growth, their adhesion ability and their proplatelet forming capacity. We also conducted competitive analyses of different matrix proteins to evaluate the degree of the influence on MKs. Furthermore, we studied the effect of collagen-unresponsive MKs on platelet biogenesis and function in mice lacking the main collagen receptors *Itga2* and/or *Gp6*.

Transplantation of HSCs requires the eradication of the pathological BM and provides new niche space for donor cells. Particularly precursor cells of the megakaryocytic background poorly engraft after transplantation resulting in a long lasting thrombocytopenia. Since decreased platelet numbers lead to an increased bleeding risk that can become life threatening (Isoyama *et al.,* 2002, 2010), it is of clinical relevance to investigate the impact of irradiation-induced damage of the BM concerning the composition of matrix proteins, the influence on the vascular integrity as well as platelet biogenesis and function. Moreover, we studied mice lacking the collagen degrading protein MMP-9 regarding the outcome of irradiation induced damage since this MMP is responsible for collagen and laminin turnover.

2 Material and Methods

2.1 Material

2.1.1 Devices and material

Table 2.1:   Devices

Device	Manufactorer
Cryotom CM1900	Leica (Wetzlar, Germany)
FACS Calibur	BD Biosciences (Heidelberg, Germany)
FACS Canto	BD Biosciences (Heidelberg, Germany)
Fluor Chem Q	Alpha Innotech (Kasendorf, Germany)
Sysmex KX 21N	Sysmex GmbH (Norderstedt, Germany)
Nanodrop 2000c	Thermo Fisher (Waltham, MA, USA)
7500 Fast Real Time PCR System	Applied Biosystems (Foster City, CA, USA)
TCS SP5 CLSM	Leica (Wetzlar, Germany)
TCS SP8 CLSM	Leica (Wetzlar, Germany)
Nikon A1 CLSM	Nikon (Chiyoda, Japan)
Zeiss Primo Vert	Zeiss (Jena, Germany)

Table 2.2:   Material

Material	Manufactorer
Adhesive cryo films 2C/(9)	Section lab (Hiroshima, Japan)
18 G, 20 G, 22 G canula	BD Biosciences (Heidelberg, Germany)
Glass slide superfrost,	Roth (Karlsruhe, Germany)
Glass slide poly-L-lysine	Roth (Karlsruhe, Germany)
Heparinized capillaries	Hartenstein (Würzburg, Germany)
Microcapillaries (100 µl)	Hartenstein (Würzburg, Germany)
Syringes (10 m)	Dispomed (Gelnhausen, Germany)
Syringe filters (70 µm)	Roth (Karlsruhe, Germany)
Well plates (48-well)	Greiner (Frickenhausen, Germany)
qPCR 96-well plates	Sarstedt (Nümbrecht, Germany)
Petri dishes (10 cm)	Techno Plastic Products AG (Trasadingen, Switzerland)

2.1.2 Chemicals and reagents

Table 2.3:   Chemicals and reagents

Reagents	Manufactorer
Adenosine diphosphate (ADP)	Sigma-Aldrich (Schnelldorf, Germany)
Agarose	Roth (Karsruhe, Germany)
Ammonium peroxidsulfate (APS)	Roth (Karsruhe, Germany)
Apyrase (grade III)	Sigma-Aldrich (Schnelldorf, Germany)
Bovine serum albumin (BSA)	AppliChem (Darmstadt, Germany)
Bradford solution	Bio-Rad (Munich, Germany)
Collagen related peptide (CRP)	CRB Cambridge Research Biochemicals (Billingham, UK)
Dimethyl sulfoxide (DMSO)	Sigma-Aldrich (Schnelldorf, Germany)
dNTP mix	Fermentas (St. Leon-Rot, Germany)
Ethylenediaminetetraacetic acid (EDTA)	AppliChem (Darmstadt, Germany)
Fat-free dry milk	AppliChem (Darmstadt, Germany)
Fluoroshield mounting medium with DAPI	Sigma-Aldrich (Schnelldorf, Germany)
GeneRuler 100 bp DNA Ladder	Fermentas (St. Leon-Rot, Germany)
Heparin sodium	Ratiopharm (Ulm, Germany)
Indomethacin	Alfa Aesar (Karlsruhe, Germany)
Isofluran CP	cp-pharma (Burgdorf, Germany)
Leupeptin	Sigma-Aldrich (Schnelldorf, Germany)
Midori Green DNA stain	Nippon Genetics (Düren, Germany)
PageRuler prestained protein ladder	Fermentas (St. Leon-Rot, Germany)
Paraformaldehyde (PFA)	Sigma-Aldrich (Schnelldorf, Germany)
Pepstatin	Roche Diagnostics (Mannheim, Germany)
Prostacyclin (PGI_2)	Sigma-Aldrich (Schnelldorf, Germany)
Proteinase K	Fermentas (St. Leon-Rot, Germany)
Roti Lumin plus ECL solution	Roth (Karsruhe, Germany)
Rotiphorese gel 30 acrylamide	Roth (Karsruhe, Germany)
Sodium orthovanadate	Sigma-Aldrich (Schnelldorf, Germany)
Sucrose	Sigma-Aldrich (Schnelldorf, Germany)
Super cryo embedding medium (SCEM)	Section lab (Hiroshima, Japan)
Taq Polymerase	Fermentas (St. Leon-Rot, Germany)
Taq Polymerase 10x buffer	Fermentas (St. Leon-Rot, Germany)
Tetramethylethylenediamine (TEMED)	Roth (Karsruhe, Germany)
Thiazole Orange	Sigma-Aldrich (Schnelldorf, Germany)
Thrombin	Roche Diagnostics (Mannheim, Germany)
Triton X-100	AppliChem (Darmstadt, Germany)
Tween 20	Roth (Karsruhe, Germany)
U46619	Enzo Lifesciences (Lörrach, Germany)

If not other stated above, all reagents and chemicals were obtained from AppliChem (Darmstadt, Germany), Roth (Karsruhe, Germany) or Sigma-Aldrich (Schnelldorf, Germany).

2.1.3 Antibodies

Commercial antibodies

Table 2.4: **Commercial antibodies**

Antibody	Manufactorer
Anti-CD105 (MJ7/18)	eBioscience (San Diego, CA, USA)
Anti-CD45 (30-F11)	eBioscience (San Diego, CA, USA)
Anti-CD41-FITC (MWReg30)	BD Biosciences (Heidelberg, Germany)
Anti-collagen I (pAb)	Abcam (Cambridge, UK)
Anti-collagen III (pAb)	Abcam (Cambridge, UK)
Anti-collagen IV (pAb)	Merck Millipore (Darmstadt, Germany)
Anti-SMA (1A4)	Dako (Hamburg, Germany)
Anti-fibrinogen (isolated from human plasma)	Dako (Hamburg, Germany)
Anti-fibronectin (pAb)	Merck Millipore (Billerica, MA; USA)
Anti-vWF (isolated from human plasma)	Dako (Hamburg, Germany)
Anti-mouse IgG Alexa 568	Life Technologies (Carlsbad, CA, USA)
Anti-rat IgG Alexa 546 and 647	Life Technologies (Carlsbad, CA, USA)
Anti-rabbit IgG Alexa 647 and Alexa 568	Life Technologies (Carlsbad, CA, USA)
Anti-goat IgG Alexa 647	Life Technologies (Carlsbad, CA, USA)
Anti-β-tubulin (clone TUB 2.1)	Sigma-Aldrich (Schnelldorf, Germany)
Anti-rabbit IgG HRP	Dako (Hamburg, Germany)
Anti-mouse IgG HRP	Dako (Hamburg, Germany)
Anti-rat IgG HRP	Dako (Hamburg, Germany)

All listed antibodies are directed against mouse proteins.

Non-commercial antibodies

Table 2.5:   Non-commercial antibodies

Antibody	Manufactorer
Anti-GPIb (15E2)	Nieswandt laboratory (Würzburg, Germany)
Anti- GPIX (56F8)	Nieswandt laboratory (Würzburg, Germany)
Anti- GPV (89H11)	Nieswandt laboratory (Würzburg, Germany)
Anti- GPVI (JAQ1)	Nieswandt laboratory (Würzburg, Germany)
Anti- α2 (12C6 and 23C11)	Nieswandt laboratory (Würzburg, Germany)
Anti- CD9 (96H10)	Nieswandt laboratory (Würzburg, Germany)
Anti- αIIbβ3 (14A3)	Nieswandt laboratory (Würzburg, Germany)
Anti- α5 integrin (25B11)	Nieswandt laboratory (Würzburg, Germany)
Anti- CLEC-2 (11E9)	Nieswandt laboratory (Würzburg, Germany)
Anti- P-Selectin (5C8)	Nieswandt laboratory (Würzburg, Germany)
Anti- laminin-α5 chain (504)	Sorokin laboratory (Münster, Germany)
Anti- laminin-α4 chain (377b)	Sorokin laboratory (Münster, Germany)
Anti- VEGFR2 (Flk1)	Ergün laboratory (Würzburg, Germany)
Anti- VE-cadherin	Ergün laboratory (Würzburg, Germany)
Anti- β_1-Tubulin	Italiano laboratory (Boston, MA, US)

All listed antibodies are directed against mouse proteins.

2.1.4 Buffers and solutions

All buffers used for this thesis were prepared with water from a MilliQPurification System. To adjust the pH, HCl or NaOH were used.

- **Cell culture medium (Gibco)**

  DMEM + GlutaMAX   -

  FCS   10%

  Penicillin/streptomycin   100 U/ml

- **Dulbecco´s phosphate buffered saline (Sigma)**

  Endotoxin free

- **Phosphate buffered saline (PBS), pH 7.14**

NaCl	137 mM
KCl	2.7 mM
KH_2PO_4	1.5 mM
Na_2HPO_4	8.0 mM

- **Hepes-Tyrode-buffer without Ca^{2+}**

NaCl	137 mM
KCl	2.7 mM
$NaHCO_3$	12 mM
NaH_2PO_4	0.43 mM
$MgCl_2$	1 mM
HEPES	5 mM
(BSA fraction V solution	0.35% v/v) freshly added
(Glucose solution	1% v/v) freshly added

- **Hepes-Tyrode-buffer with Ca^{2+}**

NaCl	137 mM
KCl	2.7 mM
$NaHCO_3$	12 mM
NaH_2PO_4	0.43 mM
$CaCl_2$	2 mM
$MgCl_2$	1 mM
HEPES	5 mM
(BSA fraction V solution	0.35% v/v) freshly added
(Glucose solution	1% v/v) freshly added

- **Protein lysis buffer, 2x, pH 7.4**

HEPES	15 mM
NaCl	150 mM
EGTA	10 mM
Triton X-100	2% v/v
(Leupeptin	1 mM) freshly added
(Pepstatin	1 mM) freshly added
(Aprotinin A	1 mM) freshly added
(PMSF	1 mM) freshly added

- **Separation gel buffer, pH 8.8**

Tris-HCl	1.5 M

- **Stacking gel buffer, pH 6.8**

Tris-HCl	1 M

- **SDS sample buffer, 4x reducing**

Tris-HCl	200 mM
Glycerol	40% v/v
SDS	8% w/v
Bromphenol blue	0.04% w/v
β-Mercaptoethanol	2% v/v

- **Laemmli buffer**

Tris	40 mM
Glycine	0.95 mM
SDS	0.5% w/v

- **Transfer buffer**

$NaHCO_3$	10 mM
Na_2CO_3	3 mM
(Methanol	20% v/v) freshly added

- **Tris buffered saline (TBS), pH 7.3**

NaCl	137 mM
Tris-HCl	20 mM

- **Washing buffer (TBS-T)**

TBS (1x)	-
Tween 20	0.1% v/v

- **Blocking buffer**

TBS-T	-
BSA or fat-free dry milk	5% w/v

- **Stripping buffer, pH 6.7**

Tris-HCl	62.5 mM
SDS	2%
(β-Mercaptoethanol	0.7% v/v) freshly added

- **Gitschier buffer (10x)**

Tris	670 mM, pH 8.8
$(NH_4)_2SO_4$	166 mM
$MgCl_2$	65 mM
Triton X-100	0.5% v/v

- **DNA lysis buffer**

Gitschier (10x)	10%
Proteinase K	1 mg/ml
β-Mercaptoethanol	1% v/v

- **TAE buffer, 50x, pH 8.0**

TRIS	200 mM
Acetic acid	5.7% w/v
EDTA	50 mM

- **Orange G, loading dye 6x**

Tris-HCl	10 mM, pH 7.6
Glycerol	60% v/v
EDTA	60 mM
Orange G	0.15% w/v

- **Washing buffer (IF-stain)**

PBS	-
FCS	5% v/v
Tween 20	0.1% v/v

- **Blocking buffer (IF-stain)**

Washing buffer	-
Serum	10% v/v

- **Coating buffer (ELISA), pH 9.5**

$NaHCO_3$	50 mM

2.1.5 Mouse models

Table 2.6:   Mouse models

Mouse line	Background	Source
Gp6^(-/-)	C57BL/6	Markus Bender, Würzburg
Itga2^(-/-)	C57BL/6	Beate Eckes, Köln
Gp6/*Itga2* DKO	C57BL/6	Own breeding
Lat^(-/-)	C57BL/6	Zhang *et al.*, 1999
Syk^(fl/fl, Pf4-Cre+)	C57BL/6	Lorenz *et al.*, 2015
Mmp9^(-/-)	FVB → C57/B6 (mixed)	Vu *et al.*, → Charles River FVB/N-Tg(Eno2-MMP-9)1Pfi
CD-1	outbred	Charles River

2.1.6 Primers

All primers were obtained from Biomers (Ulm, Germany). The following primer pairs were used for genotyping mouse strains in this study.

Table 2.7:   Primers

Primer	Sequence 5´→ 3'
GP6_Intron 2 forward (qPCR)	ACACAGAGTGGTGAGTATGTC
GP6_Intron 2 reverse (qPCR)	AATCACGGACACTAGGTTAGC
GP6_Exon 4 forward (qPCR)	GACTCTGAAGTGCCAGAGC
GP6_Exon 4 reverse (qPCR)	AAGCTGTAACACCGGTAC
ITGA2_WT forward	AAGTTGCTCGCTTGCTCTA
ITGA2_WT reverse	AATATCCGTAGAAGCTCAGC
ITGA2_KO forward	AAGTTGCTCGCTTGCTCTA
ITGA2_KO reverse	TGGCTTTTCTTCCTCCTATGG
MMP-9_WT forward	ACTCTGAAGACTTGCCGCGAG
MMP-9_WT reverse	CTCGCGGCAAGTCTTCAGAGTA
MMP-9_KO forward	CTGAATGAACTGCAGGACGA
MMP-9_KO reverse	ATACTTTCTCGGCAGGAGCA

2.2 Methods

2.2.1 Mouse studies

Animal husbandry

All animal studies were approved by the district government of Lower Franconia (Bezirksregierung Unterfranken).

Generation of transgenic mice

Gp6^{-/-}, *Itga2*^{-/-}, *Lat*^{-/-} and *Syk*[fl/fl, Pf4-Cre+] mouse lines were present at the animal facility in the institute and described originally as listed in Table 2.6. *Gp6*/*Itga2* double-deficient (DKO) mice were generated by cross breeding *Gp6*-null mice and *Itga2*-null mice. Mice constitutively lacking *Mmp9*, originally described by Vu *et al*. in 1998, were obtained from Charles River and are currently backcrossed to the C57BL/6 background. Dr. David Stegner provided *Syk*[fl/fl, Pf4-Cre+] mice and littermate controls. *Lat*^{-/-} mice with respective control animals were kindly provided by Dr. Viola Lorenz.

Genotyping of transgenic mice

Isolation of genomic DNA from ear punches

An ear punch device was used to obtain a small part of the mouse ear, which was incubated for 2 h at 56°C in 100 µl DNA lysis buffer. Afterwards, sample was boiled for 5 min at 95°C and centrifuged at 20000 g for 10 min at 4°C. For genotyping PCR 1 µl of the supernatant was applied.

Genotyping of *Itga2* mice

Primers used to genotype *Itga2* mice are listed in Table 2.7. The predicted band sizes are 230 bp for WT and 300 bp for KO.

Table 2.8: **PCR mix for *Itga2* genotyping**

Reagent	Volume in µl
H_2O	17.85
10x PCR-buffer	2.5
$MgCl_2$	2.0
dNTP´s	0.5
Primer forward	0.5
Primer reverse	0.5
Taq-Polymerase	0.15

Table 2.9: PCR program for genotyping *Itga2⁺/⁺* mice

Step	Temperature	Duration
1	94°C	4 min
2	94°C	1 min
3	52°C	1 min
4	72°C	1 min
5	4°C	∞

Repeat steps 2-4 for 35 cycles

Table 2.10: PCR program for genotyping *Itga2⁻/⁻* mice

Step	Temperature	Duration
1	94°C	4 min
2	94°C	1 min
3	54°C	30 sec
4	72°C	1 min
5	94°C	1 min
6	47°C	1 min
7	72°C	1 min
8	4°C	∞

Repeat steps 2-4 for 8 cycles

Repeat steps 5-7 for 27 cycles

Genotyping of *Gp6* mice

To genotype *Gp6* mice, quantitative real time PCR was used and the ΔΔC$_t$ method was applied to evaluate the data. The obtained C$_t$ values of Exon 4 were referred to C$_t$ values of Intron 2 and were measured in triplicates. Primers used to genotype *Gp6* mice are listed in Table 2.7.

Table 2.11: qPCR mix for genotyping *Gp6* mice

Reagent	Volume in µl
H$_2$O	3.8
Sybr-green mix	10
Primer forward	0.6
Primer reverse	0.6
DNA (10 ng/µl)	5

Table 2.12: qPCR program for genotyping *Gp6* mice

Step	Temperature	Duration
1	50°C	2 min
2	95°C	10 min
3	95°C	15 sec
4	60°C	1 min
5	95°C	15 sec
6	60°C	1 min
7	95°C	30 sec
8	60°C	15 sec

Repeat steps 3-4 for 40 cycles

Melt curve: steps 5-8

Genotyping of *Mmp9* mice

Primers used to genotype *Mmp9* mice are listed in Table 2.7. The predicted band sizes are 390 bp for WT and 172 bp for KO.

Table 2.13: PCR mix for genotyping *Mmp9* mice

Reagent	Volume in µl
H_2O	16.55
10x PCR-buffer	2.5
$MgCl_2$	2.5
dNTP´s	1.0
Primer forward	0.1
Primer reverse	0.1
Taq-Polymerase	0.25

Table 2.14: PCR program for genotyping *Mmp9* mice

Step	Temperature	Duration
1	95°C	5 min
2	95°C	1 min
3	61°C	1 min
4	72°C	1 min
5	72°C	10 min
6	4°C	∞

Repeat steps 2-4 for 35 cycles

Agarose gel electrophoresis

To visualize PCR products, 1.5% (w/v) agarose gels were prepared. Therefore, agarose was dissolved in TAE buffer by boiling it in a microwave. After cooling the solution down to approximately 50-60°C, 5 µl of Midori green per 100 ml were added to the solution. Samples were mixed 1:6 with loading dye and 20 µl were loaded onto the gel. To separate the DNA according to its size a current of 130-150 V was applied for 45 min and PCR products were visualized by UV light.

Irradiation of mice

Mice were placed in a radiation permeable box and immobilized with a cover plate. For sublethal irradiation (5Gy) mice were exposed to x-rays for 7.5 min with 160 V and 6.3 mA in a radiation device (Faxitron). Afterwards, neomycin (2 mg/ml) was given to the drinking water to prevent infections and general health conditions like weight, fur structure and behavior of the mice were assessed every day.

2.2.2 *In vitro* analyses

Isolation, cultivation and enrichment of MKs

To obtain fetal liver cell derived (FLC)-MKs, livers of E14.5 embryos were isolated from time mated mice of the respective genotype. After homogenizing the livers with a syringe in 10 ml PBS, the cell suspension was centrifuged at 200 g for 5 min. The cell pellet was resuspended in DMEM and rinsed through a 70 µm cell strainer. Additional medium was added containing 10% FCS and penicillin/streptomycin (P/S). Three livers were cultivated per 10 cm petri dish supplemented with 50 µl TPO conditioned medium for three days at 37°C and 5% CO_2. MKs were enriched via a BSA-gradient, where 1 ml of cell suspension was given on top of 3 ml BSA in PBS (1.5 ml 3% BSA + 1.5 ml 1.5% BSA) for 20 min. Afterwards, 17000 MKs per cm^2 were seeded in a 48- well plate and the percentage of proplatelet forming MKs was determined over time. For adhesion assays, 140000 MKs were seeded on uncoated, BSA- or ECMP–coated cover slips for 4 h. After removal of non-adherent cells, MKs were stained with an Alexa488 conjugated αIIbβ3-antibody and mounted with Fluoroshield mounting medium, containing DAPI. To determine the adhesion capacity, mean percentage of

covered surface was measured in 10 visual fields per coverslip with a confocal laser scanning microscope (Leica TCS SP8).

BM MKs were isolated from femora and tibiae of the respective mouse strain. Therefore, bones were dissected as described in 2.2.4. and epiphyses cropped off with scissors under sterile conditions. BM was flushed out with a PBS-filled syringe. After homogenizing the cells with a 22 gauge syringe the suspension was centrifuged at 200 g for 5 min, resuspended in 1 ml StemPro medium and rinsed through a 70 µm cell strainer to remove residual bone fragments and tissue. Further StemPro medium was added as well as SCF (50 ng/ml f.c.). BM of one mouse was cultivated per 10 cm petri dish in 10 ml medium. Two days later, medium was exchanged and SCF (50 ng/ml f.c.) as well as TPO-conditioned medium (1:1000 f.c.) was added. On day four, medium was exchanged again and only TPO-conditioned medium (1:1000 f.c.) was added to the cell suspension for one more day. A BSA gradient was performed on day five to separate MKs from other cells. Fractions were then lysed and stored at -20°C or used immediately for further analyses.

Isolation of platelets

Mice were anesthetized with isoflurane and fully bled from the retrobulbar plexus using a pre-cut glass capillary into 300 µl heparin-filled reaction tubes. Platelet rich plasma (PRP) was isolated by centrifuging blood at 60 g for 5 min at room temperature (RT) and transferring the upper phase with little of the lower red phase into a new reaction tube. This tube was centrifuged again at 60 g for 6 min and the upper phase without red cells was transferred to a new reaction tube. To obtain washed platelets, samples were centrifuged at 736 g for 5 min after addition of PGI_2 (0.1 µg/ml) and apyrase (0.02 U/ml) to the PRP. The supernatant was discarded and the pellet resuspended in 1 ml HEPES-Tyrode´s (H.T.) buffer without Ca^{2+} containing PGI_2 and apyrase. Subsequently, the samples were centrifuged again at 736 g for 5 min, resuspended in 1 ml (H.T.) buffer without Ca^{2+} and the platelet count was measured at a Sysmex KX-21N automated hematology analyzer. A final centrifugation step was conducted at 736 g for 5 min and the pellet was lysed and stored at -20°C or used immediately for further analyses.

Platelet analyses by flow cytometry

To determine expression levels of platelet surface receptors, activation of αIIbβ3 integrin and P-selectin exposure upon platelet stimulation with different agonists, 100 µl blood were taken from the retrobulbar plexus of isoflurane-anesthetized mice. The mice were bled into reaction tubes filled with 300 µl heparin and 1 ml H.T. without Ca^{2+} was added. 50 µl of diluted blood was added to 10 µl of the respective fluorophore-conjugated antibody, listed in Table 2.5, into a flow cytometry tube and incubated for 15 min, protected from light. Afterwards, the staining reaction was stopped by adding 500 µl PBS and analyses were performed at a FACS Calibur flow cytometer using the Cell Quest software (BD Biosciences). For the measurement of integrin activation and granule secretion, remaining blood was washed twice with H.T.-buffer without Ca^{2+}. Finally, the pellet was resuspended in H.T.- buffer containing Ca^{2+} and 50 µl washed platelets were incubated with 7 µl agonist (U46619, ADP; thrombin and the collagen related peptide CRP) for 6 min at 37°C and 6 min at RT in a flow cytometry tube containing phycoerythrin (PE)-coupled JON/A (4H5) and FITC-coupled anti-P-selectin (5C8) antibodies. By adding 500 µl PBS the reaction was stopped and analyses were performed at a FACS Calibur flow cytometer using the Cell Quest software (BD Biosciences).

2.2.3 Biochemical analyses

Lysate preparation

MKs and platelets were prepared as described in 2.2.2 and incubated in lysis buffer containing protease inhibitors for immunoblot analyses for 30 min at 4°C. Afterwards, the samples were centrifuged at 22000 g for 10 min at 4°C. Supernatant was transferred to a new reaction tube and stored at -20°C until the protein concentration was determined.

Determination of the protein concentration according to Bradford

To determine the protein content of cell lysates, a standard curve ranging from 100 µg/ml to 1500 µg/ml BSA was adjusted. Therefore, Bradford solution was diluted 1:6 in water, 975 µl were filled into half micro cuvettes and 25 µl of each standard was

added. After incubation for 5 min at RT, the protein standard was measured with a photometer (Nanodrop 2000c) at 450 nm. Subsequently, cell lysates were measured after adding 5 µl of the sample to 995 µl 1:6 diluted Bradford solution and incubating it for 5 min at RT.

Immunoblot analyses

For separation of proteins according to their molecular weight 4x reducing sample buffer was added to 20 µg of protein lysates, the samples were boiled for 5 min at 95°C. After cool-down, protein samples were loaded onto a 10% SDS gel. Proteins were separated at 120 V for 1.5 hours. To transfer the proteins onto a PVDF membrane a wet transfer blot was built up in the following order: sponge, 2 x filters, PVDF-membrane, SDS-gel, 2 x filters. A constant current of 350 mA was applied for one hour. After blocking free binding sites on the membrane in either 5% milk or 5% BSA in TBS-T, incubation with the primary antibody over night at 4°C was conducted. After three washing steps in TBS-T (1x 15 min, 2x 5 min), the membrane was incubated for 1 h at RT in the respective HRP-conjugated secondary antibody on the next day. Subsequently, the membrane was washed three times in washing buffer and a chemiluminescent HRP substrate was added in a 1:1 mixture followed by digital detection (Fluor Chem Q, Alpha Innotech). For detection of further protein bands on the same membrane, previously bound antibodies were detached from the membrane by incubation in stripping buffer for 30 min at 60°C. Afterwards, the membrane was washed, blocked and incubated with antibodies as described above.

Determination of antibody specificity by ELISA

For determination of antibody specificity, ELISA plates were coated with 10 µg/ml of either Col I, Col IV or a 1:1 mixture of both proteins over night at 4°C. Blockage with 5% BSA was performed for 1 h at RT followed by incubation with anti-Col I, anti-Col IV or a 1:1 mixture of both antibodies for 1 h at 37°C. After washing with PBS, samples were incubated with respective secondary HRP-conjugated antibodies for 2 h at 37°C. Prior to development with TMB One substrate in a plate reader at 450 nm, wells were washed with PBS.

2.2.4 *Ex vivo* analyses

<u>Organ preparation</u>

To isolate femora, sternae and spleens, mice were anesthetized with isoflurane and cervically dislocated. The abdominal wall was opened and bones and organs were isolated. After fixation in 4% PFA for 4 h at 4°C, organs were transferred for dehydration into sucrose solutions of 10, 20 and 30% (w/v), each for 24 h at 4°C. The bones and spleens were embedded in cryo mold dishes with SCEM medium and deep frozen at -80°C until sectioning. For IF-staining, organs were sliced into 10 µm sections on Kawamoto adhesive films with a cryotom (Leica CM1900) and fixed on superfrost glass slides. For the 3D reconstruction, mice were injected with 20 µg of an CD105-antibody coupled to Alexa 546 and an GPIX (56F8)-antibody coupled to Alexa 647 half an hour before cervical dislocation. Sternae and spleen were isolated and fixed with 4% PFA at 4°C over night. Subsequently organs were cleared with a benzyl alcohol-benzyl benzoate (BABB) –solution for 24 hours.

<u>Immunofluorescence (IF) staining</u>

For IF-staining, sections were thawed and rehydrated for 20 min in PBS. After blocking unspecific binding with blocking buffer, sections were incubated with primary antibodies for 45 min at RT. Following three washing steps with washing buffer, each for 5 min, the samples were incubated with the respective secondary antibody for 45 min at RT. The blocking – and antibody- incubation steps were repeated for each protein and after drying the sections were mounted with DAPI-containing mounting medium (Fluoroshield).

2.2.5 Imaging

<u>Transmission light microscopy</u>

To evaluate viability of cells or counting of proplatelet-forming MKs, transmission light microscopy (Zeiss Primo Vert) was conducted.

Confocal laser scanning microscopy (CLSM)

All images were taken using confocal laser-scanning microscope (Nikon A1, Chiyoda, Japan or TCS SP5 or TCS SP8, Leica Microsystems CMS, Wetzlar, Germany) with 200-, 400- or 600-fold magnification and CFI Plan Apochromat VC lenses (NA 0.75, 1.25 or 1.4) and NIS Elements AR or LAS X software for image documentation and analysis. When recording stacks or pictures used for quantitative analyses, xyz-settings were applied according to Nyquist criteria, that were calculated with the Nyquist calculator app at the Scientific Volume Imaging website and were recorded with 100-200 Hz. Deconvolution of image data was performed with Huygens essential software version 15.10 by Scientific Volume Imaging B.V. and FIJI software was used to evaluate MK areas, distances from MKs towards vessels and the contact of MKs with matrix proteins.

2.2.6 Statistical data analyses

Results are shown as mean ± SD from three individual experiments, unless indicated otherwise. All data were subjected to Shapiro-Wilk tests for determination of their distribution curve. Significant differences of pairwise comparison of means against a specified control were determined using ANOVA, student's t-test, or nonparametric Mann-Whitney rank sum test. Differences between cell size distributions of different groups were compared by Kolmogorov-Smirnov-test and frequency distributions by χ2-test. P-values < 0.05 were considered as statistically significant with: $p < 0.05$ (*,#), $p < 0.01$ (**,##) and $p < 0.001$ (***,###).

3 Results

3.1 Role of collagens on platelet biogenesis

The overall composition of the BM matrix is well characterized for years, but sectioning and visualization of the intact bone environment and architecture in situ was so far hampered due to the calcified compact bone cortex. Therefore, harsh demineralization protocols using nitric or hydrochloric acid have been typically applied. Since protein epitopes can be altered by these rough procedures it is likely that staining patterns might be incomplete or impaired. However, a new histological technique according to Kawamoto allows sectioning and four-color IF-staining of bones without previous decalcification (Hosoya *et al.*, 2005), enabling us to (co)-visualize different matrix proteins, BM-cells and vessels simultaneously.

3.1.1 MKs are equally distributed within the marrow of different bone types

In a first approach, we adopted an automated imaging system (stitching), which facilitates the visualization of whole organ- or bone-sections (Fig. 7A and B). Nuclei staining with DAPI allowed monitoring of the overall cellularity and detection of cutting artifacts to evaluate the quality of sections after the staining and washing procedures. Staining of sinusoids with anti-endoglin (CD105) and MKs with anti-CD41 fluorescently labeled antibodies followed by stitching images of sternae (Fig.7A, Ai; Aii) and femora (Fig. 7B, Bi; Bii) revealed a comparable distribution and arrangement of MKs and vessels throughout the whole bone. When we divided femora into proximal epiphysis, diaphysis and distal epiphysis, we found only minor alterations in MK distribution within the different segments of BM (Fig. 7Bi, Bii) with a slight enrichment of MKs at the distal femur epiphysis with respect to the area (Fig. 7C). MK sizes ranged from 100 µm^2 to 600 µm^2, but their distance to vessels appeared to be rather size-independent. Approximately 60% of MKs were vessel-associated (Fig. 7D) and the median distance between sinusoids was 50 µm (Fig. 7E). These results indicate that both, sternae and femora are comparable with regard to MK number and distribution and can thus be used for quantitative analyses.
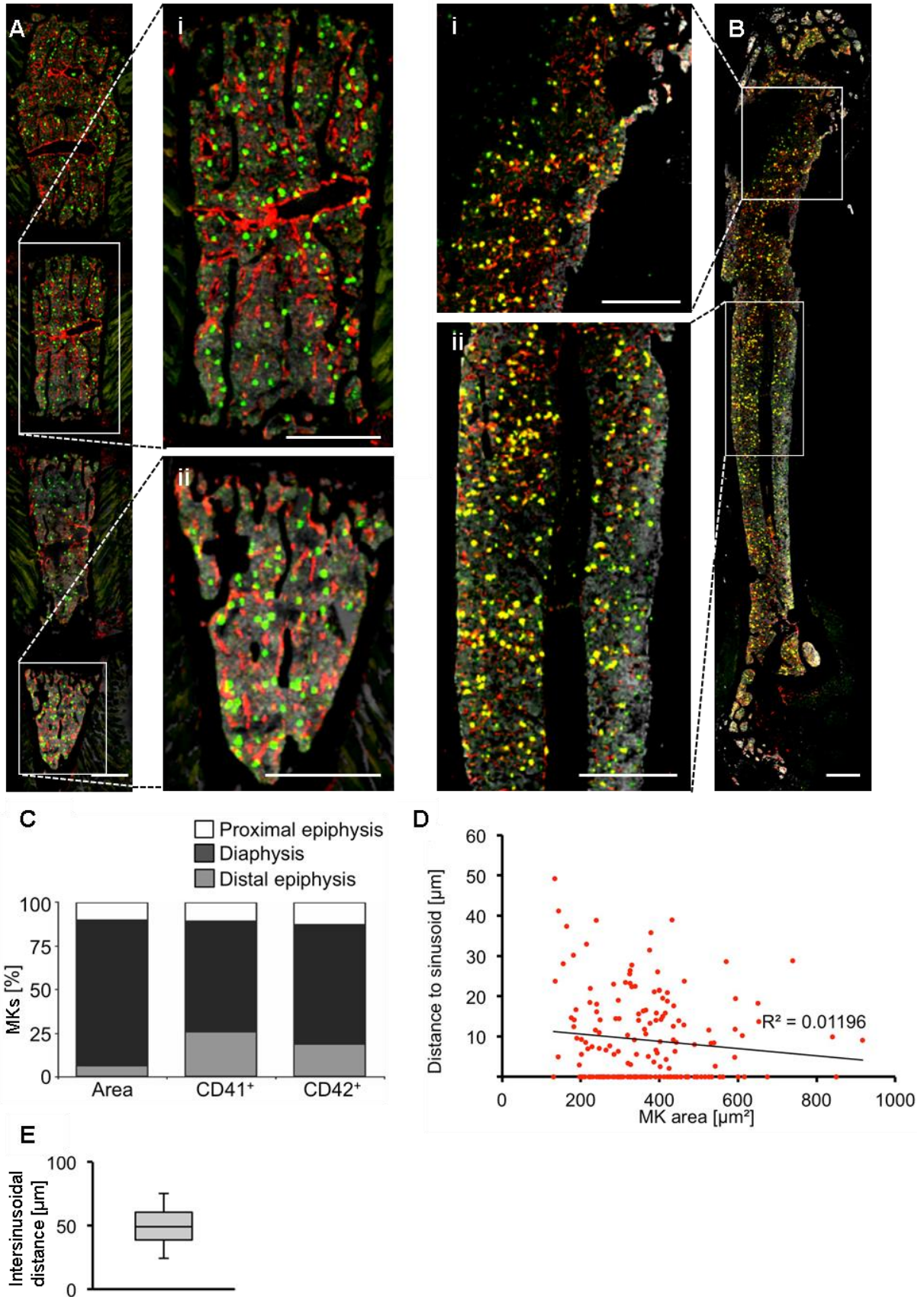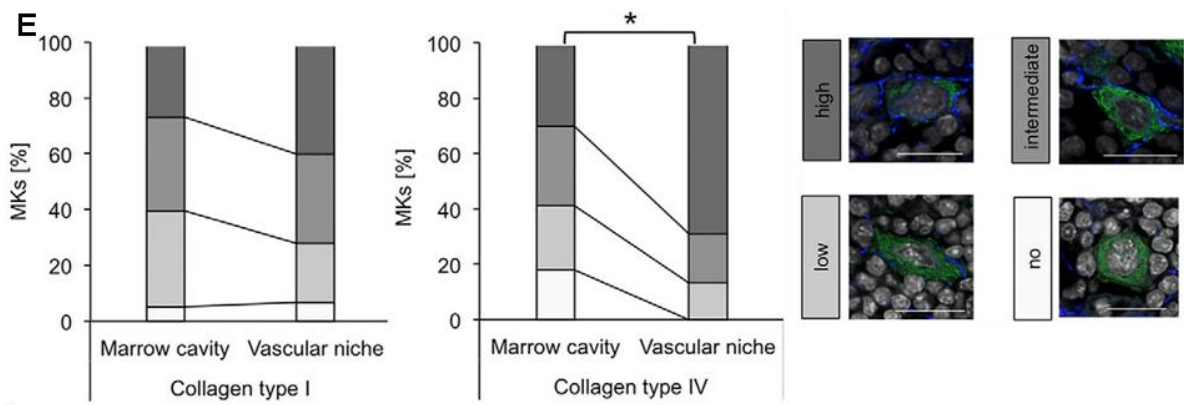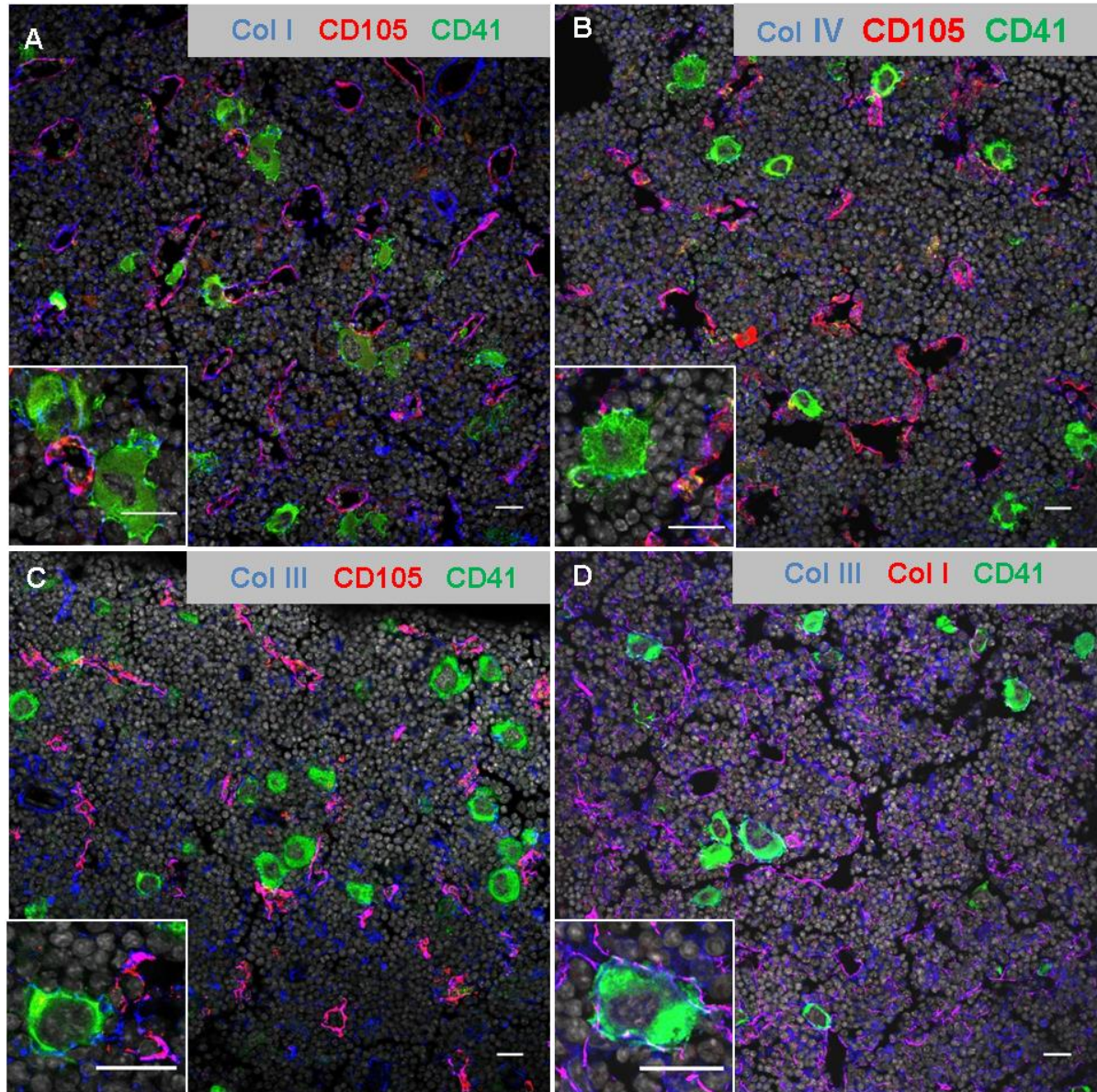
Fig. 7: Distribution of MKs throughout murine BM. Stitched images of a whole murine sternum **(A)** and femur **(B)** stained for MKs (CD41, green), sinusoids (CD105, red) and nuclei (DAPI, grey). Different segments in the sternum (Ai, Aii) as well as both femur epiphyses and the diaphysis (Bi, Bii) were easily distinguishable. Scale bars represent 1 mm in whole bone images and 500 µm in insets. **(C)** MKs were homogenously distributed throughout the different bone types with a minor enrichment in the distal

epiphysis of the femur in respect to the area. **(D)** Distance of MKs to sinusoids depicted in respect to their size indicated that larger MKs were by majority in contact to sinusoids. **(E)** The median distance between two sinusoids was 50 µm. For qualitative analysis one out of three representative experiments is shown. Box plot whiskers represent 5 resp. 95% percentile. **(C-E)** Femora of three different mice in total and five visual fields per femur were analyzed. Images A and B were generated in a collaborative project with Dr. David Stegner and Dr. Judith van Eeuwijk. Data in C were generated by Imke Meyer. Analyses in D and E were performed by Rebecca Kulawig.

3.1.2 MK-contact to Col IV is increased at the vascular niche

To evaluate the presence and localization of distinct matrix proteins at sinusoids and MKs, we developed and performed four-color IF-stainings. Col I, Col III and Col IV filaments appeared to be similarly distributed within BM and showed co-localization with sinusoids (Fig. 8A-C). Simultaneous staining for Col I and Col III revealed an overall overlapping pattern, but Col III filaments were also present solitary (Fig. 8B). Since MKs seemed to be associated with all analyzed collagen types (Fig. 8A-D, insets), we established an assay to assess alterations in contact of MKs to collagens at the vascular niche compared to marrow cavity. We defined four categories to classify the contact degree of MKs towards Col I and IV: no contact (0–5%), low contact (5–40%), intermediate contact (40–60%) and high contact (60–100%) as indicated (Fig. 8E, right). The degree of contact of MKs to Col I was almost unaltered within the marrow cavity and the vascular niche. Surprisingly, an increased amount of MKs was in contact with Col IV at the vascular niche, while the values in the BM cavity were comparable to Col I (Fig. 8E). To exclude cross reactivity of Col I and IV antibodies towards the respective other collagen type, we performed an ELISA assay. The resulting data, depicted in a heatmap, indicate that the antibodies used in this study recognize their respective epitopes with highest affinity as expected and that there is only a minimal affinity toward the other collagen types (Fig. 8F). Together, these findings imply that we can bona fide distinguish distinct collagens in the BM by IF-stainings and thus are able to perform analyses specifically for each isoform.

Fig. 8: Distribution of distinct collagen types throughout murine BM. (A) Col I, **(B)** Col IV and **(C)** Col III were abundantly expressed within BM and were present as subendothelial layers at sinusoids and arterioles. **(D)** Col I showed a partially overlapping staining with Col III and all collagen types co-localized with CD105-positive sinusoids **(A-C)**. MKs were in contact with Col I, III and IV at varying degrees. **(E)** While the degree of contact between Col I and MKs (4 categories, insets on the right) was not altered within cavity and at sinusoids, MKs residing at the vascular niche had markedly increased contact to Col IV (* $P<0.05$ by Kolmogorov-Smirnov test). Nuclei were visualized with DAPI (grey). Scale bars represent 20 µm. Five visual fields per femur and three femora of different mice in total were used to generate quantitative data. **(F)** Antibodies, directed against Col I or Col IV, showed the highest affinity towards their corresponding protein and were less sensitive towards other collagen types or mixtures in an ELISA approach. Values display the optical density (OD) measured at 450 nm. One out of three representative experiments is shown. Experiments in E were technically performed by Rebecca Kulawig.

3.1.3 Laminins, fibrinogen and FN show a diverse distribution within BM

Stainings of laminins, fibronectin (FN) and fibrinogen in combination with vessels and MKs within BM were performed in order to further map these extracellular matrix (ECM) proteins. FN appeared to be expressed as a dense network throughout the whole BM but was hardly associated with sinusoids (Fig. 9A). Fibrinogen was detectable as patches and highly co-localized with MKs (Fig. 9B). The laminin isoforms –α4 and –α5, were both expressed within BM (Fig. 3C, D) and present at arterioles, which are also positive for smooth muscle actin (Fig. 9E, F). In contrast, only laminin-α5 co-localized with the CD105-positive sinusoids (Fig. 9G, H). These results suggest that also other ECM proteins can specifically be stained and analyzed regarding their localization within BM.
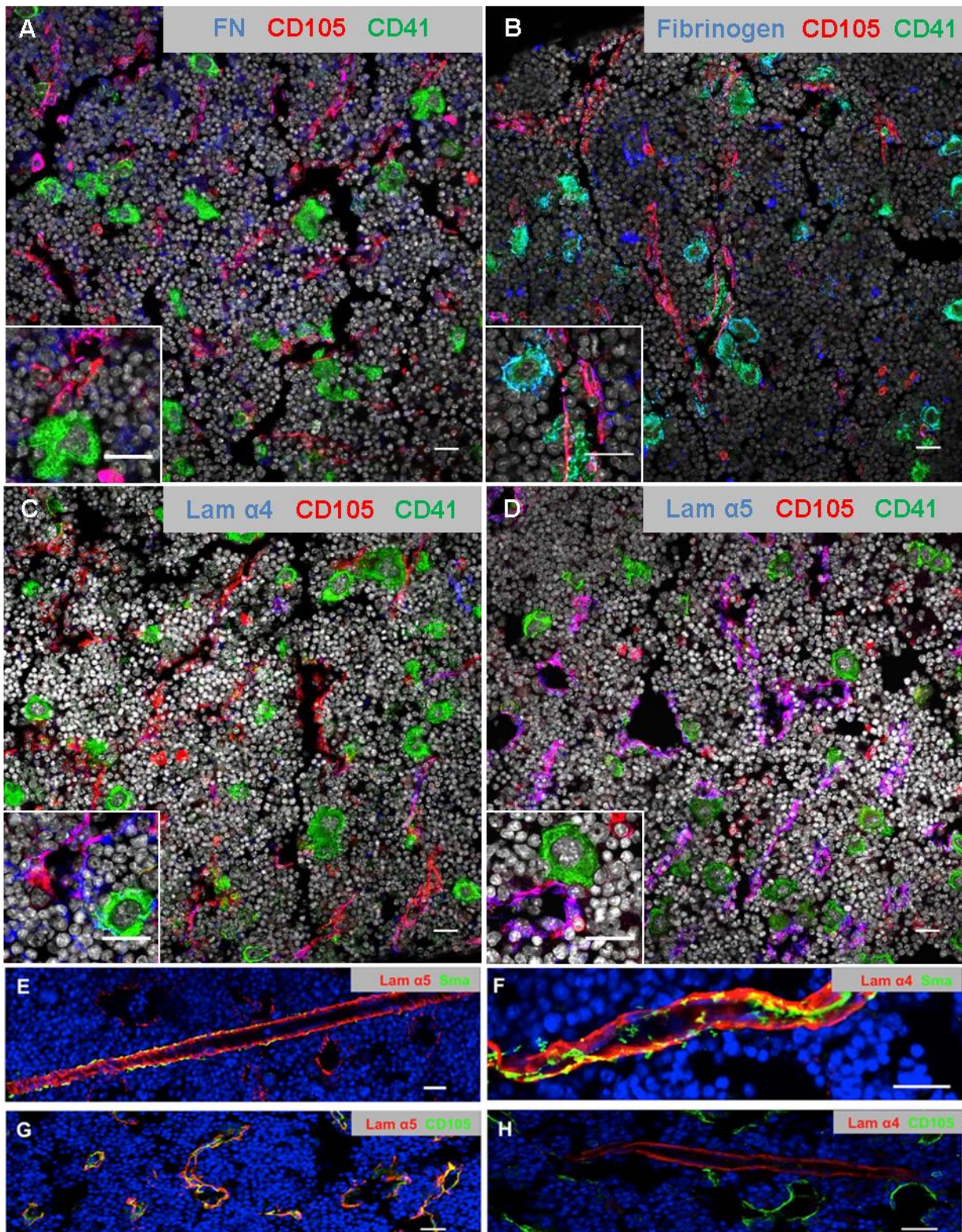
Fig. 9: Distribution of ECM proteins within murine BM. (A) Fibronectin (FN) was detected as a dense network throughout the BM but was rarely detectable near vessels. **(B)** Fibrinogen was arranged in patches and co-localized with MKs. **(C, D)** Laminin–α4 and –α5 were not present within the intersinusoidal space. **(E, F)** Arterioles, surrounded by smooth muscle actin (SMA), were in contact with laminins–α4 and –α5 but only laminin-α5 co-localized with CD105-positive sinusoids **(G, H)**. Nuclei were visualized with DAPI (grey: A-D, blue: E-H). Scale bars represent 20 µm. Shown results are

representative of three independent experiments. Experiments for pictures E-H were technically performed by Rebecca Kulawig.

3.1.4 Increased adhesion of MKs on Col I is diminished by α2β1 blockage

To assess the influence of collagens and other ECM proteins on MKs, we performed *in vitro* studies on fetal liver cell (FLC)-derived MKs. We cultured them for three days to study their ability to adhere on different ECM proteins. The area of each MK was approximately 600 μm^2 when they were allowed to adhere on BSA-coated or on uncoated cover slips. The size expanded to 1000 μm^2 on Col I. Adhesion on Col III, Col IV, laminin and fibronectin was also markedly increased compared to uncoated or BSA-coated controls (Fig. 10A). In concordance with the increased area, the surface coverage of MKs was highest (38%) on Col I. On Col III the surface coverage was less (25%), but still statistical significant while only little adhesion was observed on Col IV, laminin and fibronectin (10%-15%). Moreover, we observed hardly any (5%) adhesion on BSA or uncoated plates (Fig. 10B).

In further adhesion assays we wanted to identify the collagen receptor mediating the strong adhesion on Col I. We took advantage of the monoclonal antibodies JAQ1, to block GPVI, or LEN/B which binds to α2β1 integrin. The adhesion on Col I was increased 3-fold, compared to uncoated or BSA-coated plates, whereas adhesion on Col III was indistinguishable from controls. On Col IV the adhesion was weaker (1.5-fold increase) and on laminin even below the uncoated control level (0.7-fold). Upon blockage of GPVI with JAQ1, we could not detect changes in adhesion compared to untreated MKs. Interestingly, in the presence of LEN/B, MK adhesion was markedly decreased on all substrates, particularly on Col I (50% reduction). The treatment with both blocking antibodies had no additional effect on Col III-, IV- and laminin–adhered MKs compared to single treatments. But we observed a further diminished adherence on Col I in comparison to uncoated controls (Fig. 10C). These results suggest that α2β1 integrin is the main receptor mediating the strong adhesion of MKs on Col I.
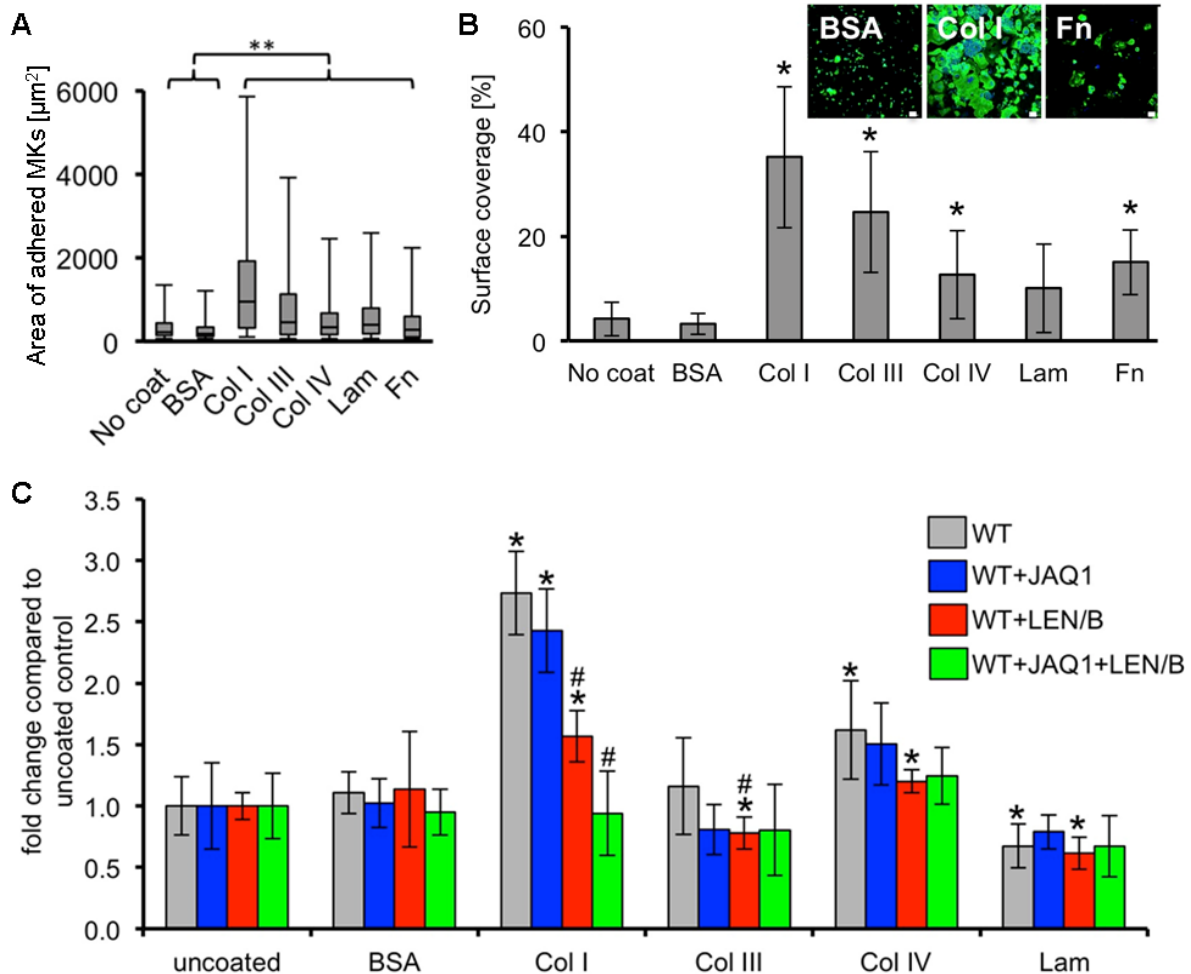
Fig. 10: Influence of ECM proteins on MK adhesion. (A) MKs, seeded on different ECM proteins, were able to spread and showed a significantly increased area on Col I-coated plates compared to uncoated and BSA controls. On all other ECM-coated plates the MK area was also slightly enhanced **(B)** Accordingly, the surface coverage of spread MKs was highest on Col I and III, and much less on Col IV and FN. **(C)** The strong adhesion of WT MKs (grey bar) on Col I could only be slightly diminished by the GPVI-blocking JAQ1 antibody (blue bar), but was markedly reduced by LEN/B antibody (red bar) blocking α2β1 integrin. The combination of both antibodies reduced adhesion to control levels (green bar). On laminin, MK adhesion was even lower than on uncoated or BSA-coated wells. Error bars indicate standard deviation, box plot whiskers represent 5 resp. 95% percentile. Significant differences of the mean (tested by Kruskal-Wallis/Mann-Whitney test) are marked by hashes when compared to wildtype (WT) or by asterisk if compared to uncoated control (*,# $P < 0.05$, ** $P < 0.01$). Data of three independent experiments, each determined in triplicates, were averaged. Experiments A-C were technically conducted by Rebecca Kulawig.

3.1.5 Proplatelet formation (PPF) is selectively inhibited by Col I

Once MKs are mature and in contact with vessels, they start to form proplatelets through the endothelial layer. In order to determine which of the ECM proteins can influence this directed process, we cultured fetal liver-derived (FLC) MKs for three days and subsequently seeded them on differently coated plates. The degree of PPF was measured on two consecutive days (day 4 and day 5). On BSA-coated or uncoated plates the PPF increased over time and reached a maximum of about 35% on day 5. Afterwards the PPF decreased, probably because MKs have already released their full

demarcation membrane system (DMS) content. The degree of PPF on laminin, fibronectin and Col IV was comparable to BSA control. Interestingly, MKs seeded on Col I exhibited less PPF. Only 17% of MKs formed proplatelets on day 5, which was comparable to what was observed for MKs seeded on BSA on day 3. This inhibition of PPF was also present on Col III, but to a much lesser extent (Fig. 11A).

In further PPF-assays, where we titrated laminin and CRP against Col IV, we wanted to address the question, whether one of the other ECM proteins can compensate for the inhibitory effect of Col I on PPF. Laminin was not able to revert the inhibition of PPF by Col I. Only when Col I was absent from the culture, PPF could be restored to 54%. When titrating Col IV against Col I, we observed a dose-dependent increase of PPF culminating in 46%. A similar effect was determined for CRP, which carries a condensed GPO-motif of Col I, with an even stronger increase but a comparable end point value (Fig. 11B). These data indicate that the inhibition of PPF is Col I-mediated and that CRP behaves like Col IV, although it resembles rather Col I.
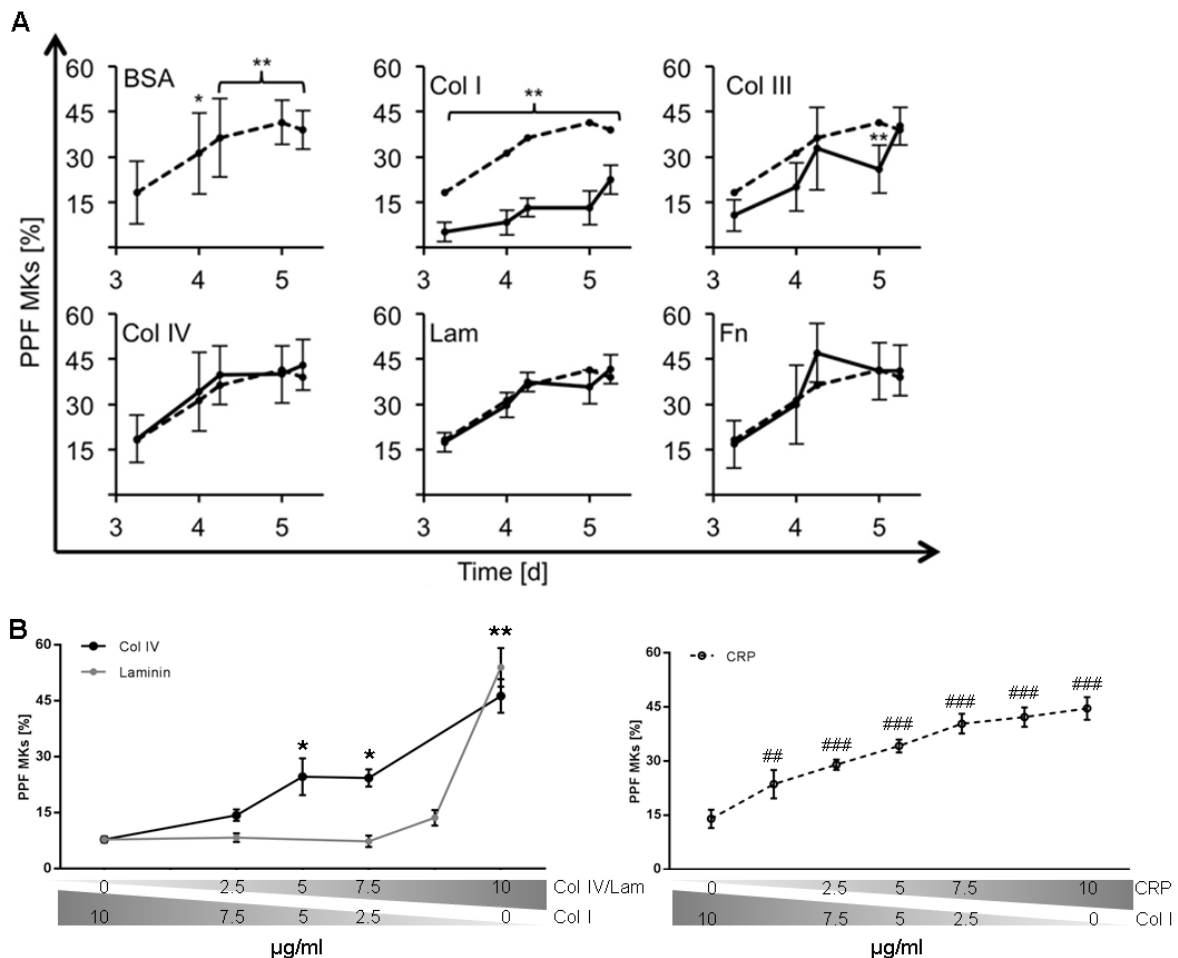
Fig. 11: Influence of ECM proteins on PPF. (A) MKs plated on Col I and III showed a reduced and attenuated PPF, compared to the BSA-control (dashed line). None of the other ECM proteins [Col IV, laminin (Lam) or fibronectin (Fn)] could support PPF to levels beyond that of BSA control. **(B)** When titrating Col IV, laminin or CRP against Col I, only CRP (dashed line) and Col IV (black line) were able to abrogate the inhibition of PPF by Col I in a dose-dependent manner. In the mixture of Col I with laminin, even 10% of Col I were sufficient to inhibit PPF. Asterisks indicate the difference of Col IV to pure Col I and hashes mark differences of CRP to pure Col I (* $P < 0.05$; **, ## $P < 0.01$, ### $P < 0.001$). **(A, B)** Error bars indicate standard deviation. All tests were performed according to Kolmogorov-Smirnow. Data of three independent experiments, each determined in triplicates, were averaged. Experiments for A and in parts also B were technically performed by Rebecca Kulawig.

3.1.6 Inhibition of PPF is GPVI-dependent

To elucidate the signaling events, which are responsible for the inhibition of PPF on Col I, we applied genetic as well as pharmacological approaches. We seeded FLC-MKs of WT mice either on BSA, as a control, or on Col I and determined PPF. On BSA, approximately 35% of MKs formed proplatelets, whereas PPF on Col I was diminished to roughly 8%. When using MKs lacking the collagen receptor GPVI or blocking this receptor with JAQ1 in WT MKs, the degree of PPF on Col I was comparable to the BSA control, thus fully reverting the inhibitory effect of Col I. In contrast, LEN/B-mediated blockage of α2β1 integrin in WT MKs or usage of α2-deficient MKs did not affect the reduced PPF on Col I. The simultaneous blockage of both receptors in WT MKs had no additional effect on PPF beyond the *Gp6*-null values (Fig. 12A).

In titration assays where we mixed two matrix proteins in a certain ratio, we investigated whether laminin, Col IV or CRP could compensate for the Col I-mediated inhibition of PPF (Fig. 12B, C, D). PPF was diminished in a dose-dependent manner when using Col IV or CRP, whereas inhibition of PPF remained unaltered upon laminin titration. The blockage of α2β1 integrin had no influence on PPF and was comparable to untreated MKs. However, blockage of GPVI alone or in combination with α2β1 integrin resulted in normalization of PPF. Similar results were obtained by using JAQ1 Fab-fragments (Fig. 12D). These findings indicate that GPVI is the receptor mediating the inhibition of PPF on Col I.

We therefore performed further assays to identify Col I-induced signaling events downstream of GPVI. Assuming that the GPVI signaling cascade is comparable to platelets, in which activation via GPVI occurs through phosphorylation of Src family kinases (SFKs), Syk and the linker of activated T-cells (LAT), we first conducted PPF analyses of mice lacking either LAT or Syk. PPF of MKs derived from either knockout mice was still profoundly inhibited on Col I (Fig. 12E, F). Because there were no mice

available lacking the SFKs Lyn and Fyn we further took advantage of the SFK blocker PP2, treated WT MKs with this reagent and determined the degree of PPF. Surprisingly, the treatment with 10 µM PP2 led to normalized PPF on Col I compared to control. DMSO, serving as a vehicle control, had no effect on the inhibition of PPF. Additional blockage of GPVI with JAQ1 restored PPF back to untreated control (Fig. 12G). Interestingly, we saw this abrogation of PPF inhibition also when we used CRP. These results suggest that the signaling downstream of GPVI in PPF is partially different from that in platelet activation. While SFKs are crucial for platelet activation and the inhibition of PPF, signaling via Syk and LAT seems to be dispensable for the latter, indicating a branching point downstream of SFKs.
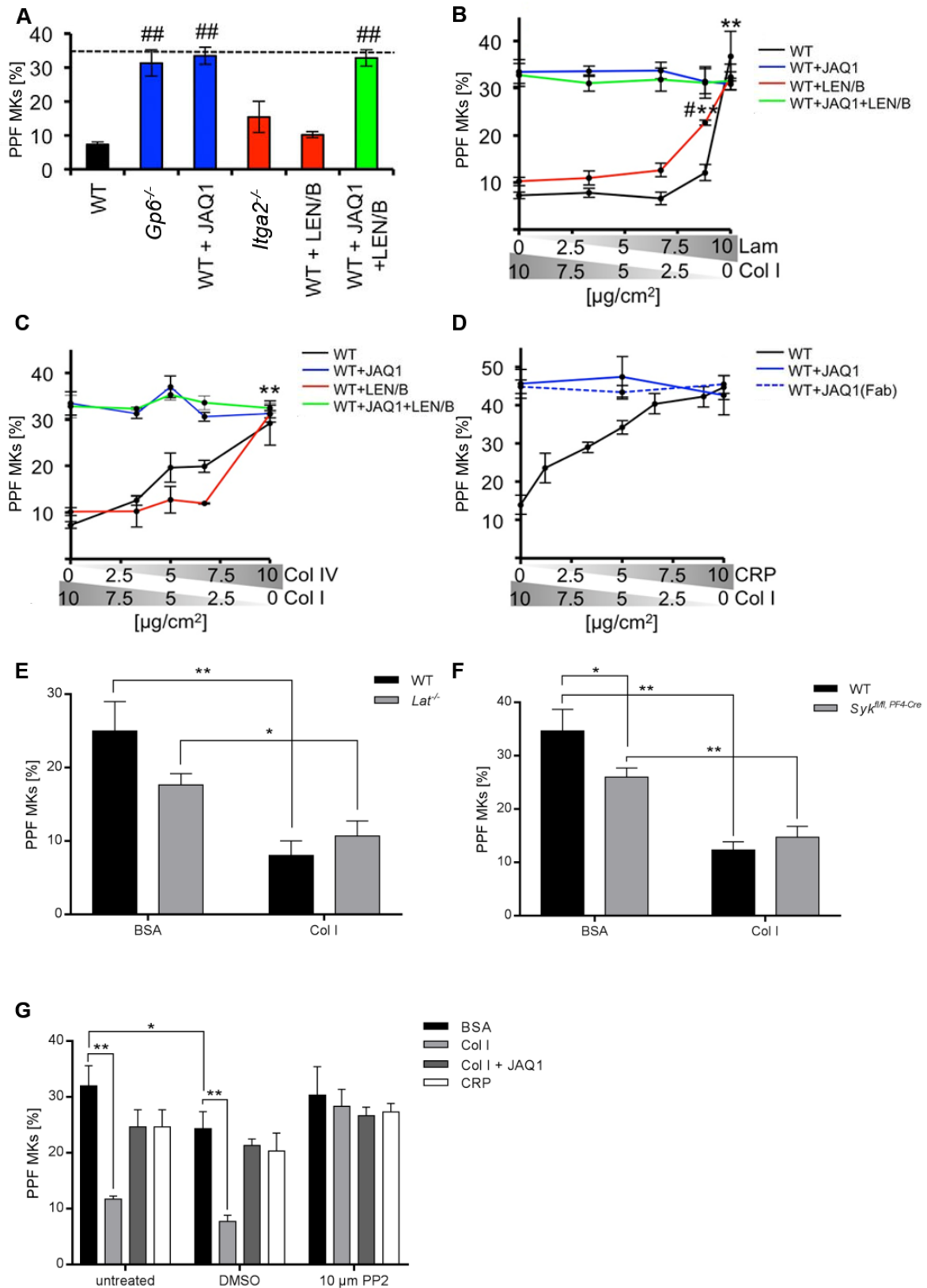
Fig. 12: Collagen-mediated signaling events during PPF. (A) PPF of WT MKs seeded on Col I was inhibited (black bar). When *Gp6-/-* MKs were used or GPVI was blocked with JAQ1 (blue bars), the inhibition of PPF on Col I was normalized to values of BSA-coated control (dashed line). In contrast, Col I still reduced PPF of *Itga2-/-* or LEN/B blocked WT MKs (red bars). By blocking both collagen receptors (green bars), no additinal effects beyond the JAQ1-blocked MKs were observed. **(B-D)** In titration assays using laminin **(B)**, Col IV **(C)** or CRP **(D)** against Col I, PPF was diminished in a dose dependent manner when using Col IV or CRP, whereas laminin titration did not influence the inhibition of PPF. Blockage of

α2β1 integrin had no influence on PPF and was comparable to untreated MKs. However, blockage of GPVI alone or in combination with α2β1 integrin resulted in abolished inhibition of PPF. This was also detected when using JAQ1 Fab-fragments. **(E-F)** PPF ability of **(E)** *Lat^-/-* or **(F)** *Syk^fl/fl, PF4-Cre* MKs revealed no differences to WT MKs seeded on Col I- or BSA-coated plates. **(G)** When WT MKs were plated on Col I and additionally treated with PP2 or DMSO as a control, the inhibition of PPF was abolished. Blocking the GPVI receptor with JAQ1 or plating MKs on CRP always restored PPF back to untreated control. Data of three independent experiments, each determined in triplicates, were averaged (E-G) (* $P < 0.05$; ** $P < 0.01$). Error bars indicate standard deviation. Asterisks in B,C,F,G mark statistically significant differences of the means compared to MKs plated on BSA (F,G) or pure Col I (B,C). Hash marks statistically significant differences of the mean compared to WT MKs (*, # $P < 0.05$; **, ## $P < 0.01$). All tests were performed according to Kolmogorov-Smirnow.

In immunoblot analyses we wanted to confirm the dispensability of Syk by investigating the phosphorylation of this protein. MKs and platelets were allowed to adhere on Col I– or CRP-coated plates and cells were lysed 15, 45 and 120 min afterwards. Untreated MKs and platelets were lysed immediately after seeding. As a positive control, platelets activated with 2.5 µg CRP under stirring conditions were used. Neither on Col I nor on CRP, MKs showed phosphorylation of Syk at tyrosine 525/26, whereas in platelets seeded on CRP a slight phosphorylation was detectable at all time points. In contrast, we could not verify phosphorylation upon spreading of platelets on Col I (Fig. 13A), which might be due to the lack of stirring conditions. These data indeed confirmed that Syk does not become phosphorylated in MKs upon Col I-mediated signaling.

In addition, we investigated phosphorylation of ERK, an ubiquitously expressed kinase involved in signal transduction, in MKs and platelets seeded on Col I or CRP. Use of culture medium led to phosphorylation of ERK in both MKs and platelets. In platelets, the signal was strongest after 5 min and decreased over time. In MKs a constant phosphorylation signal was detected, but was also present in untreated control samples (Fig. 13B).

It is known that ERK phosphorylation can also occur only by cultivation of cells with serum. In consideration of this fact we serum-starved MKs prior to the immunoblot analysis. MKs seeded in PBS on Col I showed no phosphorylation of ERK. However, phosphorylation of ERK was detectable in platelets seeded for 15 min in PBS on CRP, indicating a medium- and stimulus- dependent phosphorylation of ERK (Fig 13C).
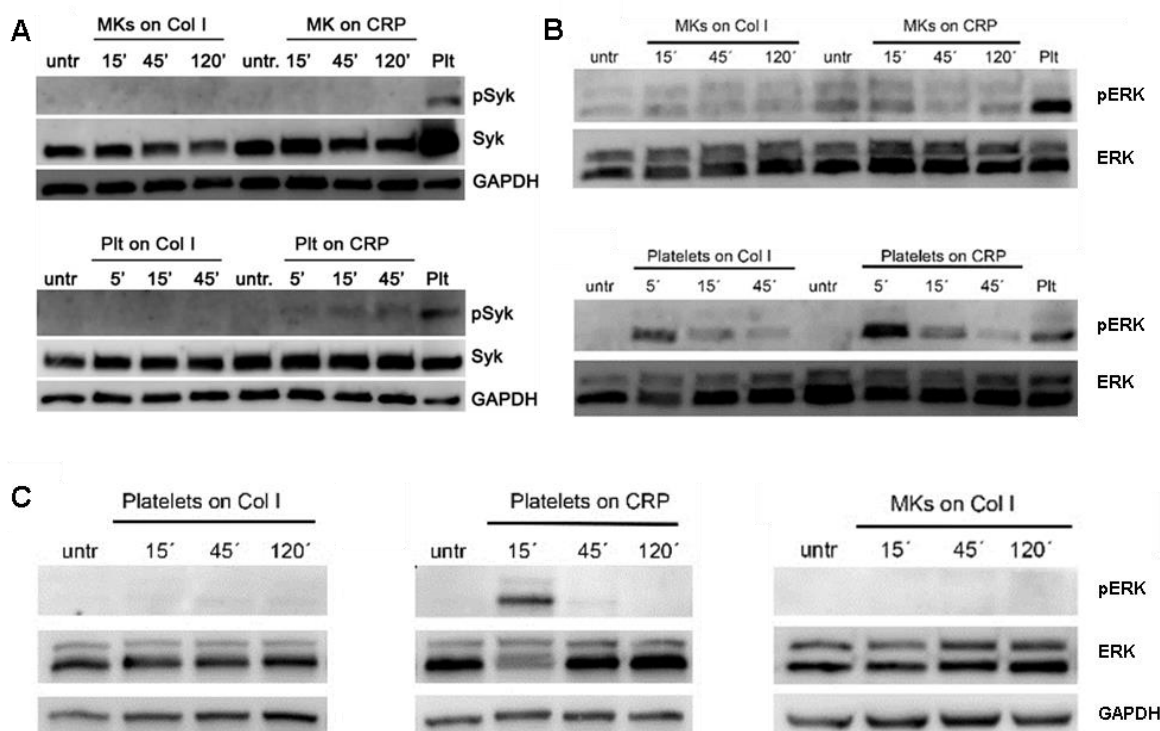
Fig. 13: Phosphorylation events in platelets and MKs. (A) When MKs or platelets were seeded in medium onto Col I, no phosphorylation of Syk525/26 could be observed at all time points. In platelets, but not MKs, phosphorylation occured upon stimulation with CRP. **(B)** Phosphorylation of ERK was detected in platelets on both Col I and CRP, with the strongest signal at 5 min. In contrast, MKs showed a weaker phosphorylation, which, however, was also present in untreated MKs. As a positive control, platelets stimulated with 2.5 µg CRP under stirring conditions, were used. **(C)** No phosphorylation of ERK was detectable when MKs and platelets were seeded in PBS onto Col I. Only on CRP a phosphorylation occurred in platelets after 15 min.

3.2 Characterization of platelet biogenesis in mice lacking GPVI and integrin α2β1

Because mice lacking either GPVI or α2β1 integrin showed no alterations in platelet counts and only displayed a mildly impaired hemostasis, the composition and functionality of the BM has not yet been investigated. In the previous chapter we could show in *in vitro* assays that especially Col I and Col IV are essential for a proper platelet biogenesis. We assumed that mice lacking one of the collagen receptor assure their normal platelet count by remodeling their BM environment regarding MK number, size or localization and tried to answer this question by analyses of the BM *in situ*.

Holtkötter and colleagues, who were the first in 2002 to describe mice lacking α2β1 integrin (Holtkötter *et al.,* 2002), showed a normal platelet count and tail bleeding times in these mice. The expression of other glyco-proteins was overall unaltered with the exception of the β1-integrin subunit, which was diminished to 70% of control levels. Concomitantly the α5- and α6- subunits, that also form heterodimers with the β1-integrin, were increased. The activation of platelets in different assays was unaffected

thus leading to a normal aggregation response on fibrillar collagen despite a slightly delayed onset in *Itga2*-null mice.

Out of the two existing *Gp6*$^{-/-}$ mouse strains, for our studies we used the strain described by Bender and colleagues in 2011 (Bender, Hagedorn and Nieswandt, 2011). Platelet counts in these mice were normal, but the *Gp6*-null platelets were not able to adhere on soluble or fibrillar collagen, thus subsequently showing an inability to form aggregates on collagen *in vitro*. In addition, these mice were unable to form an occlusive thrombus in all tested *in vivo* models, suggesting a general thrombotic defect in the absence of GPVI. Surprisingly, the tail bleeding time in *Gp6*-null mice was only slightly increased and granule secretion as well as integrin activation were impaired only upon GPVI-stimulation.

IF-stainings of WT MKs or MKs lacking either GPVI or α2β1 integrin with JAQ1 and LEN/B antibodies confirmed the absence of the surface receptors in the respective knockout, while the other glyco-protein was unaffected compared to WT (Fig. 14A). When measuring the absolute MK numbers per mm^2 (Fig. 14B) as well as the MK area (Fig. 14C) we found a similar density and size of BM MKs in *Gp6*$^{-/-}$ and WT mice, whereas the MK numbers in *Itga2*$^{-/-}$ mice were almost doubled compared to the WT control. In contrast, the area of α2β1-deficient MKs was slightly decreased.

In both knockout strains, approximately 45% of MKs showed an association with sinusoids (Fig. 14D). We could not detect significant differences between the genotypes for contact of MKs to Col I at the sinusoids and in the marrow cavity, whereas the contact to Col IV was increased at the vascular niche in both *Gp6*$^{-/-}$ and *Itga2*$^{-/-}$ mice. In the marrow cavity MKs lacking GPVI showed a higher degree of Col IV contact, while contact to Col IV was slightly reduced in *Itga2*-null MKs compared to WT (Fig. 14E). These results indicate that MK localization and thus platelet biogenesis is indeed affected in mice deficient for *Gp6* or *Itga2* and that their unaltered platelet counts may be a result of compensatory mechanisms within the BM.

In PPF assays, where either Col IV (Fig. 14F) or laminin (Fig. 14G) was titrated against Col I, the inhibition of PPF by Col I was abrogated in *Gp6*$^{-/-}$ MKs independent of the Col I concentration. In *Itga2*$^{-/-}$ MKs the PPF on laminin/Col I was inhibited and comparable to WT levels. In addition, when titrating Col IV against Col I, *Itga2*-null MKs behaved like WT MKs and showed a dose-dependent abrogation of PPF inhibition.

Taken together these results suggest that MKs deficient for *Gp6* or *Itga2* can compensate the lack of these receptors by an altered size (*Itga2$^{-/-}$*) and Col IV-association, which might lead to the normal platelet counts in the single knockouts. But it remains unclear whether the altered size of MKs in *Itga2$^{-/-}$* mice is a primary or secondary effect of the knockout. Furthermore, the degree of PPF in mice deficient for one respective collagen receptor was comparable to WT MKs where the same receptor was blocked with a specific antibody (Fig. 12B, C), indicating that the pharmacological approach can fully mimic the results of the genetic knockout mice *in vitro*.
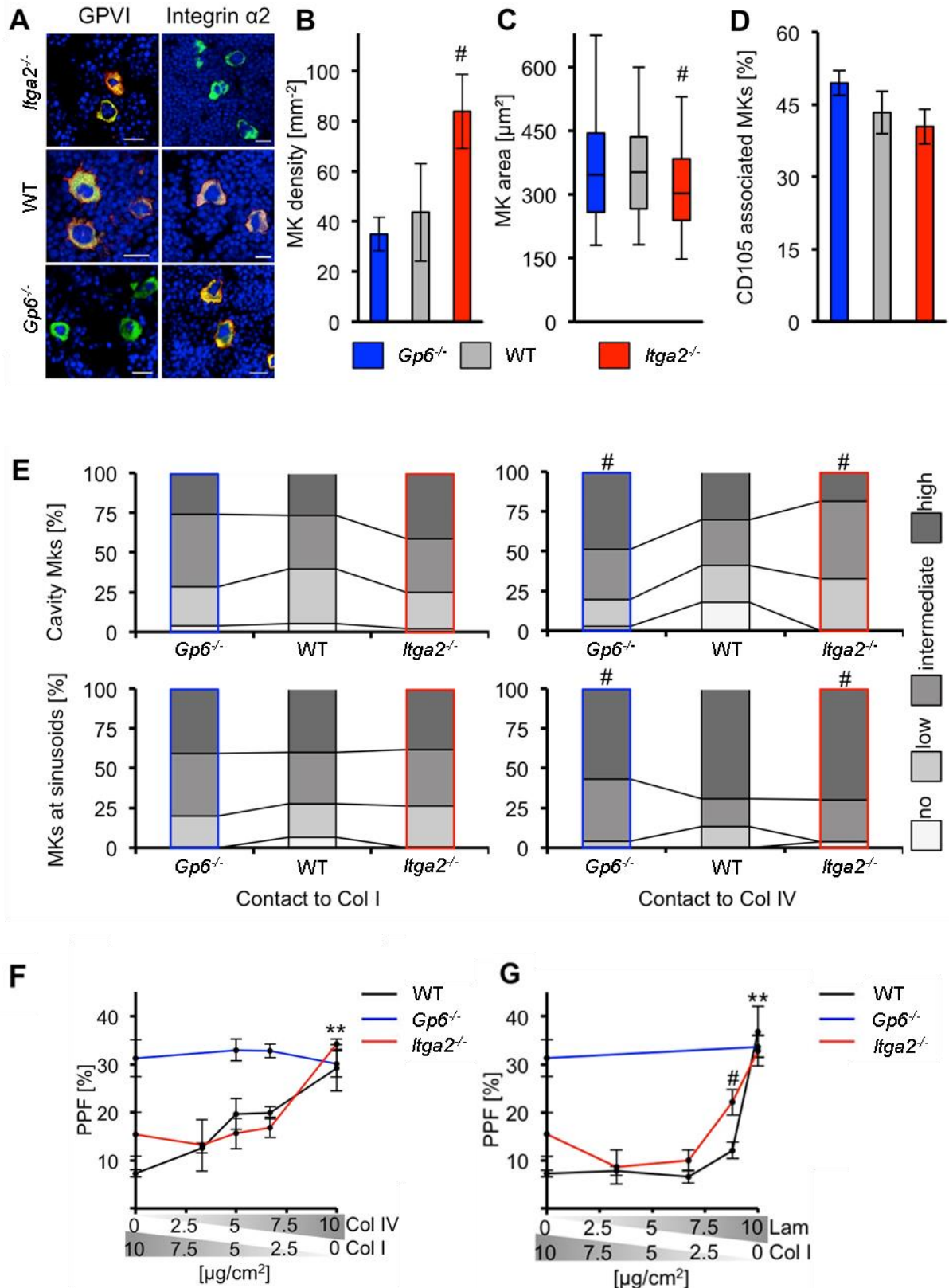
Fig. 14: MK and PPF analyses of mice lacking collagen receptors. (A) IF-stainings of *Gp6*^{-/-} and *Itga2*^{-/-} MKs (green) with JAQ1 and LEN/B (red) antibodies and *vice versa* confirmed the specific loss of the collagen receptors. Nuclei are depicted in blue. **(B)** Measurement of MK numbers revealed a density of approximately 41 MKs/mm^2 in WT mice. *Gp6*^{-/-} mice had comparable MK numbers, whereas *Itga2*^{-/-} mice showed a doubled MK density. **(C)** Mice lacking α2β1 integrin were smaller as WT and *Gp6*-knockout MKs. **(D)** The distance to sinusoids was comparable to WT in both knockout strains. **(E)** *In situ,* the contact of *Gp6*- (blue) and *Itga2*-null (red) MKs with Col I within BM cavity or vascular niche did not differ from WT MKs. However, contact to Col IV significantly changed when MKs lack one of the

collagen receptors. MK to collagen contact categories: no contact (0–5%), low contact (5–40%), intermediate contact (40–60%) and high contact (60–100%). **(F)** PPF in $Gp6^{-/-}$ MKs was unaffected, independent of the Col I and Col IV concentrations. MKs of $Itga2^{-/-}$ MKs showed comparable PPF and Col I-dependent inhibition could be reduced with increasing Col IV concentrations. **(G)** Inhibition of PPF was present in WT and $Itga2$-null MKs even with the lowest Col I concentration, when titrating it against laminin. In $Gp6$-null MKs, inhibition of PPF was normalized in all laminin-Col IV mixtures. Error bars indicate standard deviation. Asterisks mark statistically significant differences of the mean compared to pure Col I (** $P < 0.01$). Hashes mark statistically significant differences of the mean compared to WT (# $P < 0.05$). Data of three independent experiments, measured in triplicates, were averaged.

3.2.1 MKs in $Gp6^{-/-}$ and $Itga2^{-/-}$ mice are unaltered after platelet depletion

Next, we investigated the generation of new platelets in response to platelet depletion by use of an anti-GPIbβ antibody to address the question whether one of the collagen receptors influences platelet production after an induced demand. We analyzed the recovery of platelets and subsequently the MKs within BM in single deficient mice. Platelet counts dropped already one day after injection of 50 µg antibody, confirming the successful platelet depletion (Fig. 15A). The recovery of platelet counts started on day 3 with slightly more platelets in $Gp6^{-/-}$ mice. A significantly higher platelet count was present in $Gp6$-null mice 5 days after depletion compared to WT and $Itga2^{-/-}$ mice, suggesting a faster platelet recovery. Nonetheless, this effect could also be due to the already higher platelet count before depletion (Fig. 15A). These results suggest that none of the two collagen receptors influences platelet production after an acutely increased demand.

MK numbers in the different knockout mice were comparable to WT after platelet depletion with roughly 40-50 MKs per visual field (Fig. 15B). The discrepancy of MK numbers before (Fig. 14E) and after depletion in $Itga2^{-/-}$ mice might be due to different investigators (Rebecca Kulawig in Berlin and Daniela Semeniak in Würzburg). Furthermore, the MK area and size at the three distinct time points after platelet depletion was overall unaltered between the knockout and WT mice (Fig. 15C-E). The majority of MKs had an area between 300 and 400 µm^2, which could already be seen before depletion (Fig. 14C). The overall unaltered MK number and size after depletion indicates that the platelet recovery appears to be independent of the presence of either collagen receptor, but this does not exclude compensatory mechanisms for one another with respect to platelet production.
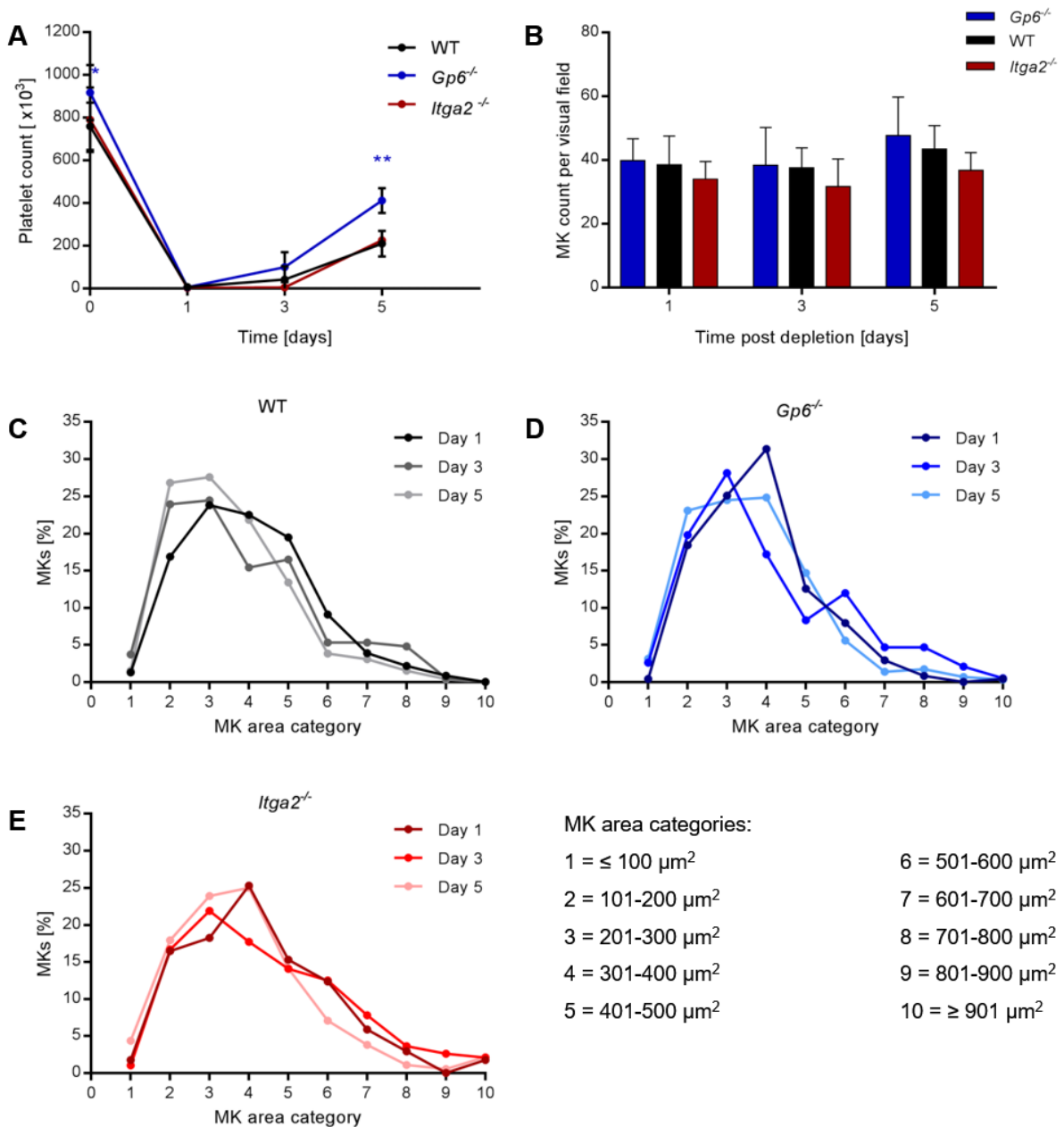
Fig. 15: Comparative analyses of MK area and number after platelet depletion in mice lacking collagen receptors GPVI or α2 integrin. (A) Successful depletion was confirmed by complete loss of platelets 24 h after injection of 50 µg antibody. Platelet recovery started on day 3 post depletion and further increased over time with slightly more platelets present in *Gp6*-/- mice on day 5 compared to WT controls. **(B)** MK numbers appeared unaltered after depletion for all genotypes. **(C-E)** The majority of MKs had an area between 200 and 400 µm^2 in WT, *Gp6*-null and *Itga2*-null mice and there was no shift towards smaller or bigger MKs observable at any time point after depletion. Error bars indicate standard deviation. Asterisks mark statistically significant differences of the mean compared to WT controls (* P < 0.05; ** P < 0.01). At least 5 sections and 5 visual fields per section of 3 different mice were analyzed for each time point and genotype.

3.2.2 The MK-vessel association is unaltered in *Gp6*-/- and *Itga2*-/- mice after platelet depletion

We were next interested whether MKs increased their association with vessels to achieve the comparable platelet recovery in mice lacking one of the collagen receptors.

We used femur sections of either genotype, stained for MKs and the vessel marker CD105 and measured the contact degree of MKs to vessels as well as the MK area with respect to the vessel distance. Vessel contact was overall unaffected after platelet depletion in all analyzed genotypes (Fig. 16A) and no obvious changes in MK- and vessel- structure were detectable (Fig. 16B). The BM sinusoids showed a staining pattern partially overlapping with Col I as well as with Col IV filaments and MKs were in contact with both collagen types. The MK area with respect to the sinusoid distance was unaltered, when comparing consecutive days after platelet depletion in the different genotypes (Fig. 16C). The same was true when we compared the genotypes at the different time points (Fig. 16D). These results suggest that loss of either collagen receptor does not affect the MK to vessel association within the BM upon platelet depletion.
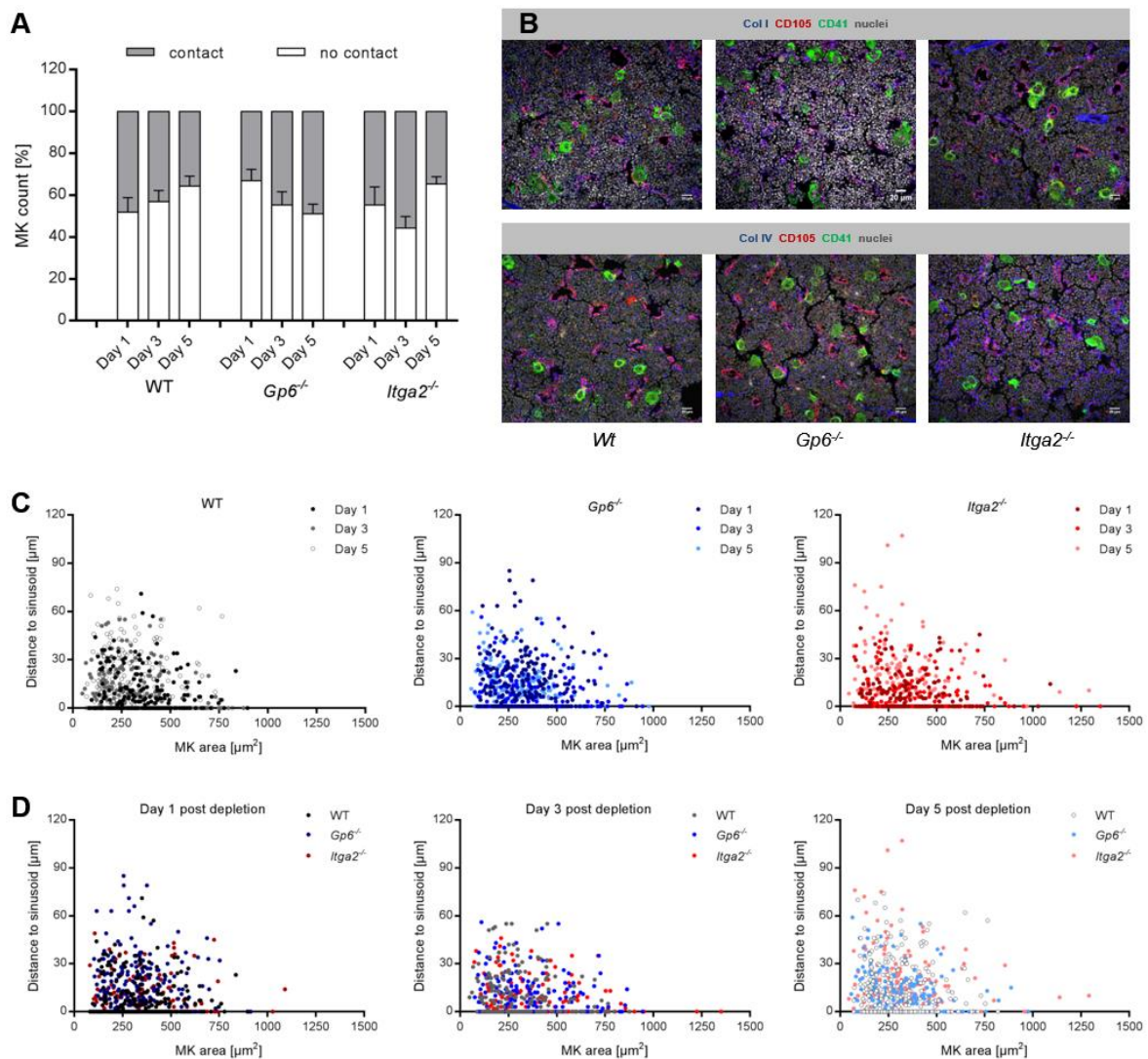
**Fig. 16: MK-vessel association in mice lacking collagen receptors GPVI or α2-integrin. (A)** No differences in MK contact to vessels were observed after platelet depletion in *Gp6*-null and *Itga2*-null mice compared to WT mice. **(B)** Representative IF-stainings of WT, *Gp6⁻/⁻* and *Itga2⁻/⁻* BM revealed no obvious differences in MK and vessel structure, as well as Col I and Col IV staining patterns. Scale bars

represent 20 μm. **(C-D)** MK area in respect to distance to sinusoids of WT and knockout MKs was unaltered when comparing time points after platelet depletion in the different genotypes **(C)**, or between genotypes at days 1, 3 and 5 after depletion **(D)**. Error bars indicate the standard deviation. At least 5 sections and 5 visual fields per section of 3 different mice were analyzed for each time point and genotype.

3.2.3 MK-Col I contact is diminished after platelet depletion

Platelets of mice, lacking either GPVI or the α2β1 integrin show a reduced response towards collagens. We suspected that also MKs in these animals might be influenced in their interaction with different collagen types. Such an impaired interaction might compensate for the deficiency of one collagen receptor, thus culminating in normalized platelet recovery after depletion. To investigate this hypothesis, we analyzed the contact of MKs with Col I and Col IV after platelet depletion. One day after platelet depletion, the interaction of collagen receptor–deficient MKs with Col I as well as Col IV was unaffected and comparable to WT MKs (Fig. 17A, B). In contrast, we found that MKs had generally less contact to Col I on day 3 compared to the first day (Fig. 17C). The Col IV-association was overall unchanged between genotypes and comparable to day 1 (Fig. 17D). However, on day 5 after depletion the Col I contact was normalized in all genotypes and comparable to day 1 (Fig. 17E), while MK-Col IV contact remained unaltered (Fig. 17F). The analyses indicate that platelet biogenesis after depletion might be stimulated via decreased interaction of MKs with Col I.
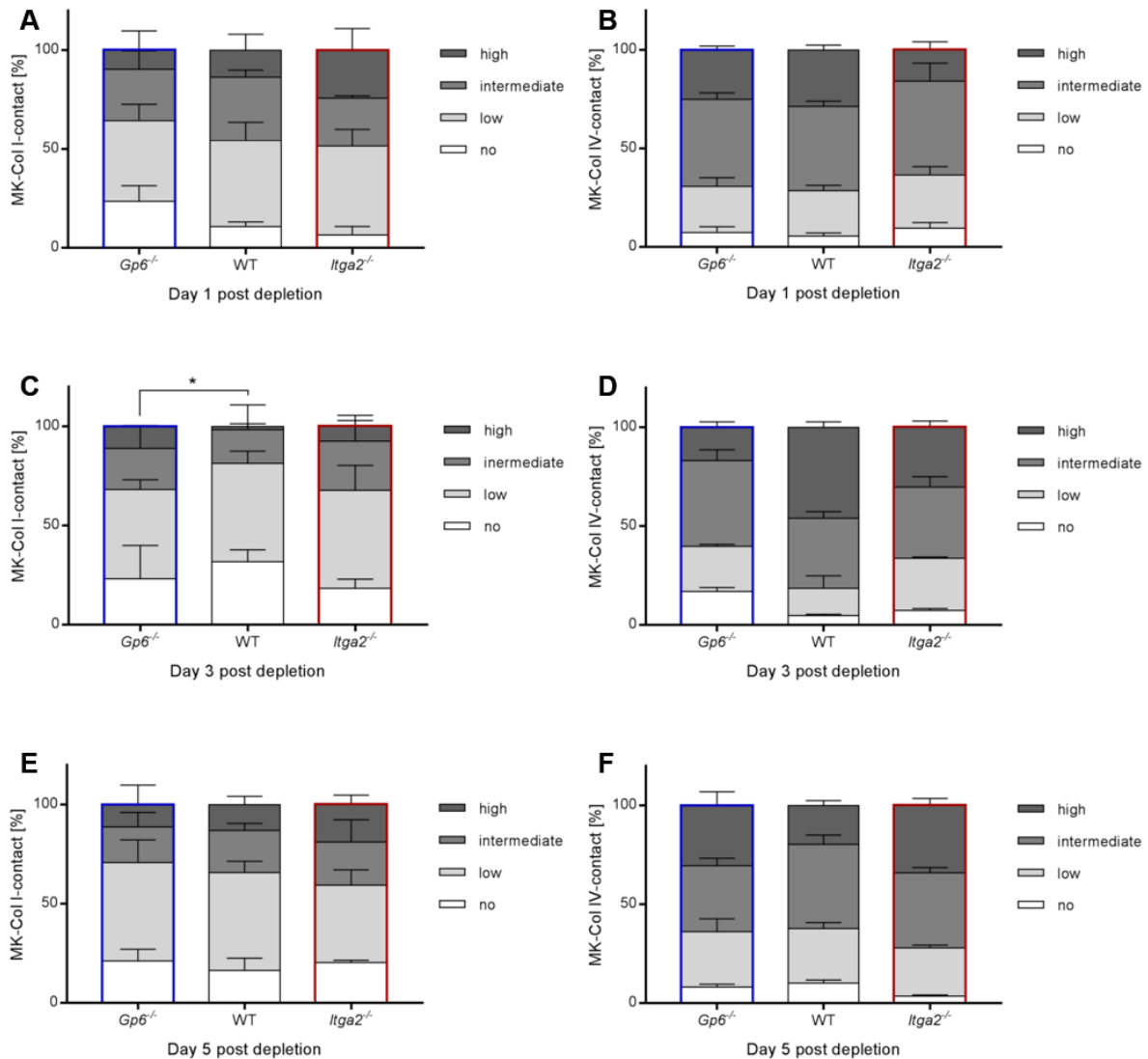
Fig. 17: Degree of contact of MKs to Col I and Col IV within BM after platelet depletion. (A, B) One day after platelet depletion no alterations in Col I and Col IV contact to MKs was detectable between *Gp6*-null and *Itga2*-null mice compared to WT. **(C, D)** While on day 3 the Col IV contact to MKs in all mice was unaltered compared to day 1, the contact to Col I decreased in all genotypes **(E, F)** Five days after platelet depletion the contact to collagen types was normalized and comparable to day 1. Error bars indicate standard deviation. At least 5 sections and 5 visual fields per section of 3 different mice were analyzed for each time point and genotype. Asterisks mark statistically significant differences of the mean compared to WT animals, analyzed with students t-test (* $P < 0.05$). MK to collagen contact categories: no (0–5%), low (5–40%), intermediate (40–60%) and high (60–100%).

3.2.4 Diminished MK-Col I contact appears at both BM niches after platelet depletion

In further analyses we wanted to investigate whether the Col I contact is impaired at the vessels or distant from sinusoids. Thus, we determined the MK to collagen contact in both "niches". At the vascular niche MKs of all genotypes showed a comparable association to Col I as well as to Col IV (Fig. 18A). The association of MKs to Col I and Col IV was also unaltered in the marrow cavity for any of the different genotypes (Fig. 18B).

On day 3 after platelet depletion, the MK contact to Col I in both niches decreased in all genotypes (Fig. 18C, D). However, the Col IV contact at the vascular niche overall increased and was more pronounced in WT mice. In the marrow cavity WT MKs showed an unaltered Col IV contact on day 3 compared to day 1, while Col IV interaction was decreased in the collagen receptor-deficient MKs at that time point (Fig. 18C, D).

Five days after depletion, the contact towards Col I and Col IV at both niches normalized between genotypes and associations were comparable to the first day after platelet depletion (Fig. 18E, F). Taken together, these data suggest that the decreased Col I contact at both niches might be important for the recovery of platelets and that MKs can directly influence platelet biogenesis by altering their contact to collagens within BM rather than changing MK numbers, MK size or the vessel contact.
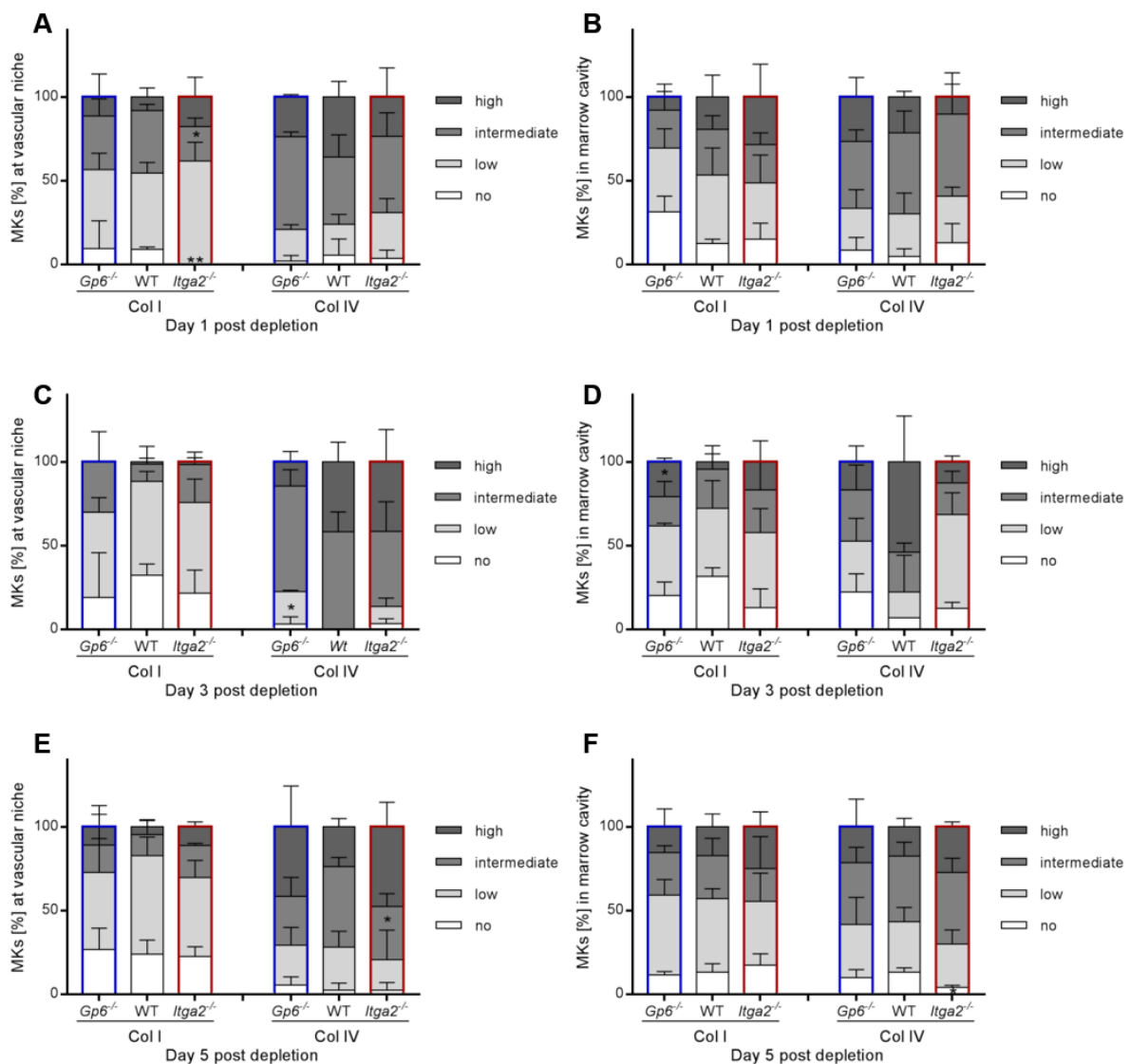
Fig. 18: Degree of MK contact to Col I and Col IV at the vascular niche and marrow cavity after platelet depletion. (A) On day 1 after platelet depletion the Col IV contact in mice lacking collagen receptors was comparable to WT at sinusoids. Col I contact was comparable between all genotypes, although *Itga2*-null mice showed significant differences in the distribution pattern. **(B)** Distant from sinusoids, the contact to Col I and Col IV was unaltered in knockout mice compared to WT. **(C)** Three days after platelet depletion the contact of MKs to Col I at the vascular niche decreased in all genotypes compared to day 1, whereas the Col IV contact was mildly increased in general, but to a lesser extent in *Gp6*$^{-/-}$ mice compared to WT. **(D)** MKs within the marrow cavity the had less contact to Col IV and this decreased interaction was even more pronounced in knockout mice compared to WT and to MKs of all genotypes at the vascular niche. Col I contact of WT mice in the marrow cavity was comparable to Col I contact at sinusoids. In contrast, *Gp6*-null mice and *Itga2*-null mice showed slightly more contact to Col I. **(E, F)** Five days after depletion Col I and Col IV contact at sinusoids and in the marrow cavity were comparable in all genotypes, except for a slightly reduced amount of *Itga2*-null MKs in the "low" category. Error bars indicate standard deviation. Asterisks mark statistically significant differences of the mean compared to WT (* $P < 0.05$; ** $P < 0.01$). At least 5 sections and 5 visual fields per section of 3 different mice were analyzed for each time point and genotype. MK to collagen contact categories: no contact (0–5%), low contact (5–40%), intermediate contact (40–60%) and high contact (60–100%).

### 3.2.5 DKO mice show abrogated platelet activation upon GPVI-stimulation

In a second approach we investigated the process of platelet biogenesis in mice deficient for both collagen receptors simultaneously. In the previous chapter we could show that mice lacking *Gp6* or *Itga2* might assure their normal platelet count by changing the degree of contact of collagens to MKs. Additionally, the question arose whether in single collagen receptor deficient mice the other collagen receptor can compensate for the absence of the other one and whether MKs, that are unable to respond to collagen (double-deficient for *Gp6* and *Itga2*), can thus still generate platelets. In several previous studies of platelet function, only specific antibodies were intravenously injected to transiently block or deplete both receptors on circulating platelets. However, this approach cannot be easily adopted to investigations regarding MKs for platelet biogenesis *in situ* or *in vivo*. We thus generated and characterized double-deficient mice (in the following designated as DKO).

Platelet counts and size, measured by flow cytometry, revealed no differences compared to WT platelets (Fig. 19A, B). Other blood parameters were also unaltered (Fig. 19C). The expression of glyco-proteins on the platelet surface showed reduced MFI values for GPVI and α2 integrin, thus confirming the absence of both collagen receptors in the DKO mice. In contrast, the MFI for the integrin α5-subunit was increased compared to WT-values, which had already been described for *Itga2*$^{-/-}$ mice. MFIs for all other glyco-proteins were comparable to WT values (Fig 19D).

Platelet degranulation, measured by the exposure of P-selectin was comparable upon stimulation of G-protein coupled receptors (GPCRS) with ADP, U46619 (U46), or

thrombin. As expected we found that stimulation of GPVI with CRP was fully abolished in DKO mice (Fig. 19E). Accordingly, activation of αIIbβ3 integrin, determined by the binding of the epitope-specific antibody JON/A was selectively defective in DKO platelets when they were stimulated with CRP (Fig. 19F). These results confirmed that the lack of both collagen receptors specifically affected platelet activation upon GPVI stimulation, whereas platelet activation by G-protein coupled receptors was unaffected.
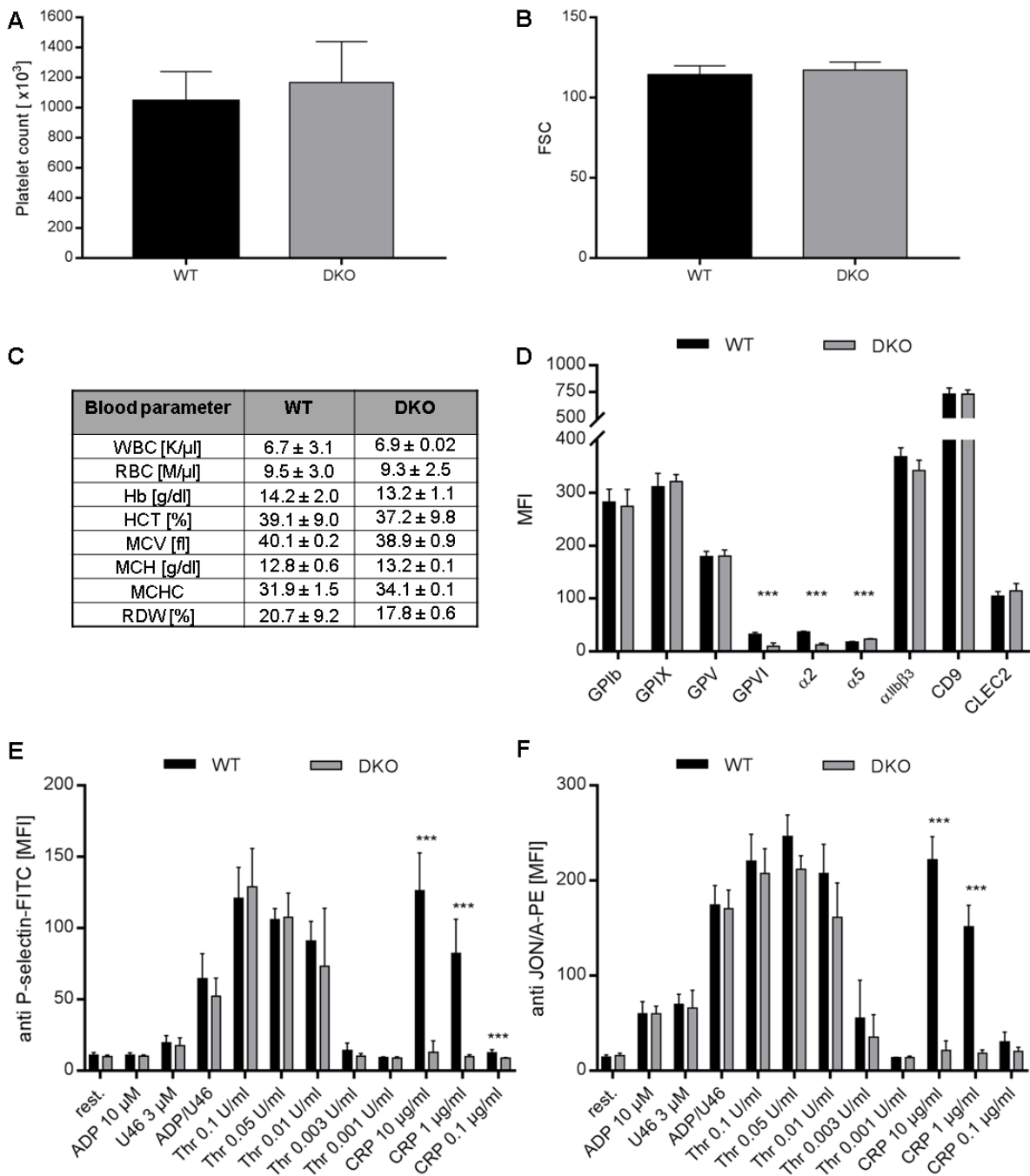
Fig. 19: Immunophenotyping of resting and activated platelets in DKO mice. DKO mice showed an unaltered platelet count **(A)** and size **(B)** compared to WT controls. **(C)** Other blood parameters were also not influenced. WBC = white blood cell count; RBC = red blood cell count; Hb = hemoglobin; HCT
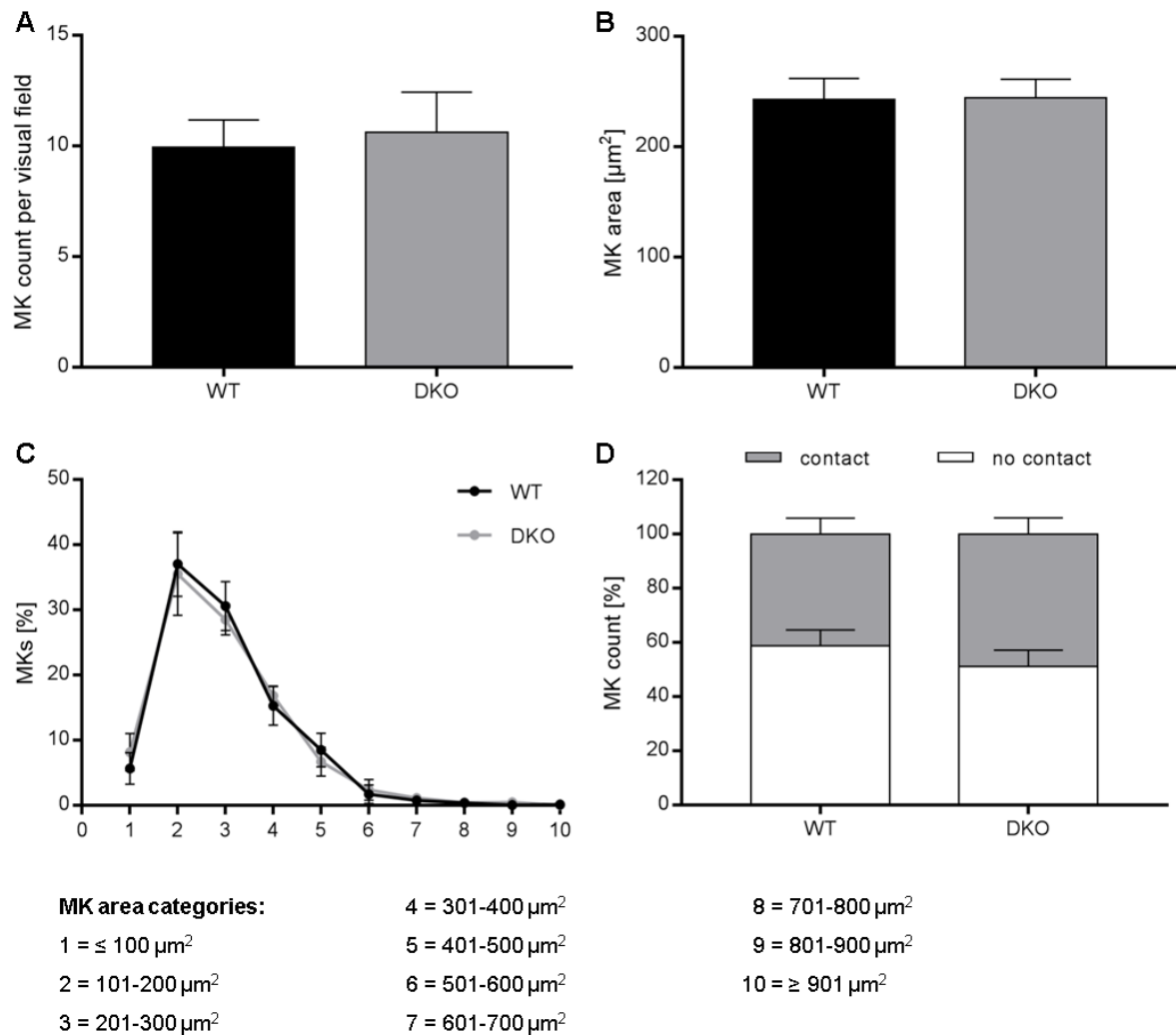
= hematocrit; MCV = mean corpuscular volume; MCH = mean corpuscular hemoglobin; MCHC = mean corpuscular hemoglobin concentration; RDW = red blood cell distribution width. **(D)** Flow cytometric measurements confirmed the absence of both collagen receptors on the platelet surface and no alterations were detectable in the MFI values of other glyco-proteins with the exception of the fibronectin receptor α5β1 integrin, which showed higher MFI values. **(E)** Platelet α-degranulation was measured by P-selectin exposure and revealed decreased MFI values in DKO upon GPVI stimulation compared to WT. **(F)** αIIbβ3 activation was analyzed by binding of the JON/A-PE antibody and showed a decreased MFI in DKO upon CRP stimulation. Error bars indicate standard deviation. Asterisks mark statistically significant differences of the mean compared to WT mice (*** $P < 0.001$). Data of two independent experiments, each determined with 5 vs. 5 mice, were averaged.

3.2.6 MK number and size as well as their contact to vessels are unaltered in DKO mice

In order to investigate whether the unaltered platelet counts were due to compensatory mechanisms in the process of platelet production, we determined MK numbers and size, as well as their contact to vessels within the BM. We observed no alterations in numbers and size of DKO MKs compared to WT (Fig. 20A, B). The majority of WT and DKO MKs had an area between 200 and 300 μm^2 (Fig. 20C) and approximately 60% of MKs were in contact with vessels in both WT and DKO mice (Fig. 20D). These data suggest that the lack of *GPVI* and *Itga2* does not affect MKs and their localization within BM at steady state.

MK area categories:

1 = ≤ 100 µm²	4 = 301-400 µm²	8 = 701-800 µm²
2 = 101-200 µm²	5 = 401-500 µm²	9 = 801-900 µm²
3 = 201-300 µm²	6 = 501-600 µm²	10 = ≥ 901 µm²
	7 = 601-700 µm²	

Fig. 20: MK analyses of DKO within BM. (A) MK numbers and **(B)** MK area of DKO were comparable to WT. **(C)** The majority of MKs had an area between 200 and 300 µm² and there was no shift towards smaller or bigger MKs in DKO mice. **(D)** Approximately 60% of MKs had no contact to vessels in WT and DKO, whereas 40% were associated with sinusoids. Error bars indicate standard deviation. At least 5 sections and 5 visual fields per section of 5 different mice were analyzed.

3.2.7 MK-Col I contact is reduced in DKO mice

In mice lacking either *Gp6* or *Itga2* the contact of MKs to Col I was transiently diminished, which might stimulate platelet generation. This alteration in collagen contact might also explain the normal platelet production in DKO mice. To address this hypothesis, we analyzed the association of MKs towards collagens. In general, the Col I contact was diminished in DKO, whereas the Col IV contact was increased (Fig 21A, B). The reduced Col I contact was found at the vascular niche as well as in the marrow cavity, but the decline was more profound at sinusoids. In contrast, the Col IV contact was only increased in the marrow cavity (Fig. 21C, D). These results imply that, similar to the single deficiency, also in DKO mice the diminished contact of MKs to Col I might stimulate platelet production.
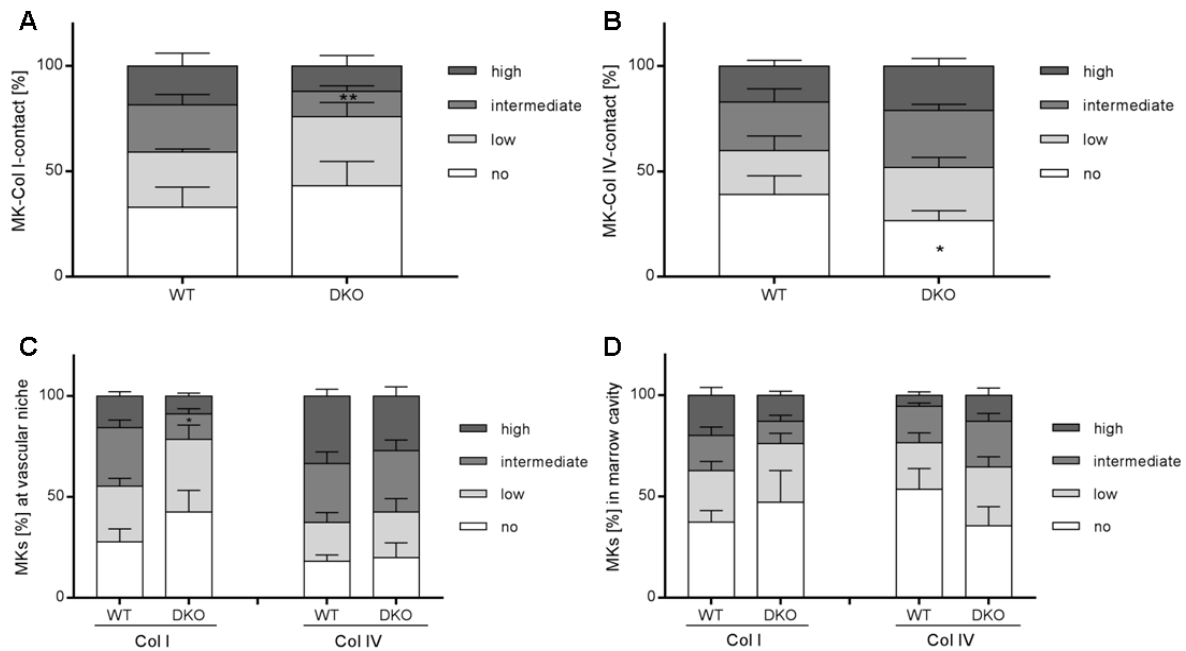
Fig. 21: Degree of MK contact to Col I and Col IV within BM of DKO mice. (A) Col I contact was overall reduced in DKO mice, whereas **(B)** Col IV contact was markedly increased compared to WT. **(C)** The decreased Col I contact was detectable at the vessels as well as **(D)** in the marrow cavity. In contrast, the Col IV contact at sinusoids was comparable between WT and DKO, but distant from vessels, DKO MKs showed an increased contact compared to WT. Scale bars represent 20 µm. Error bars indicate standard deviation. Asterisks mark statistically significant differences of the mean compared to WT controls (* $P < 0.05$; ** $P < 0.01$). At least 5 sections and 5 visual fields per section of 5 different mice were analyzed.

3.2.8   DKO mice show an increase of MK numbers in spleen

In contrast to humans, the spleen is a hematopoietic organ in mice. We investigated, whether - and if, to what degree - platelet biogenesis might also be present in the spleen of DKO animals compared to WT control animals, by determining MK numbers in spleen sections. IF-stainings of WT and DKO spleens revealed no differences in the spleen structure. White and red pulp were readily distinguishable by the absence or presence of αIIbβ3 integrin-positive stainings, respectively (Fig. 22A). In images recorded with higher magnification, MKs could clearly be identified by their size, their staining for αIIbβ3 integrin and their polyploid nucleus (Fig. 22B). Strikingly, MK counts in spleens of DKO mice were 3-fold higher than in WT controls (Fig. 22C), suggesting that the spleen of DKO mice might indeed contribute to platelet generation upon absence of both GPVI and integrin α2β1 by upregulating the MK count in the spleen.
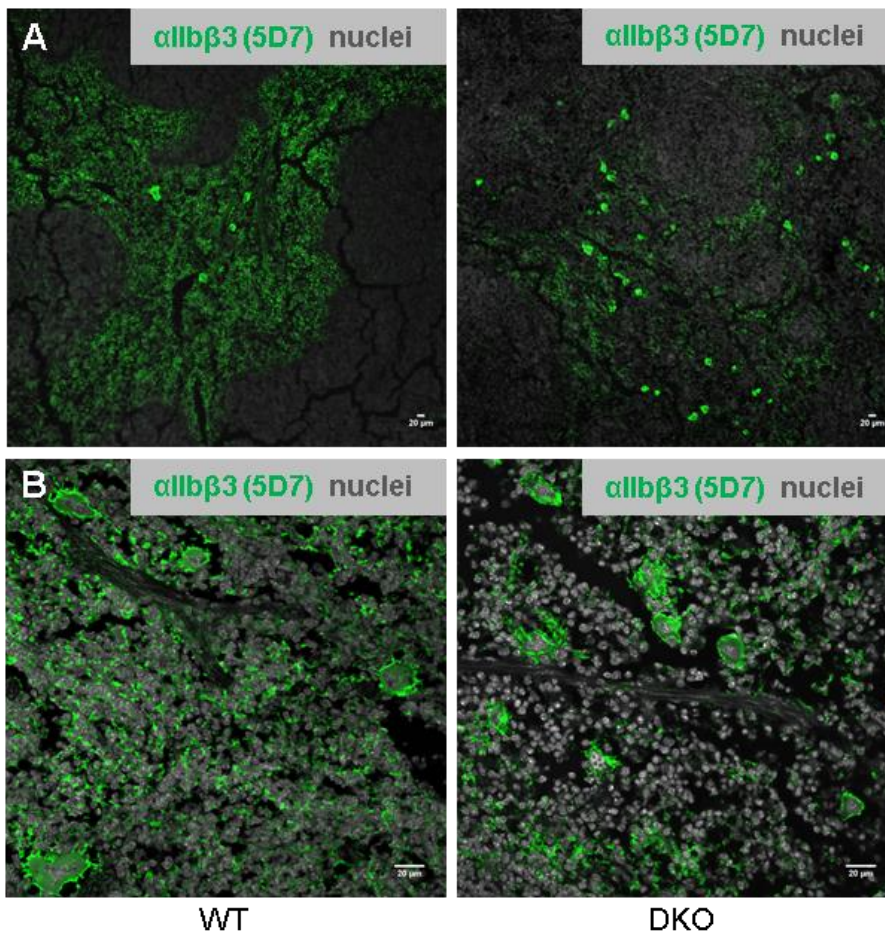
Fig. 22: MK analyses in spleens of DKO mice. (A) Representative IF-stainings of spleens revealed no structural differences between WT and DKO mice. Red and white pulp were clearly distinguishable (10x dry objective). **(B)** MK structure was unaltered between DKO and WT (40x oil objective). Scale bars represent 20 μm. **(C)** MK numbers were three-fold increased, compared to sections of WT animals. Error bars indicate standard deviation. Asterisks mark statistically significant differences of the mean compared to WT (*** $P < 0.001$). At least 5 sections and 5 visual fields per section of 5 different mice were analyzed.
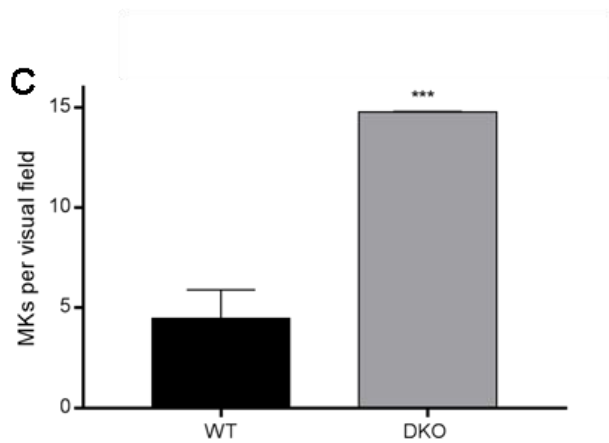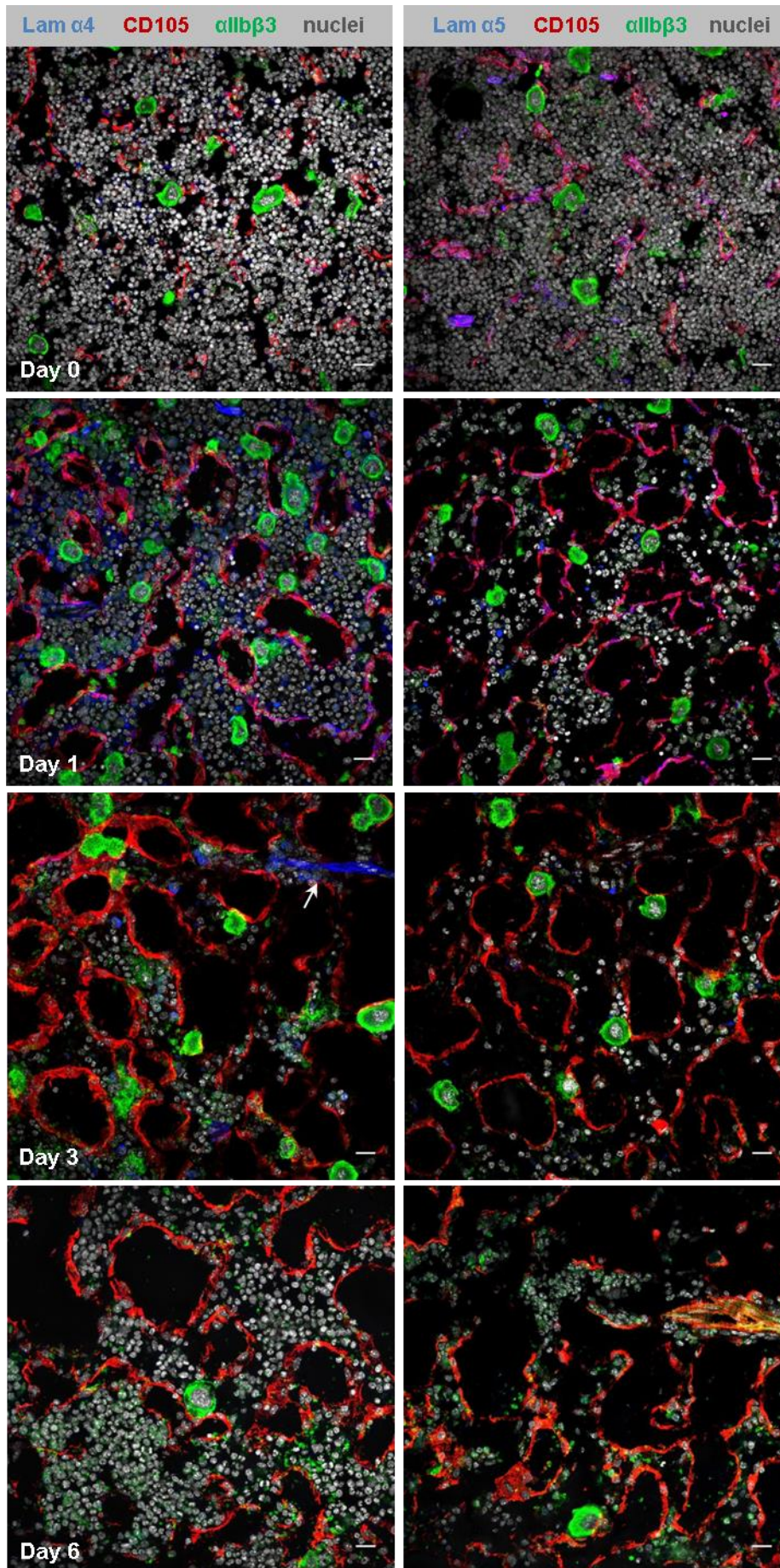
3.3 Influence of irradiation on BM

Platelets are among the last cells that recover after irradiation of the BM. The mechanisms for this are so far poorly understood. This chapter aims to address how irradiation affects the bone marrow matrix in respect to the MK biology as well as platelet production and function.

We performed a series of experiments where mice were irradiated to mimic the conditions for BM transplantation in order to study the influence of irradiation on the BM environment. We focused on cell and MK cellularity, the vessel structure (especially the microvasculature) and the expression and localization of the ECM protein families collagens and laminins. The results we gained are preliminary and thus can only be carefully interpreted.

3.3.1 Irradiation-induced loss of Col IV and laminin-α5 at sinusoids

In untreated femora, laminin-α5 (Lam α5) showed an overlapping staining pattern with sinusoids and arterioles, whereas laminin-α4 (Lam α4) expression was restricted to arterioles. In a first approach, we determined the localization of laminins within BM after sublethal irradiation with 5 Grey (Gy) by IF-stainings. Immediately after irradiation both isoforms were detectable. Surprisingly, only laminin-α4 co-localized with arterioles on day 3, while laminin-α5 was absent from sinusoids, suggesting a specific loss of laminin-α5 between day 1 and 3 (Fig. 23).

Fig. 23: Influence of sublethal irradiation on expression and localization of laminins α4 and α5. Laminins-α4 (Lam α4) and -α5 (Lam α5) were stained together with vessels, depicted in red, (CD105) and MKs in green (αIIbβ3) before irradiation and one, three and six days after sublethal irradiation (5 Gy). Nuclei were visualized with DAPI (grey). Laminins (blue) were both detectable before irradiation (day 0). While laminin-α4 was still present at arterioles on day 3 (arrow), laminin-α5 was not detectable anymore. Scale bars represent 20 μm. At least 5 sections and 5 visual fields per section of 5 different mice were analyzed.

In IF-stainings for Col I and Col IV before irradiation (day 0), both collagens showed an overlap with sinusoids and a filamentous pattern distant from vessels. One day after irradiation, a progressive vasodilatation could be observed, but Col I and Col IV were still expressed in a subendothelial pattern at the sinusoids. On day 3 after irradiation the staining for Col I and Col IV was much stronger and both collagens co-localized with sinusoids. However, while six days after irradiation Col I was still detectable, Col IV expression was restricted to arterioles and only present distant from sinusoids, indicating a specific loss of Col IV at sinusoids between day 3 and 6 after irradiation (Fig. 24).
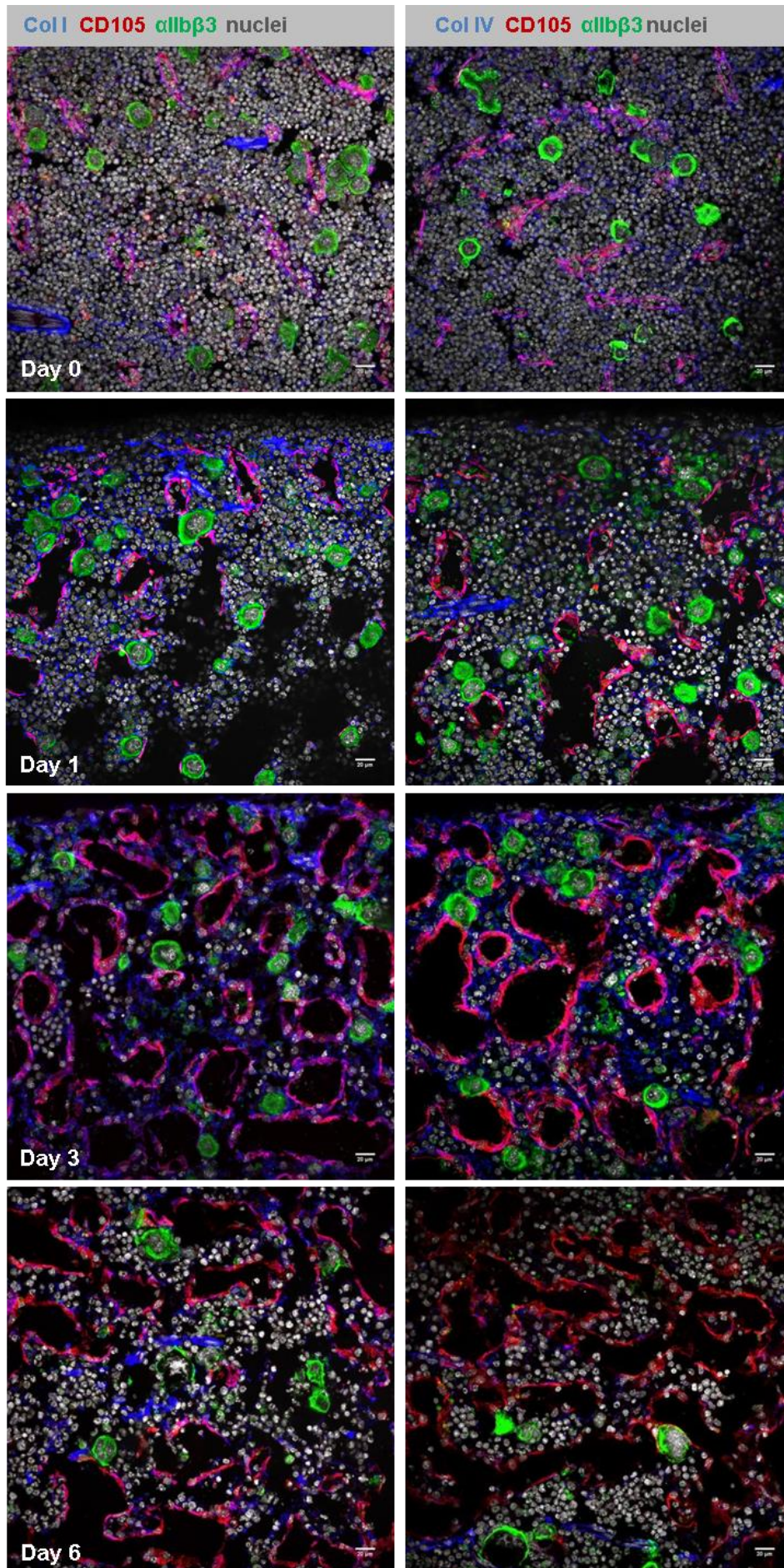
Fig. 24: Influence of sublethal irradiation on the expression and localization of Col I and Col IV. Col I and Col IV were stained together with vessels (CD105) and MKs, depicted in green, (αIIbβ3) before irradiation as well as one, three and six days after irradiation (5 Gy). Nuclei were visualized with DAPI (grey). Collagens (blue) were both detectable before irradiation (day 0) until three days after irradiation (day 3). While Col I was still present at sinusoids (red) and within BM on day 6, Col IV was not detectable at vessels anymore. Scale bars represent 20 µm. At least 5 sections and 5 visual fields per section of 5 different mice were analyzed.

3.3.2 MMP expression increases after irradiation

Since collagens as well as laminins can be degraded by matrix metalloproteinases (MMPs), we performed also IF-stainings for the two main collagen degrading MMPs, MMP-2 and MMP-9 before and after irradiation. Even before irradiation individual MMP-2- and MMP-9-positive cells were detectable, likely due to the steady remodeling of the BM environment. One day after irradiation the staining intensity for MMP-2 was markedly increased, whereas MMP-9 staining was comparable to day 0. However, on day 3 we found that MKs - among other cells - became strongly positive for MMP-9, while MMP-2 appeared rather intercellular (Fig. 25), indicating an increased turnover of laminin-α5 and Col IV and that MKs might participate on matrix remodeling, especially when MMP expression becomes upregulated after irradiation.
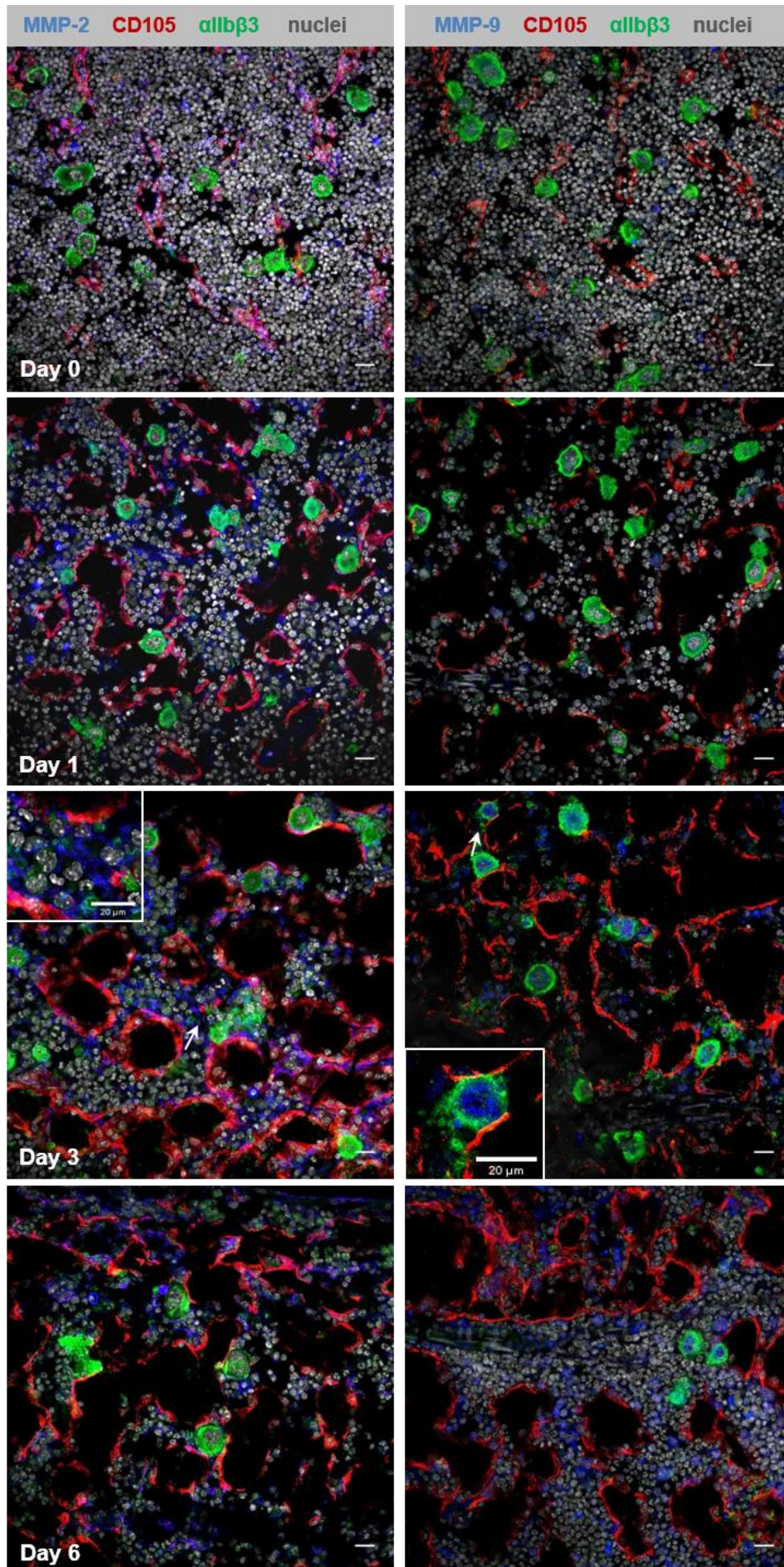
Fig. 25: Influence of sublethal irradiation on the expression of matrix metallo-proteinases (MMPs). MMP-2 and MMP-9 were stained together with vessels, depicted in red, (CD105) and MKs (αIIbβ3) before irradiation as well as one, three and six days after sublethal irradiation (5 Gy). Nuclei were visualized with DAPI (grey). Both MMPs (blue) were present before irradiation, but MMP-2 expression increased over time after irradiation within BM (inset). However, on day three after irradiation MKs (green) became positive for MMP-9 (inset) and a general increase in MMP-9-positive cells was detectable. Scale bars represent 20 μm. At least 5 sections and 5 visual fields per section of 5 different mice were analyzed.

3.3.3 Vasodilatation after irradiation is a BM-specific phenomenon

In addition to the observed alterations in ECM protein expression, a massive vasodilatation was detectable at all time points after irradiation (Fig. 23-25). We investigated, whether the observed vasodilatation within BM also occurred in other organs by a 3D image reconstruction of sinusoids in sternae and spleen. Sinusoids (red) in sternae also exhibit a massive vasodilatation compared to untreated WT control, whereas the vessel structure in spleen was overall indistinguishable between irradiated and non-irradiated samples. A GPIX-counterstain (green) labeled MKs and platelets in the BM, but also revealed the presence of smaller platelet-like particles, that appeared to be more disrupted after irradiation. Surprisingly, the abundance of these particles was found to be markedly increased in spleens of irradiated mice compared to non-irradiated controls, suggesting an accumulation of platelet- or MK fragments in the spleen. Taken together these data imply that the vasodilatation appears to be a BM-specific phenomenon that is not induced in spleen (Fig. 26). Furthermore, the accumulation of GPIX-positive particles in the spleen suggests a degradation of MKs and platelets.
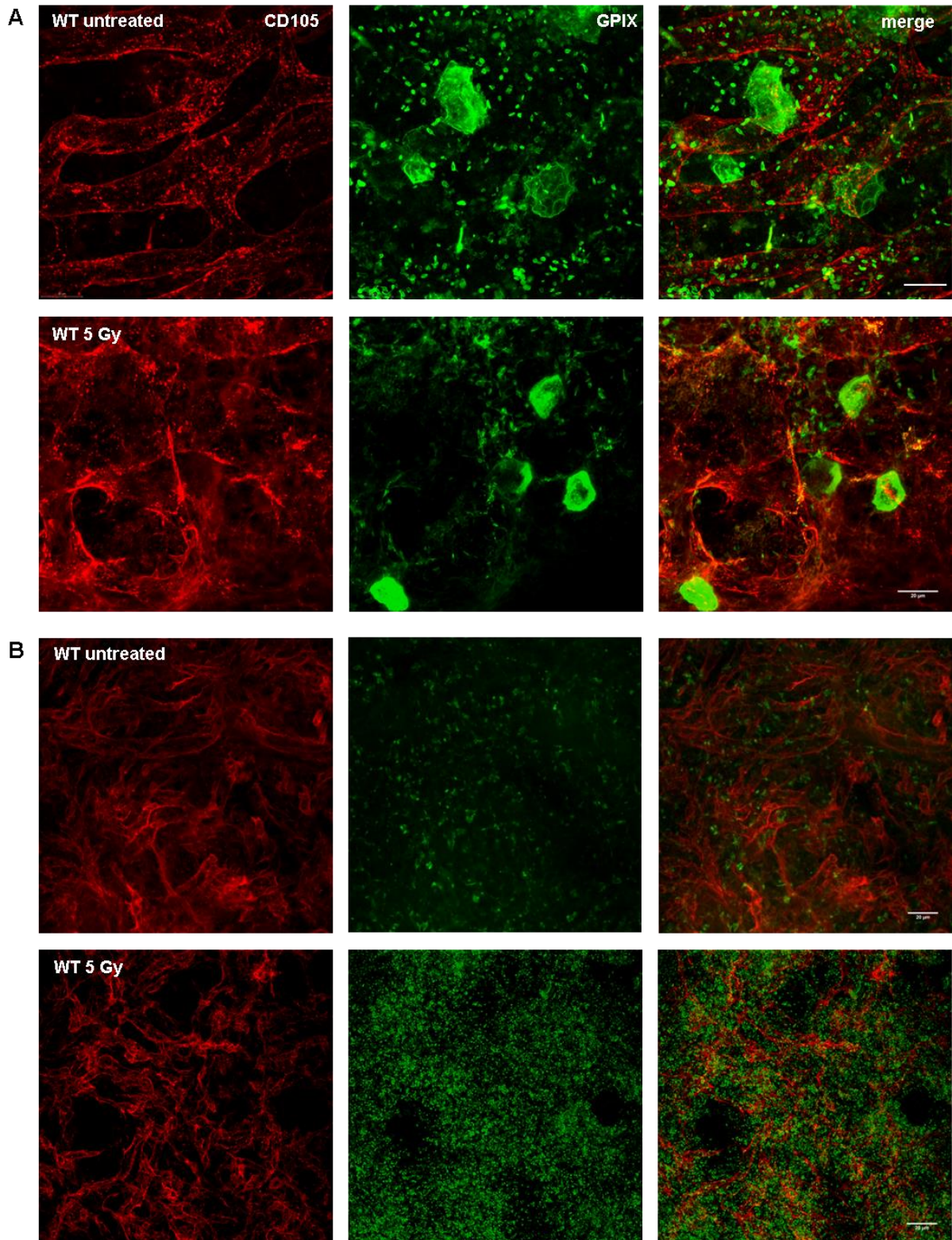
Fig. 26: Influence of sublethal irradiation on sinusoids of murine bones and spleen. Either **(A)** sternae or **(B)** spleens of untreated and sublethally irradiated WT mice were isolated, fixed and cleared with BABB. A 50 µm stack of a visual field was recorded according to Nyquist criteria and a maximal intensity-projection was reconstructed. CD105-positive sinusoids, depicted in red, show a massive dilatation in sternae after sublethal irradiation compared to non-irradiated WT control. In contrast, the morphology of sinusoids in spleens was comparable to the untreated WT animals. MKs and platelets, depicted in green, were stained with an anti-GPIX antibody and revealed a massive increase of GPIX-

positive fragments in spleen, whereas the staining pattern was comparable in sternae of untreated and irradiated mice. Scale bars represent 20 µm.

3.3.4 Irradiation-induced MK reduction results in macrothrombocytopenia

The application of irradiation to the BM is aimed to deplete all existing hematopoietic cell types prior to HSC transplantation. As platelets have a rather short life span of 6-10 days, we were interested how irradiation affects MKs and subsequently platelet counts and their function in response to sublethal irradiation. Before irradiation, we identified 12 MKs per visual field with a mean size of 386 µm^2. One day after irradiation slightly more MKs (15) were present per visual field. Afterwards, the MK number per visual field dropped to 11 MKs on day 3 and three MKs on day 6 after irradiation. In contrast, the average area of the remaining MKs increased significantly on day 3 and was even higher on day 6, indicating an influence of irradiation on MKs (Fig. 27A). It is also possible that the younger, still proliferating MKs are more prone to irradiation, whereas mature, highly polyploid MKs, which are not in the cell cycle anymore are more resistant and thus still detectable on day 6 after irradiation.

Furthermore, we wanted to assess the impact of the reduced MK numbers on platelet turnover and function and whether the absence of MMP-9 might affect the outcome. We observed by flow cytometric analyses of platelets in *Mmp9*$^{+/+}$ and *Mmp9*$^{-/-}$ mice that these mice developed a macrothrombocytopenia over the time period (Fig. 27B). Interestingly, the remaining MKs within BM were still able to generate new platelets. Both genotypes showed an increase in TO-positive cells over time, with a significantly profound increase of reticulated platelets in *Mmp9*$^{-/-}$ mice 12 days after irradiation (Fig. 27C). Taken together these data imply that irradiation induces a macrothrombocytopenia starting on day 6 due to the reduced MKs in BM, while platelet biogenesis from the remaining MKs in the BM is still possible.
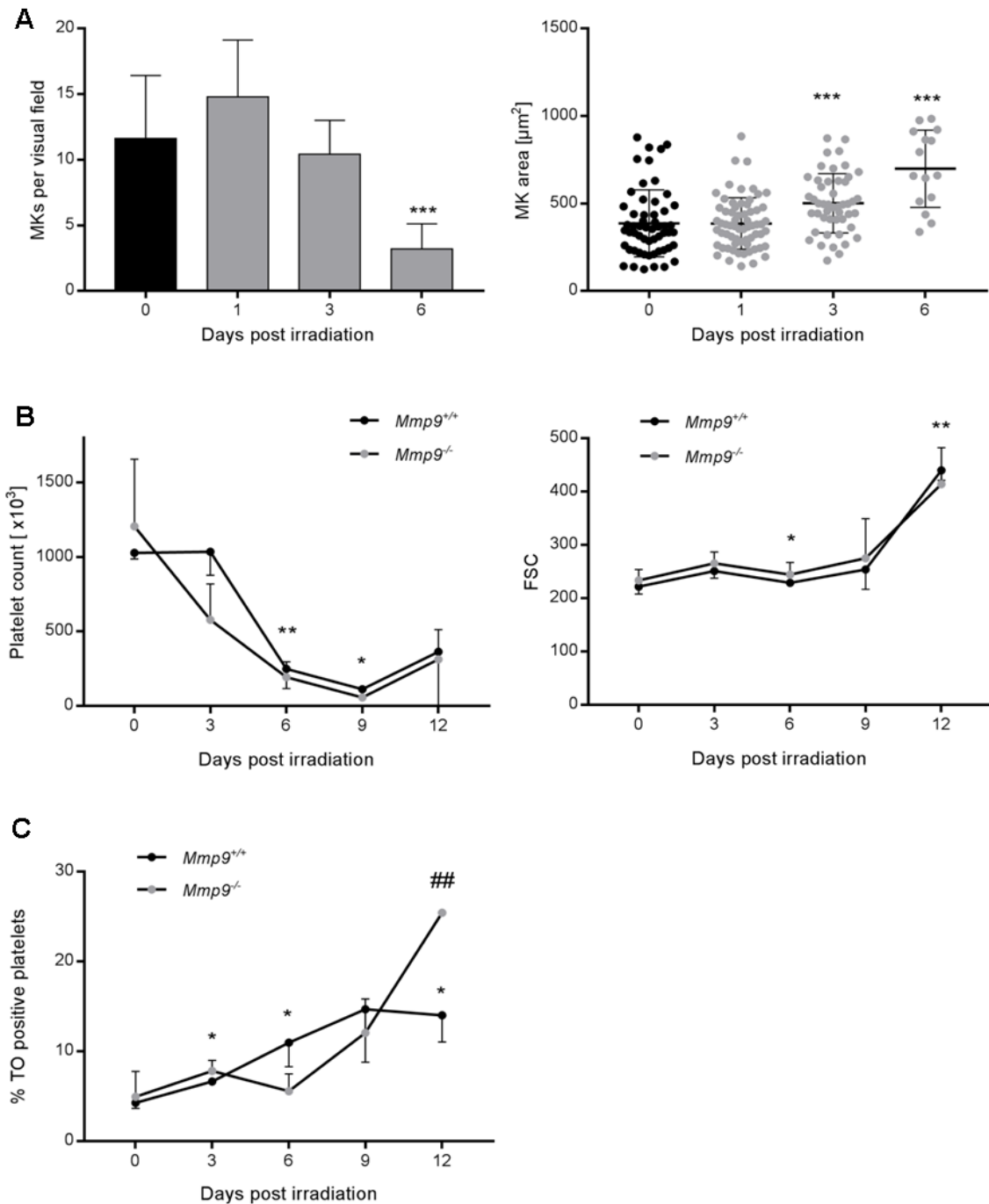
Fig. 27: Influence of irradiation on MKs and platelets. (A) While the MK number increased on the first day after irradiation and then decreased until day 6, the area of remaining MKs increased over time. **(B)** In concordance with the fewer but bigger MKs, mice developed a macrothrombocytopenia. **(C)** The remaining MKs within BM were still able to generate new platelets. We observed an increase of reticulated platelets over time. Error bars indicate standard deviation. Asterisks mark statistically significant differences of the mean compared to untreated control (black bar and dots) (*** $P < 0.001$). At least 5 sections and 5 visual fields per section of 5 different mice were analyzed. For B and C 3 vs. 3 mice were analyzed in one experiment.

3.3.5 Expression patterns of platelet surface receptors are heterogenous after irradiation

Alterations in the expression of glyco-proteins (GP) on the platelet surface might influence the platelet function. Thus, we determined the expression levels of several surface receptors after irradiation by flow cytometry analyses on the remaining as well as at the newly generated platelets. In order to investigate whether MMP-9 might affect the outcome, comparative analyses were performed in $Mmp9^{+/+}$ and $Mmp9^{-/-}$ mice. Expression levels of GPIb, GPV and GPIX, which form the vWF-receptor complex, were overall normal on the platelet surface in both, in $Mmp9^{+/+}$ and $Mmp9^{-/-}$ mice. The MFI-values slightly decreased until day 9 and normalized again on day 12. While the expression levels of α2β1, α5β1 and αIIbβ3 were overall unaltered after irradiation, the (hem)ITAM-based receptors GPVI and CLEC-2 showed a slight decrease in expression over the observed time period. Surprisingly, expression of the highly abundant tetraspanin CD9 was markedly reduced until day 12. Expression levels of all glyco-proteins were overall comparable between $Mmp9^{+/+}$ and $Mmp9^{-/-}$ mice, suggesting that MMP-9 is dispensable for the observed alterations in platelet surface receptor expression in response to irradiation (Fig. 28).
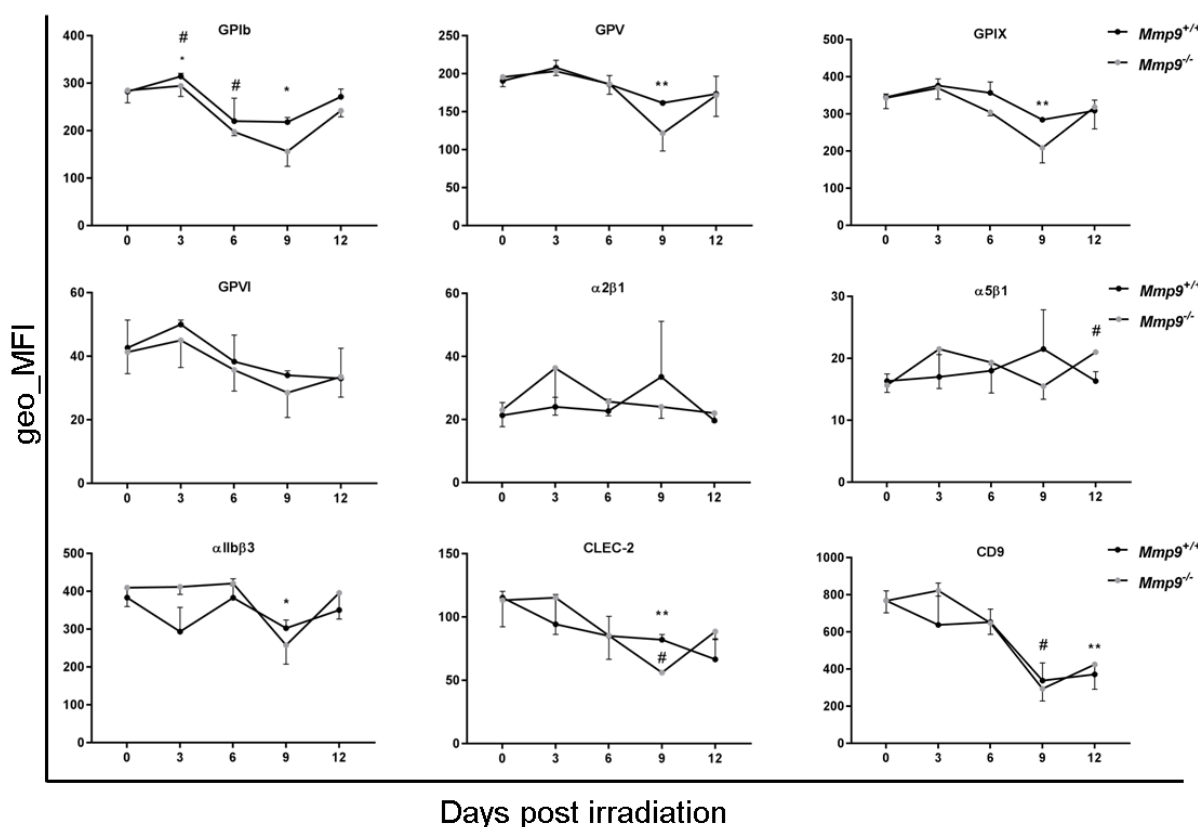
Fig. 28: Surface receptor expression on platelets after sublethal irradiation. A decrease in GPIb, GPV and GPIX expression was found until day 9 after irradiation, which normalized on day 12. For GPVI and CLEC-2 a slight decrease in expression was still present on day 12. In contrast α2β1, α5β1 and

αIIbβ3 expression was unaltered over time. CD9 showed a constant reduction in expression over time. Error bars indicate standard deviation. Asterisks mark statistically significant differences of the mean in *Mmp9+/+* mice compared to untreated (day 0) mice (* $P < 0.05$; ** $P < 0.01$). Hashes mark statistically significant differences of the mean in *Mmp9-/-* compared to untreated (day 0) mice (# $P < 0.05$). Data of one experiment, determined in triplicates is shown.

3.3.6 Platelets develop a hyporesponsiveness upon activation

Our findings imply that irradiation affects the expression levels of glyco-proteins on the platelet surface. As this alterations might affect the reactivity of platelets toward certain agonists, we next aimed to investigate whether platelet function changes in response to irradiation.

Since we observed diverse expression patterns of the tested glyco-proteins after irradiation, we analyzed the α-degranulation and αIIbβ3 integrin activation of platelets with different agonists in *Mmp9+/+* and *Mmp9-/-* mice. Upon stimulation of GPCR-coupled receptors with ADP or the prostaglandin H2 mimetic U46619 (U46), we could hardly detect any degranulation at any of the indicated time points (Fig. 29A, B). Only when both agonists were used in combination, we found a significant degranulation until day 3 after irradiation. Afterwards platelet reactivity declined further and was finally indistinguishable from unstimulated samples on day 9 and 12 after irradiation, as depicted by the red dashed line (Fig. 29C). In contrast, αIIbβ3 integrin activation could be achieved with either agonist (Fig. 29A, B) or in combination (Fig. 29C). In accordance with the degranulation defect, integrin activation also decreased over time. The hyporesponsiveness of platelets that starts to develop on day 6 after irradiation indicates that only the newly generated platelets have a defective function upon ADP or U46 stimulation, but MMP-9 seem to be dispensable for the maintenance of platelet function.
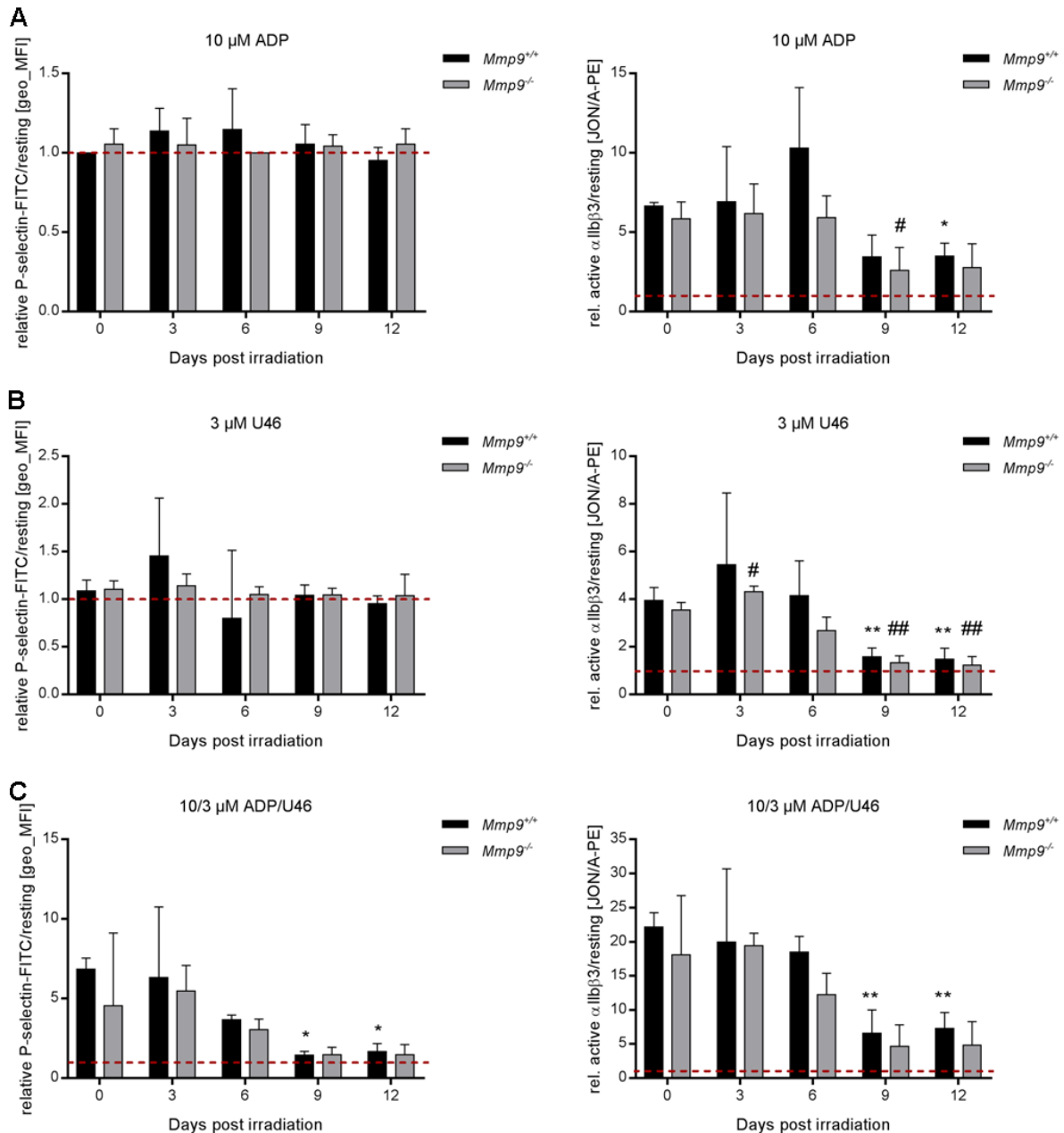
Fig. 29: Platelet activation upon GPCR stimulation. Platelets of *Mmp9+/+* or *Mmp9-/-* mice did not show any degranulation (CD62P expression) upon ADP **(A)** or U46 **(B)** stimulation after irradiation compared to resting values (red dashed line). **(C)** Platelet activation was only detected when ADP and U46 were used in combination until day 3 after irradiation. Afterwards, platelet activation decreased until day 9 and subsequently no degranulation was present anymore. Activation of integrin αIIbβ3 was unaltered upon stimulation with ADP and/or U46 until day 6 after irradiation. Nine days after irradiation, activation decreased upon stimulation with all agonists. Error bars indicate standard deviation. Asterisks mark statistically significant differences of the mean in *Mmp9+/+* mice compared to untreated (day 0) mice (* $P < 0.05$; ** $P < 0.01$). Hashes mark statistically significant differences of the mean in *Mmp9-/-* mice compared to untreated (day 0) mice (# $P < 0.05$; ## $P < 0.01$). Data of one experiment, determined in triplicates, is shown.

However, when stimulating platelets with a high dose of thrombin (0.1 U/ml), P-selectin exposure as well as αIIbβ3 integrin activation on day 3 was comparable to values before irradiation. While degranulation decreased until day 9 and then normalized,

integrin activation was markedly reduced until day 12 (Fig. 30A). With a low dose of thrombin (0.003 U/ml) hardly any degranulation or αIIbβ3 integrin activation was detectable (Fig. 30B).
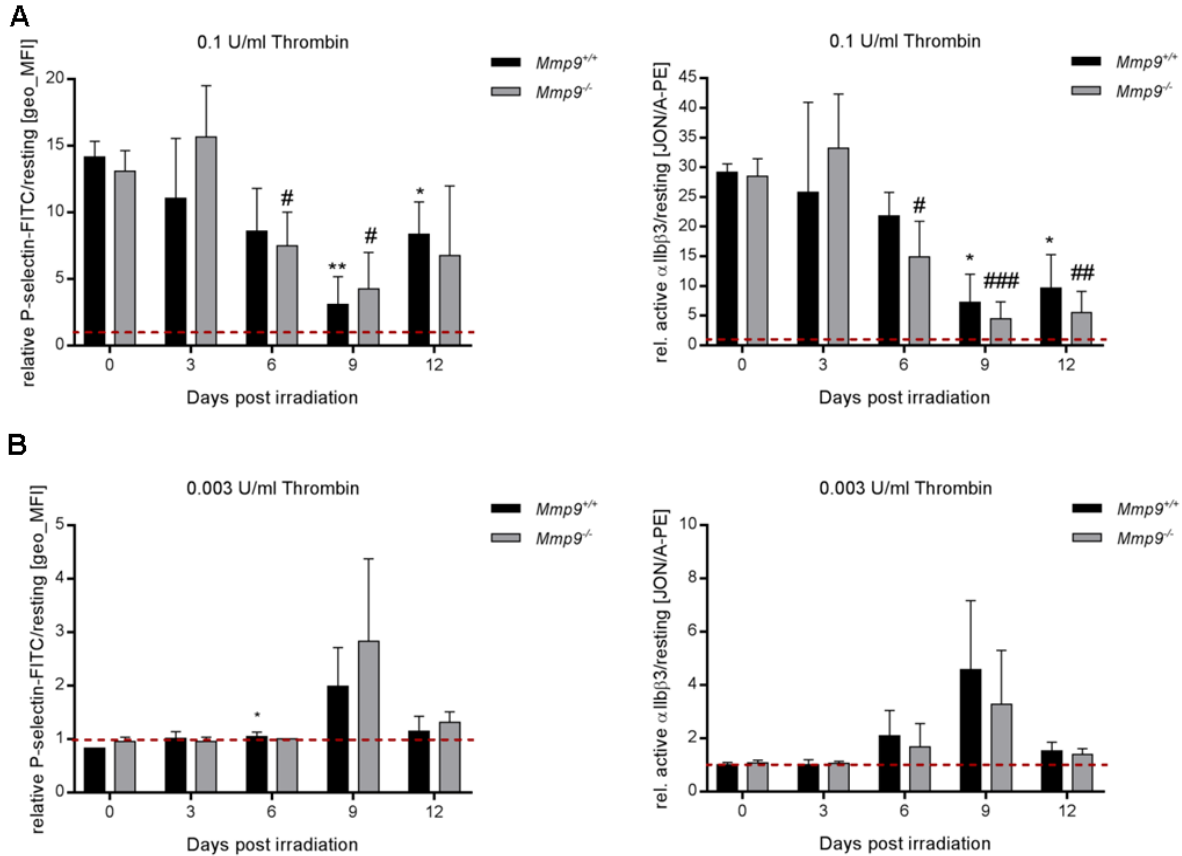
Fig. 30: Platelet activation in irradiated mice upon thrombin stimulation. (A) A transient decrease in degranulation and αIIbβ3 integrin activation was observable only upon stimulation with the highest thrombin concentration in *Mmp9+/+* and *Mmp9-/-* mice. **(B)** The lowest dose of thrombin hardly led to any activation and was comparable to resting values (red dashed line) except for day 9, where a slight activation was detectable. Error bars indicate standard deviation. Asterisks mark statistically significant differences of the mean in *Mmp9+/+* mice compared to untreated (day 0) mice (* $P < 0.05$; ** $P < 0.01$). Hashes mark statistically significant differences of the mean in *Mmp9-/-* mice compared to untreated (day 0) mice (# $P < 0.05$; ## $P < 0.01$; ### $P < 0.001$). Data of one experiment, determined in triplicates is shown.

On day 3 post irradiation, the stimulation of GPVI with a high dose of CRP (10 µg/ml) led to a normal α-degranulation and to an unaltered αIIbβ3 integrin activation compared to non-irradiated control animals. On day 6, αIIbβ3 integrin activation and α-degranulation decreased and hardly any activated platelets were detectable after day 9 (Fig. 31A). With a low dose of 0.1 µg/ml CRP, integrin activation as well as P-selectin exposure was measurable until day 3. On day 9 and 12 we could neither detect any degranulation or integrin activation (Fig. 31B). The lack of *Mmp9* had no effect on the outcome of platelet activation in any shown assay (Fig. 28-30). Taken together the

results from these experiments provide several independent lines of evidence that platelets after irradiation lose their ability to secrete their granule contents as well as to properly activate their αIIbβ3 integrins upon stimulation in response to a variety of different agonists. Of note, the the GPVI defect seemed to be more profound than that of G-protein coupled receptors.
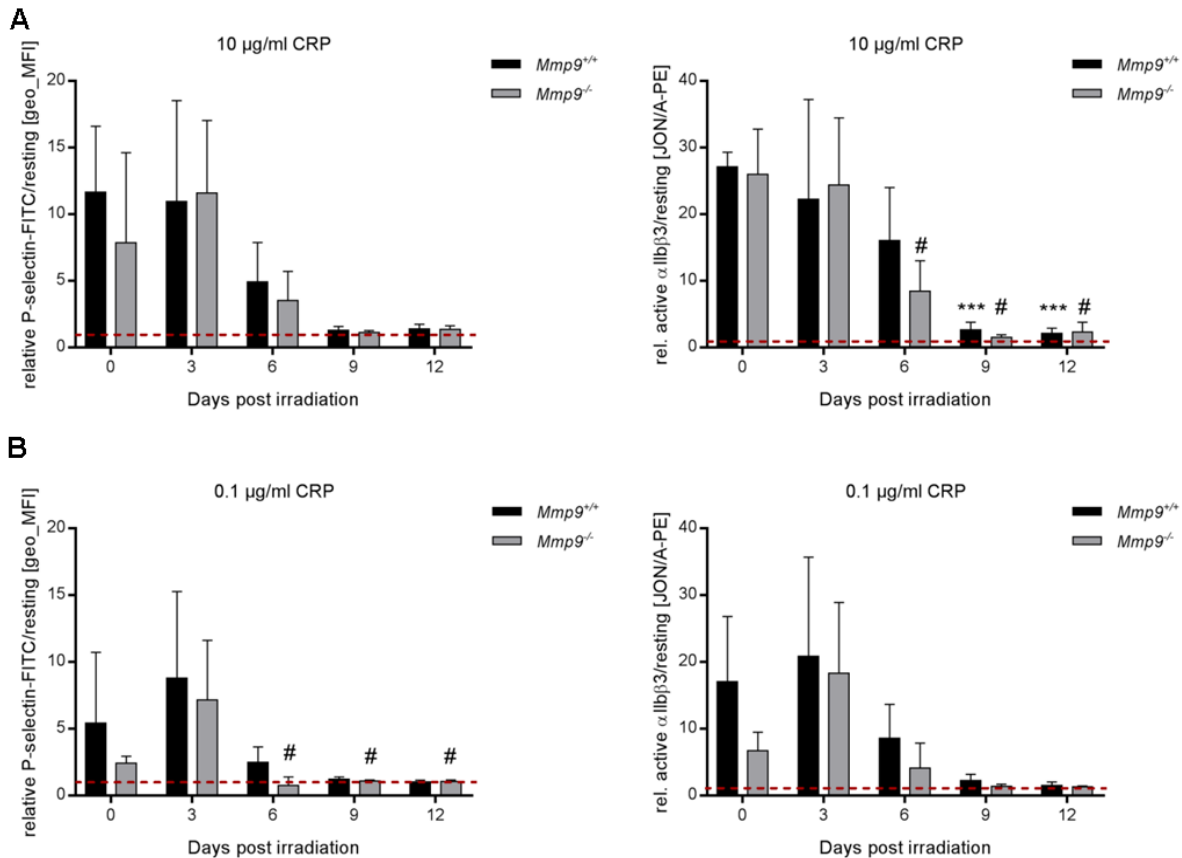
Fig. 31: Platelet activation in irradiated mice upon GPVI stimulation. (A-B) *Mmp9*^{+/+} and *Mmp9*^{-/-} mice showed a decreased activation upon stimulation with all concentrations of CRP until day 6. At later time points, no activation was found as all MFI-values were comparable to resting platelets. Error bars indicate standard deviation. Asterisks mark statistically significant differences of the mean in *Mmp9*^{+/+} mice compared to untreated (day 0) mice (* $P < 0.05$; *** $P < 0.001$). Hashes mark statistically significant difference of the mean in *Mmp9*^{-/-} mice compared to untreated (day 0) mice (# $P < 0.05$). Data of one experiment, determined in triplicates is shown.

3.3.7 BM regeneration already starts 12 days after irradiation

Since the low platelet count in response to irradiation ameliorated and the reduced platelet activation responses in *Mmp9*^{+/+} and *Mmp9*^{-/-} mice started to recover on day 12 after irradiation, we were interested how the expression of ECM proteins in the BM of irradiated mice alters over time. To address this question experimentally, we investigated the expression and localization of Col I, Col IV and the BM-specific laminin subunits α4 (Lam α4) and α5 (Lam α5) by IF-stainings in comparison to expression of

MMP-2 and MMP-9. BM-sections were stained by multiple antibodies and analyzed by confocal laser-scanning microscopy. First, we assessed whether a regeneration process was already initiated within BM. Further, stitching of images was adopted to facilitate the visualization of MK-distribution throughout the whole bone. We found that laminin-α5 showed was still absent from sinusoids, whereas Col IV staining was partially overlapping with some sinusoidal markers. Laminin-α4 and Col I expression was not affected and comparable to day 6 after irradiation (Fig. 23, 24). While six days after irradiation MKs appeared to be positive for MMP-9, MMP-2 expression was rather detected intercellularly. On day 12 no MMP expression was detectable anymore (Fig. 32).
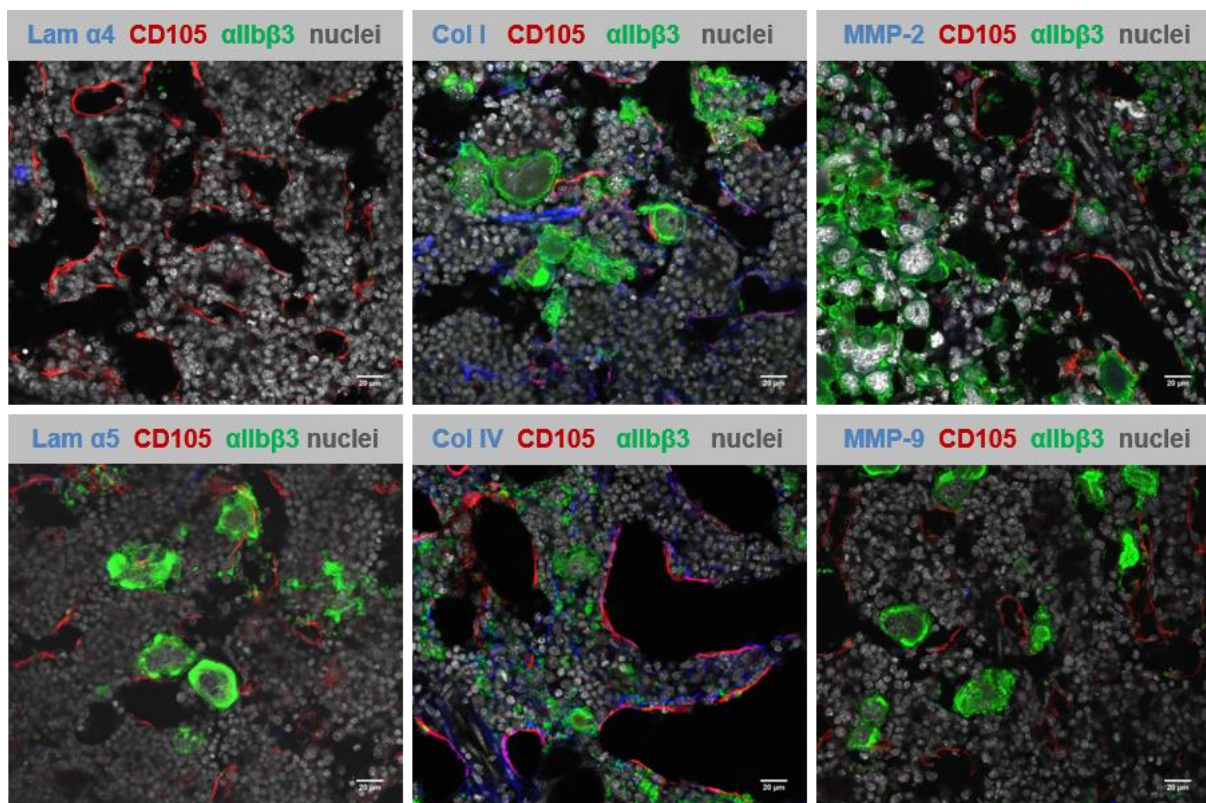
Fig. 32: Distribution of laminins, collagens and MMPs in BM on day 12 after sublethal irradiation. Laminin isoforms α4 and α5 were not detectable on day 12 after irradiation (blue, left panels). In contrast, Col IV (blue, middle panels) already was present at some sinusoids (red) and within BM as well as Col I (blue). MKs (green) showed no positive staining for MMP-9 (blue, right panels) anymore and MMP-2 (blue) was also absent from BM. Vasodilatation started to recede at some areas within BM. Scale bars represent 20µm.

Stitching of *Mmp9*^{+/+} (Fig. 33A) and *Mmp9*^{-/-} (Fig. 33B) femora images revealed that the general cellularity, illustrated by the nuclei depicted in grey, was increased and almost comparable to untreated WT femora (Fig. 1B). Surprisingly, MK numbers also increased, but their distribution appeared in an insular pattern within BM (Fig. 33Ai, ii,

Bi). This phenomenon also occurred in *Mmp9$^{-/-}$* mice, which have, according to the mouse line description, a 10% shorter femur than *Mmp9$^{+/+}$* mice (Fig. 33B). These results indicate that the reconstitution of the MK lineage within BM already begins between day 6 and day 12 after sublethal irradiation.

Investigation of the effects after sublethal irradiation on BM and platelets revealed massive alterations regarding microvasculature structure, ECM protein expression and localization as well as MK cellularity and platelet function. Unexpectedly, specifically laminin-α5 and Col IV became undetectable at the subendothelial layer after irradiation, which is probably caused by the upregulated MMP-9. Moreover, the higher expression of MMP-9 in MKs implies that these cells might contribute to the turnover of ECM proteins. The lack of Col IV and laminin-α5 might also contribute to the instability of the vessels, thus leading to the vasodilatation after irradiation.

Furthermore, we observed a reduction of MKs within BM, which subsequently results in a thrombocytopenia. Interestingly, platelet biogenesis still took place after irradiation but the newly generated platelets were less functional although the expression of glyco-proteins on platelet surface was overall unaltered. Since we observed on day 12 after irradiation a reconstitution process of the BM, we assume that MK as well as platelet numbers will recover within the next days after our last measured time point. But it still is unclear whether these platelets stay defective for a longer time period.

Taken together the combination of the numerous alterations within BM might contribute to the delayed recovery of the platelets compared to other hematopoietic cells after HSC transplantation.
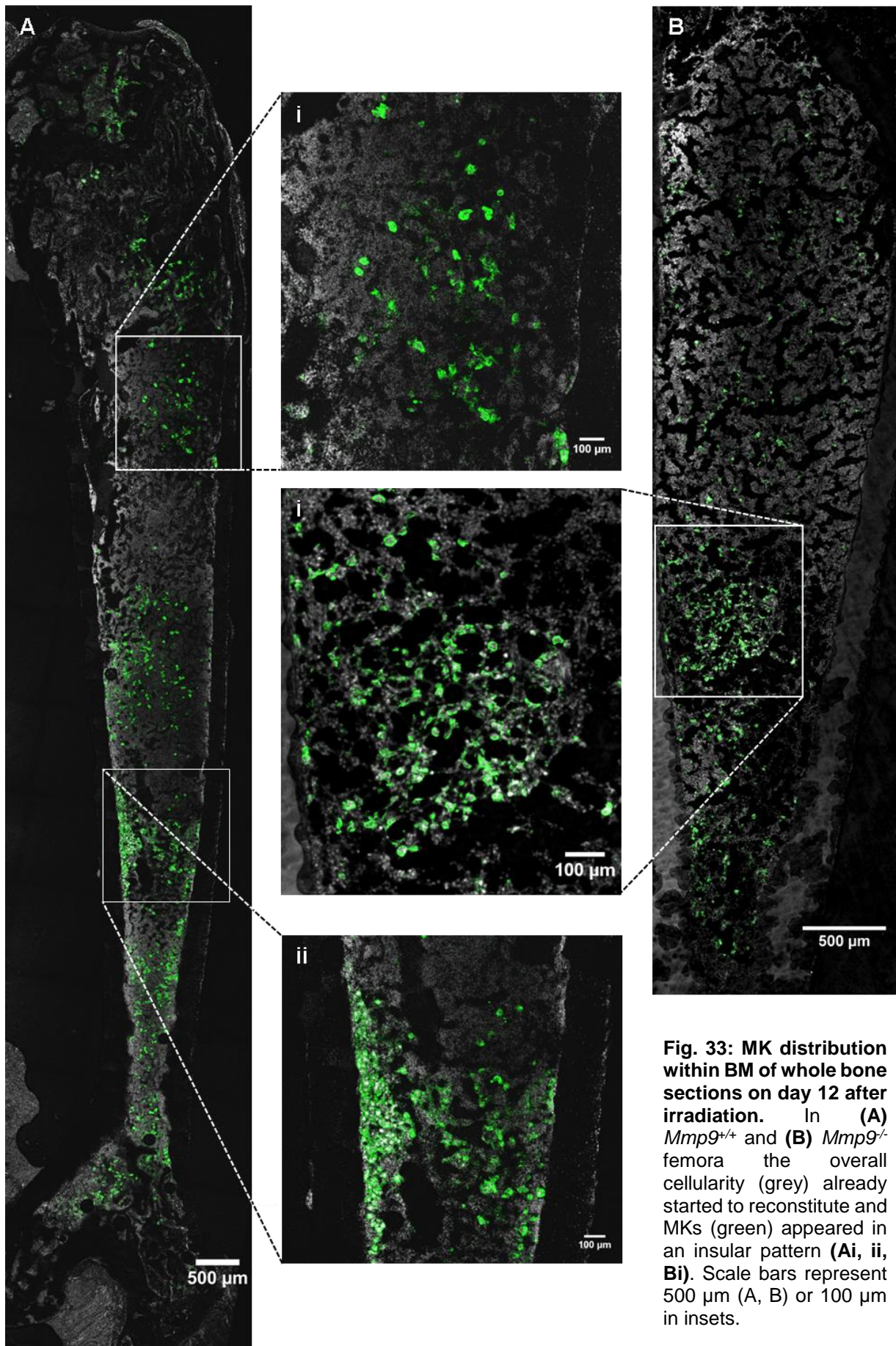
Fig. 33: MK distribution within BM of whole bone sections on day 12 after irradiation. In **(A)** *Mmp9+/+* and **(B)** *Mmp9-/-* femora the overall cellularity (grey) already started to reconstitute and MKs (green) appeared in an insular pattern **(Ai, ii, Bi)**. Scale bars represent 500 µm (A, B) or 100 µm in insets.

4 Discussion

The BM is the system responsible for the generation of all hematopoietic cells. The extracellular matrix proteins, representing the major part of the bone, form a three-dimensional network within the BM, defining thereby environmental niches and allowing the orientation and migration of hematopoietic cells (Thews, Mutschler and Vaupel, 1999). So far it was difficult to investigate the intact organ due to its restricted accessibility, but over the past few years new techniques developed that allow to study the BM and its cells (a) *ex vivo* and *in vitro*, (b) *in situ* by maintaining the overall topology of the BM and (c) the altered dynamics in response to trauma and damage like irradiation. These three aspects have also been addressed in the Results section of this thesis.

In the present study, new approaches were established and exercised to facilitate microscopical analysis of the BM regarding structure and composition. Furthermore, the role of ECM proteins on platelet biogenesis was investigated with an emphasis on distinct collagen types. Therefore, pharmacological approaches with specific antibodies against the different ECM proteins or their receptors were applied in *in vitro* systems. Comparative, genetic mouse models, which lack the main collagen receptors GPVI and/or α2β1 integrin were analyzed. In the last part of this study, the hematopoietic system was challenged by irradiation, to determine the effects on microvaculature structure, ECM protein expression and localization as well as platelet biogenesis and function.

4.1 Improvement in sample preparation and microscopical techniques allow insights into bone structure and composition

Over the last decades high resolution microscopic techniques like confocal laser scanning microscopy (CLSM) became accessible and thus more and more important for biological questions, since they can provide insights into cellular structures and interactions in a nanometer scale. Along with the progress in the development of recording and processing techniques, also the preparation of samples improved and even *in vivo* imaging is now possible.

The tissue cutting method according to Kawamoto that was applied in this study, allows sectioning of compact tissues like bones without previous decalcification. The

subsequent application of multi-color IF-stainings, established by our group, conceded insights into the BM topology regarding, MK-, vessel- and ECM protein localization or their physical interactions at the same time. The recording of whole bone sections revealed a homogenous distribution of MKs throughout the BM and a dense vessel network (Fig. 7). This is contradictory to an architectural niche concept, where HSCs residing at the endosteal niche migrate towards vessels meanwhile they differentiate (Aguilar *et al.*, 2017). Moreover, stainings of HSCs with an antibody against the SCF receptor, also performed by our group, revealed a rather uniform distribution of HSCs within the complete BM (data not shown). An elegant study by Stegner and colleagues (Stegner & van Eeuwijk *et al.,* 2017) confirmed that MKs cannot migrate within BM due to spatial limitations within the dense microvascular system. Even with an SDF-1 stimulus or when platelets were depleted to initiate PPF, the number and localization of MKs remained overall unaffected.

IF-stainings of collagens revealed that Col I and IV are present throughout the BM and co-localize with sinusoids (Fig. 8), which is in line with a recent study (Malara *et al.*, 2014), In contrast, a study by Nilsson and colleagues shows Col I exclusively in the cortical bone and Col IV only associated with vessels (Nilsson *et al.*, 1998). This discrepancy to our findings might be attributed to different preparation and staining procedures. A harsh decalcification (typically hydrochloric acid) of the bone to facilitate the sectioning might destroy epitopes on the protein surface and change the binding of antibodies, finally leading to an impaired and incorrect staining pattern (Athanasou *et al.*, 1987). Also the application of cross-reactive antibodies itself can result in staining artifacts. Therefore it is essential to determine the specificity of all used antibodies (Fig. 8F).

Indeed, bone sections are a static and descriptive system but nonetheless quantifications regarding localization and distribution of proteins (Fig. 7, 8, 9) can be performed with meaningful results. Our analyses of the 2D sections showed that the majority of MKs are in vessel contact and the distance between two vessels represents 50 μm (Fig. 7). These dimensions are in line with analyses made by *light sheet fluorescence microscopy* (LSFM) and subsequent 3D reconstruction (Stegner & van Eeuwijk *et al.,* 2017). Also kinetic processes can be illustrated to a certain extent (Fig. 17, 23, 26). Of course, those kinetic analyses are restricted to the velocity of the investigated biological process. Fast progressions like PPF are usually traced by

intravital two-photon microscopy (2P-IVM) and cannot be depicted by 2D cryo sections. In contrast, long lasting processes and also changes that take place in a range of days, can be analyzed (Fig. 23-25).

Quantitative analyses of three dimensions are more difficult. Cryo sections only allow investigations in x- and y- dimension with a very limited size in z-direction (typically 7-10 μm). Therefore, analyses that were performed to evaluate the degree of collagen wrapping of MKs or the vessel contact can only be a rough estimate. But, since the vessel contact of MKs, determined in the 2D cryo sections was consistent with the values determined by Stegner and colleagues in their 3D reconstructions, we can assume that collagen association with MKs also reflects roughly the 3D situation. We could show that the Col I contact of MKs was homogeneous in the marrow cavity as well as at sinusoids. In contrast, Col IV association of MKs was much higher at vessels than in the marrow cavity (Fig. 8E).

To overcome the limitation in z-dimension to some degree, we modified the tissue preparation technique used for LSFM where vessels, MKs and platelets are labeled in the living mouse via injection of specific antibodies coupled to fluorophores with an excitation spectra at high wavelengths. Afterwards, the living animal is transcardially perfused with PBS to wash out the blood and the tissues become subsequently fixed with PFA. To allow penetration of the light sheet through the tissue, the organs have to be made transparent. This is achieved by clearance with BABB for 24h (Stegner & van Eeuwijk *et al.,* 2017). Due to general autofluorescence of tissues at lower wavelenghts (blue-green), *in vivo* labelings are limited to fluorophores of higher wavelengths (light red-dark red), thus currently limiting the staining to only two colors simultaneously. For the comparison of the vasodilatation in bones and spleens after irradiation, a visual field of 50 μm in z-dimension was sufficient. Thus it was not necessary to clear the whole organs. Bones and Spleens were fixed after tissue preparation instead of perfusion with fixation at the living animal. We cleared the whole organs with BABB over night and recorded a stack with x-, y- and z- values according to Nyquist criteria, which determines the minimal sample density that is needed to gather all information from the microscope into the recorded image. Is the sampling distance larger than the distance according to Nyquist (undersampling), some information about the image gets lost. But also an oversampling is problematic, since the acquisition times would be longer, which subsequently leads to bleaching effects

in the sample. In consideration of the Nyquist criteria we were thus also able to detect changes in 3 dimensions in bone and spleen by CLSM (Fig. 26).

However, this 3D imaging is limited to a small penetration depth of 50 µm and LSFM would be necessary to image the whole organ. Despite the availability of imaging techniques in three dimensions, IF-stainings of 2D samples are still a valuable tool to investigate not only the BM compartment, since currently no other imaging method is able to image such a broad range of proteins simultaneously.

4.2 Pharmacological and genetic approaches revealed a crucial role of Col I in platelet biogenesis

Collagens are the most abundant ECM proteins within the BM and constitute almost 25% of the total protein content in animals. It is the major component of several connective tissues like skin, tendons, ligaments, cartilage, bone, basement membrane and blood vessels but differs by their composition. In vertebrates, the known 28 different collagen types (I – XXVIII) all form a triple helical structure either of heterotrimic or homotrimeric chains. The fibril forming Col I represents the archetype of all collagens and is the most abundant collagen type in the body, whereas Col IV is mainly found in the basal lamina. Due to up to 26 interruptions in the triplet sequence, Col IV is more flexible and allows cell binding and interchain- crosslinking (Vandenberg *et al.*, 1991). Posttranslational modifications that occur in all collagens are mainly caused by hydroxylations of proline and lysine residues (Kadler *et al.*, 2007).

For studies on platelets as well as for megakaryocytic research, standardized and pure collagen preparations are critical for *in vitro* and *ex vivo* analyses. Besides fibrillar collagen also artificial synthesized 'soluble' collagens like CRP (Knight *et al.*, 1999) or the rattlesnake venom purified protein, convulxin (CVX) are typically used for platelet receptor activation (Francischetti *et al.*, 1997). In a previous study we could show that the sequence difference between species of one collagen type is smaller than the difference between the different collagen types (Semeniak *et al.*, 2016), which emphasizes the importance to select the specific collagen type for platelet assays (Fig. 34).
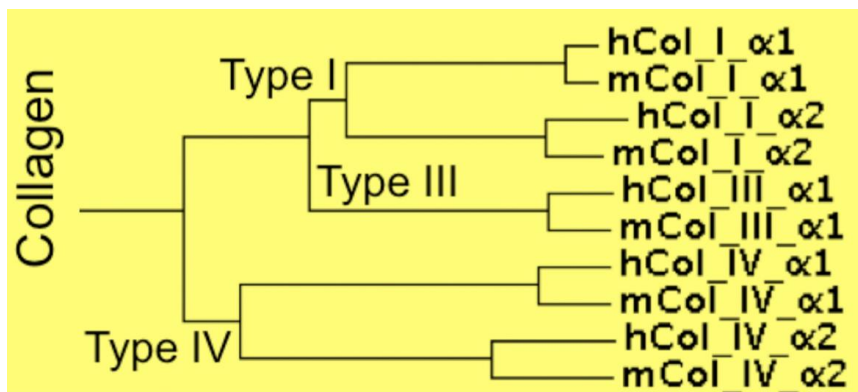
Fig. 34: Sequence alignment of different collagen types in humans and mice. Calculations by ClustalW2 using the BLOSUM matrix revealed higher sequence homologies between species than between distinct collagen types. Analysis performed by Rebecca Kulawig.

This prompted us to investigate the role of distinct collagen types and other ECM proteins on adhesion and the PPF of MKs. Interestingly, we could unravel that mainly Col I plays a crucial role in adhesion as well as in PPF but the underlying signals are mediated via different collagen receptors. On Col I, MKs showed the strongest adhesion and only when the collagen receptor α2β1 was blocked with the antibody LEN/B this adhesion was diminished (Fig. 10). In platelets, α2β1 integrin is already known as the receptor mediating adhesion at sites of injury (Sarratt *et al.*, 2005). In contrast, the inhibition of PPF on Col I (Fig. 11) was specifically abrogated when the collagen receptor GPVI was either blocked with the antibody JAQ1 or when mice were used lacking this receptor (Fig. 12).

Several collagen receptors have been described that show distinct spatiotemporal expression in the megakaryocytic lineage. While GPVI and α2β1 integrin are two well-characterized receptors on platelets (Nieswandt and Watson, 2003; Watson, 1999) and are expressed as late markers on MKs compared to αIIbβ3 or the GPIb/GPV/GPIX complex (Lagrue-Lak-Hal *et al.*, 2001; Lepage *et al.*, 2000), the collagen receptors LAIR-1 and DDR1 are less well characterized and only expressed on very early megakaryocytic progenitor cells (Steevels *et al.*, 2010, Smith *et al.*, 2017). LAIR-1 has been shown to act as an inhibitory receptor for collagen, which shows a decreasing expression with progressing MK maturation resulting in the complete absence on the platelet surface. A role of DDR1 in modulating the motility of MKs on Col I was reported recently, but so far only in humans (Abbonante *et al.*, 2013). It is still unclear whether this receptor is also expressed in mice. In addition also glyco-protein V (GPV), expressed on mature MKs and platelets, can bind to collagen (Moog *et al.*, 2001).

Laminins that have been considered a key protein family to support PPF, had in our experimental settings no effect on PPF beyond the BSA control. Since only laminin-α5 is expressed at sinusoids (Fig. 9), this specific isoform was tested, but showed also no alterations on PPF. Furthermore, it was not able to counteract the inhibition mediated by Col I (Fig. 11B). Fibronectin showed also no effect on PPF beyond the BSA control in our *in vitro*-approach. Its sinusoidal-distant distribution within BM makes it unlikely that it can counteract the Col I-mediated inhibition (Fig. 11A). Only the collagen type IV was able to abrogate the inhibition of PPF by Col I in a dose dependent manner, while it has no effect on PPF alone compared to BSA control.

Surprisingly, crosslinked CRP behaved in our titration-based PPF-assays exactly like Col IV and abrogated the inhibition mediated by Col I, although it carries the condensed GPO-motif of Col I. Col IV was shown to contain a GFOGER-peptide than a GPO-motif. This is partly in contrast to a study by Sabri and colleagues in 2004, who showed inhibition of PPF when MKs were kept adherent for a longer period of time on a GFOGER peptide. But these conflictive results might be due to several technical differences between the assays: First and most striking, Sabri and colleagues used MKs derived from human cord blood HSCs. Furthermore, other experimental conditions like the addition of bivalent cations might have influenced the findings. Moreover, there is evidence that α2β1 integrin harbors different binding sites for distinct collagen epitopes (Leitinger, 2011; O'Connor *et al.*, 2006; Schulte *et al.*, 2001), which is corroborated by our results.

In addition, the activation status of α2-integrin is also important in thrombopoiesis (Zou *et al.*, 2009), indicating an important mode of feedback where GPVI activation increases the fraction of integrins being in an active state. Since the α2β1 integrin mediates adhesion of MKs on Col I and GPVI acts as the mediator for the inhibitiory signal of Col I on PPF, we assume that both receptors have different functions for Col I binding and signaling.

In platelets, GPVI activation appears downstream of the non-covalently bound FcγR-chain via phosphorylation of Src family kinases (SFKs), and subsequently the signaling proteins Syk and LAT. When the inhibition of PPF mediated by GPVI takes place through the same signaling cascade as found for GPVI-based platelet activation by collagen, PPF should also be abrogated in MKs lacking these proteins. Interestingly, Syk- or LAT- null MKs also displayed reduced PPF on Col I, whereas application of the

Discussion

SFK inhibitor PP2 fully phenocopied MKs lacking GPVI, suggesting a branching point downstream of SFKs (Fig. 12). A similar bifurcation has been identified for the targeted downregulation of GPVI through internalization or ectodomain shedding, respectively, providing an independent line of evidence that there are two distinct signaling pathways downstream of GPVI (Rabie *et al.*, 2007).

Furthermore, we could not detect Syk tyrosine phosphorylation in MKs plated on collagen or CRP, in contrast to platelets cultured on CRP which resulted in Syk phosphorylation. This finding strengthens our hypothesis of a branching point downstream of SFKs. Typically platelets become also activated upon collagen stimulation. The fact that we could not determine this activation in platelets plated on collagen might be due to the absence of shear stress in our assay systems. In previous studies we could only detect platelet activation upon collagen stimulation by Syk phosphorylation under stirring conditions at 37°C (data not shown). Moreover, the GPVI signaling cascade in MKs might differ from platelets, where ERK proteins become transiently phosphorylated when plated on collagen I, whereas in MKs, we found only weak and attenuated ERK phosphorylation.

The finding that ERK phosphorylation was partly already present in unstimulated MKs prompted us to check the ERK phosphorylation status, when MKs were serum starved and instead cultivated in PBS prior to collagen stimulation (Neel and Lebrun, 2013). Under these culturing conditions we could not detect ERK phosphorylation in MK but in platelets, further confirming two different signaling pathways in platelet activation and inhibition of PPF. The branching point downstream of SFKs indicates as an independent line of evidence that the signaling cascade with distinct branching points can function to prevent premature GPVI signaling MKs.

BM explants are an additional method to study PPF (Eckly *et al.*, 2012). The femur bone is cut in small segements and placed into medium, where MKs start to migrate out of the central marrow and immediately form proplatelets. This shows independently that PPF is a cell autonomous process (Lecine *et al.,* 1998). Thus, the signal for PPF might be constitutively active and is inhibited by several 'brakes' within the BM cavity, which are not present or reduced at the subendothelial layer surrounding the BM sinusoids. These results prompted us to create the following model: Distant from vessels Col I filaments are abundant and bind to MKs via the integrin α2β1. This binding brings Col I in close contact to GPVI, which mediates the signal for the

inhibition of PPF, thus preventing premature release of platelets into the marrow cavity. At sinusoids, collagen binding sites for the α2β1 integrin are rather occupied by Col IV whose density is increased at vessels, thereby hampering Col I binding and preventing the transduction of the inhibitory signals (Fig. 35) (Semeniak *et al.*, 2016).
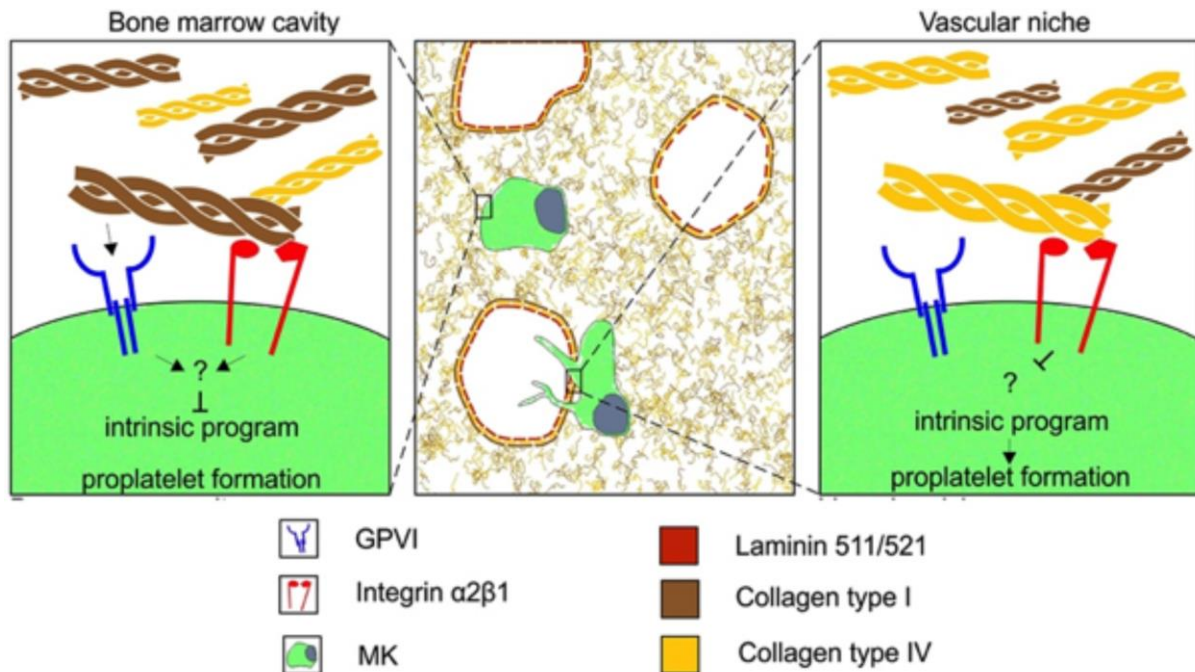
Fig. 35: Model depicting the process of PPF. MKs, distant from vessels, bind with high affinity to Col I (brown filaments) via α2β1 integrin and an inhibitory signal is transmitted by GPVI to prevent premature release of platelets into the BM (left panel). At sinusoids, MKs show increased contact to Col IV (yellow filaments), which displace Col I from α2β1 integrin. This leads to the abrogation of the inhibitory signal and PPF takes place (right panel). Image generated by Rebecca Kulawig and taken from Semeniak *et al.*, 2016.

Interestingly, mice lacking GPVI or integrin α2 have normal platelet counts. Furthermore, no signs of premature platelet release in the BM can be detected in these mice. Also platelet depletion, which encourages MKs to generate new platelets did not show altered platelet recovery rates in collagen receptor-deficient mice and was comparable to WT mice (Fig. 15A). The significant difference that we observed in mice deficient for *Gp6* compared to WT control animals might be due to the different platelet counts before depletion. By normalization of platelet counts relative to their starting values, the slightly higher platelet counts in *Gp6*^{-/-} mice were not detectable anymore, indeed confirming no differences in platelet recovery rates in *Gp6*^{-/-} mice. Unfortunately we had no opportunity to determine the platelet counts at later time points, where we should have seen an overshoot of platelet counts, which than normalizes again. This has to be analyzed in future experiments to exclude alterations at these later time points in mice deficient for *Gp6* or *Itga2*.

The assumption that collagen receptor deficient mice show altered MK numbers or distribution to compensate the inability to recognize collagen could not be confirmed. The doubled MK number in *Itga2*^{-/-} mice (Fig. 14B) might be due to different experimenters, mice and resources used to quantify the MK numbers. Since we also could not detect impairments in MK numbers in mice lacking both collagen receptors (Fig. 20A), we do not assume that the increase of MK numbers in *Itga2*^{-/-} mice is reproducible and has a physiological relevance. MKs are rather sessile and do not change localization or their numbers, which also was shown by Stegner and colleagues in 2017. Only the association towards Col I was transiently reduced after depletion. Since platelet depletion did not affect MK motility (Stegner & van Eeuwijk *et al.,* 2017), Col I remodeling might be impaired. In order to investigate this, expression levels of Col I as well as the Col I-degrading protein MMP-2 have to be determined on mRNA level and on protein level and finally MMP-2 activity needs to be determined.

Our data also show that PPF on Col I was not completely abolished, but rather attenuated (the level of PPF on day 5 on Col I was comparable to day 3 on BSA, Fig. 11). It is thus very likely that *in vivo* more than one inhibitory signal can act simultaneously, which cannot be reflected by our *in vitro* approach. These additional 'brakes' would still be active in mice lacking GPVI, explaining the normal platelet counts in these mice.

Although *in vitro* assays are often the only possible way to investigate kinetics in megakaryopoiesis and platelet biogenesis, these technical approaches have well known weaknesses. FLC-derived MKs are the tool of choice to study PPF *in vitro*. The amount of MKs that can be isolated from fetal livers allows analyses of many different conditions in parallel. In contrast to the *in vivo* situation, MKs show an unpolarized PPF in cell culture. So far no cytokine or cell culture condition is known to mimic the directed PPF across the endothelial barrier, occurring within BM. This suggests that there are still unknown factors and conditions, which influence platelet biogenesis *in vivo*. It is also known that FLC-derived MKs produce platelets that are hyporesponsive upon GPVI stimulation. This is a phenomenon described in human fetal platelets that show less responsiveness in aggregation due to decreased surface receptor expression (Israels *et al.*, 2003; Andres, Schulze and Speer, 2015).

Unfortunately, BM-derived MKs, which would reflect the *in vivo* situation the best, are hardly able to form proplatelets in our experimental settings. Interestingly, the addition

of the anti-thrombin anticoagulant hirudin, can markedly increase PPF of BM-derived MKs (Strassel *et al.*, 2012). However, the underlying mechanism remains unknown.

So far, we focused on mouse models that lack either GPVI or the α2-integrin on the cell surface. In order to investigate PPF in MKs that are completely 'blind' for collagen, we generated mice that lack both collagen receptors. Surprisingly, these mice also showed normal platelet counts and size. Furthermore, platelet activation was not impaired except for the expected inability to respond to any GPVI agonist. In these mice only the fibronectin receptor α5β1 integrin was upregulated at the surface of platelets. Since FN can also bind collagens (Nègre *et al.*, 1994), this increased expression might already be present at the level of MKs and thus compensate for the lack of the two major collagen receptors resulting in normal platelet counts. This upregulated α5 expression was already present in mice only lacking α2 integrin subunit, indicating that the FN receptor might adopt the function of the α2β1 integrin in the signal transduction during PPF.

So far, it remains unclear which protein could compensate for the lack of GPVI in the double-deficient mice. The aforementioned additional 'brakes' that inhibit PPF prematurely could provide an explanation. Certain laminin isoforms might also play a crucial role in regulating PPF. Here especially the laminin-α5 subunit, the only isoform being present at BM sinusoids, could contribute to the maintenance of PPF via its receptor α6β1 integrin. Nigatu and colleagues described that laminin-α5 can be secreted by activated platelets from α-granules and promote the adhesion via integrin α6β1. They indicated that laminin-α5 might provide a temporary extracellular matrix upon secretion to assist wound healing after injury (Nigatu *et al.*, 2006; Maynard *et al.*, 2007). Since α-granules are already present in MKs, they also might secrete laminin-α5 and thus compensate for the lack of adhesion properties by α2β1 integrin. In order to further investigate a possible role of laminin-α5 or its receptor, the expression levels of these proetins in DKO mice should be studied in flow cytometric analyses or in immunoblot analyses.

The Col I association of MKs was also diminished in DKO mice, whereas the Col IV contact was increased. This further emphasizes that other ECM protein receptors might adopt the role of α2β1 integrin and GPVI and thus recognizing the distinct collagen types and mediating the signals for PPF. The PPF has not yet been investigated in these mice, but the normal PPF in WT mice where both receptors were

blocked with the specific antibodies JAQ1 and LEN/B suggest also a normal PPF in double-deficient mice.

Surprisingly, DKO mice showed a three-fold increase of MK numbers in spleen. Whether this is also true for single-deficient mice has to be investigated, since platelet counts are unaltered in these mice. In contrast to humans, the spleen is a hematopoietic organ in mice. It has to be determined whether the spleen contributes to the normal platelet counts or whether it functions as the site for degradation of defective, collagen-non responsive MKs. A splenectomy in DKO mice would give indirect evidence for one of the two possibilities. If the platelet count decreases after splenectomy, this might account for an increased thrombopoietic role of the spleen in these mice. It also would indicate that the signaling for PPF in spleen is different from signals in BM, since MKs are able to form proplatelets in spleen but not in BM.

We know from previous studies that at least the vessel structure and composition differs between spleen and BM. The angiopoietin receptor Tie-2 is described to be expressed in endothelial cells (Makinde and Agrawal, 2008). Interestingly, we could not detect Tie2 protein in BM sinusoids (data not shown). Also after irradiation, the sinusoids in BM and spleen respond differently. While BM sinusoids develop a massive vasodilatation, the microvessels in spleen remain overall unaffected (Fig. 26). The question remains how relevant the extramedullary hematopoiesis in mice is, since in humans this type of hematopoiesis only takes place in disease-conditions like beta-thalassemia or fibrosis when space for normal hematopoiesis in the BM becomes very restricted. A recent study that is controversially discussed describes the lung as the tissue, where about half of the platelet production takes place (Lefrançais *et al.*, 2017). We never observed MKs in such an amount in lung tissue that it could contribute so substantially to the overall platelet poulation. The contradictory results might be due to poorly conceived calculations in their studies.

4.3 Outlook and concluding remarks

The results, derived from the experiments performed in this study provide novel insights into the role of ECM proteins in the process of platelet biogenesis. We could show for the first time that distinct collagen types contribute differently to the regulation of this process. This might also be of clinical relevance, for example for BM transplantations that are performed since the late 1950s. Due to an increased

availability of suitable donors, the transplantations of HSCs increased tremendously over the last decades. In 2015, approximately 40000 HSC transplantations were reported from 48 countries (Passweg *et al.*, 2015). Although the number of HSC transplantations increase, little is known about the impact of the preceding irradiation on the bone marrow matrix itself and how these alterations contribute to the engraftment of the different cell lineages after transplantation.

Over the last years some groups investigated the transient vasodilatation after irradiation (Zhou, Ding and Morrison, 2015), but the influence on the ECM proteins or MKs remains unclear. This is of relevance, since many patients suffer from mild to life-threatening bleedings due to thrombocytopenia in response to the irradiation (Labrador *et al.,* 2015; Holler *et al.*, 2009). Compared to other cells of the hematopoietic system, platelets engraft rather delayed after transplantation (Isoyama *et al.*, 2010).

With the application of the new bone sectioning and staining protocols, we were for the first time able to characterize the BM after irradiation regarding the cellularity and ECM protein composition. We could show that specifically Col IV (Fig. 24) and laminin-α5 (Fig. 23) became undetectable from the sinusoids after irradiation and that MMP-9 expression was strongly upregulated in MKs (Fig. 25). Whether this increased MMP-9 expression results also in an increased activity, thus leading to the degradation of Col IV or laminin-α5, has to be analyzed by zymographic assays of isolated cells or direct *in situ* zymography in cryo sections (Hadler-Olsen *et al.*, 2010).

In contrast, the expression of Col I and laminin-α4 remained unaffected. The reason why specifically ECM proteins that are found mainly at sinusoids are impaired in their expression has to be investigated in the future. It is likely that the altered expression is correlated to the observed transient vasodilatation in the BM (Fig. 26). In spleen, where no vessel alteration was detectable, also Col IV and laminin-α5 were unaffected (data not shown). Although the general cellularity in BM was decreased after irradiation and hardly any MKs remained, we found that the remaining cells were still able to generate new platelets for an extended period of time post irradiation (Fig. 27). However, the circulating platelets after irradiation have an increased size, most likely due to the increased demand, as found for other diseases. The decreased glyco-protein expression is accompanied by a general hyporesponsiveness of platelets.

Discussion

By flow cytometric analyses of spleen-derived hematopoietic cells, we observed an increase in GPIX-positive fragments of different sizes after irradiation, suggesting a rapid clearance of defective platelets from the circulation and also a possible degradation of MKs. Whether this clearance contributes to the long lasting thrombocytopenia could in the future be investigated by studying platelet counts after splenectomy. A positive effect of splenectomy after transplantation was already observed for red blood cells (Anklesaria *et al.*, 1989).

Surprisingly, we observed that 12 days after sublethal irradiation the vasodilatation vanished and the microvasculature became normal again. MKs appeared in an insular pattern throughout the complete femur bone, indicating that only few single HSCs in the BM differentiated to MKs (Fig. 33). It would be of interest whether those MKs and derived progeny remain in this insular distribution for an extended period of time or whether the cells within BM achieve the distribution pattern before irradiation. So far, our results are only the first approaches to study sublethally irradiated mice and the impact of lethal irradiation (typically applied for malignant disorders) remains to be analyzed. It is likely that the observed impairments of ECMP expression and the numbers and size of BM MKs as well as the number and function of circulating platelets appear affected to a stronger degree in lethally irradiated mice. Interestingly, the lack of MMP-9 had no obvious influence on the outcome of platelet biogenesis and function, indicating no substantial contribution to the thrombocytopenia after irradiation.

In the future, we want to address the question which influence matrix proteins have on the cell engraftment after BM transplantation. Mice deficient for different ECMPs shall be transplanted after sub(lethal) irradiation and the engraftment will be analyzed.

Furthermore, we want to elucidate whether the general MMP-9 activity or the activity specific in the hematopoietic system might influence the engraftment of cells. By transplantation of BM with eYFP-expressing MKs we can trace the process of engraftment, since it is also unclear how the intravenously injected HSC and megakaryocytic progenitor cells can find the correct niche place within the BM.

The results gained in this study and the experiments planned in the future shall help to understand the molecular mechanisms of platelet biogenesis, which might contribute to better therapeutical treatments of patients suffering from thrombocytopenia, especially those who underwent HSC transplantation.

5 Bibliography

Abbonante V., Gruppi C., Rubel D., Gross O., Moratti R., Balduini A. (2013) Discoidin domain receptor 1 protein is a novel modulator of megakaryocyte-collagen interactions. *J Biol Chem* 288: 16738- 16746

Aguilar A., Pertuy F., Eckly A., Strassel C., Collin D., Gachet C., Lanza F., and L´eon C. (2017) Importance of environmental stiffness for megakaryocyte differentiation and proplatelet formation. *Blood* 128: 2022-2032

Aimes RT. And Quigley JP. (1995) Matrix metalloproteinase-2 is an interstitial collagenase. Inhibitor-free enzyme catalyzes the cleavage of collagen fibrils and soluble native type I collagen generating the specific ¾- and ¼-length fragments. *J Biol Chem* 270: 5872– 6

Akashi K., Traver D., Miyamoto T. and Weissmann IL. (2000) A clonogenic common myeloid progenitor that gives rise to all myeloid lineages. *Nature* 404: 193–197

Amour A., Knight CG., Webster A., Slocombe PM., Stephens PE., Knäuper V., Docherty AJ., Murphy G. (2000) The in vitro activity of ADAM-10 is inhibited by TIMP-1 and TIMP-3. *FEBS Lett.* 473: 275–279

Amour A., Slocombe PM., Webster A., Butler M., Knight CG., Smith BJ., Stephens PE., Shelley C., Hutton M., Knäuper V., Docherty AJ., Murphy G. (1998) TNF-alpha converting enzyme (TACE) is inhibited by TIMP-3. *FEBS Lett.* 435: 39–44

Andres O, Schulze H. and Speer CP. (2015) Platelets in neonates: central mediators in haemostasis, antimicrobial defence and inflammation. *Thromb Haemost.* 113: 3-12

Angénieux C., Maître B., Eckly A., Lanza F., Gachet C., de la Salle H. (2016) Time-Dependent Decay of mRNA and Ribosomal RNA during Platelet Aging and Its Correlation with Translation Activity. *PloS One* 11

Anklesaria P., FitzGerald TJ., Kase K., Ohara A., Greenberger JS. (1989) Improved hematopoiesis in anemic Sl/Sld mice by splenectomy and therapeutic transplantation of a hematopoietic microenvironment. *Blood* 74: 1144-1151

Antkowiak A., Viaud J., Severin S., Zanoun M., Ceccato L., Chicanne G., Strassel C., Eckly A., Leon C., Gachet C., Payrastre B., Gaits-Iacovoni F. (2016) Cdc42-dependent F-actin dynamics drive structuration of the demarcation membrane system in megakaryocytes. *J Thromb Haemost* 14: 1268-84

Athanasou NA., Quinn J., Heryet A., Woods CG. and McGee JO. (1987) Effect of decalcification agents on immunoreactivity of cellular antigens. *J Clin Pathol* 40: 874-878

Becker RP. and DeBruyn PP. (1976) The transmural passage of blood cells into myeloid sinusoids and the entry of platelets into the sinusoidal circulation; a scanning electron microscopic investigation. *Am J Anat* 145: 1046-1052

Bender M., Hagedorn I. and Nieswandt B. (2011) Genetic and antibody-induced glycoprotein VI deficiency equally protects mice from mechanically and FeCl$_3$-induced thrombosis. *J Thromb Heamost.* 9:1423-1426

Bleakley M. & Riddell SR. (2004) Molecules and mechanisms of the graft-versus-leukaemia effect. *Nature Rev. Cancer* 4: 371–380

Bleyer WA., Hakami N., Shepard TH. (1971) The development of hemostasis in the human fetus and newborn infant. *J pediatr.* 79: 838–853

Buckwalter JA., Glimcher MJ., Cooper RR., Recker R. (1995) Bone biology part I: structure, blood supply, cells, matrix, and mineralization. *J Bone Joint Surg.* 77: 1256–1275

Eckly A., Strassel C., Cazenave JP., Lanza F., Léon C., Gachet C. (2012) Characterization of megakaryocyte development in the native bone marrow environment. *Methods Mol Biol.* 788: 175-92

Ferrebee JW., Lochte HL., Jaretzki A., Sahler OD., Thomas ED. (1958) Successful marrow homograft in the dog after radiation. *Surgery* 43: 516–20

Flaumenhaft R. (2003) Molecular basis of platelet granule secretion. *Arterioscler Thromb Vasc Biol* 23: 1152-1160

Flaumenhaft R. & Koseoglu S. (2017) Molecular and Cellular Biology of Platelet Formation: Implications in Health and Disease; Part II Platelet Biology: Signals and Function; Platelet contents. Schulze H. & Italiano J. (Editors). *Springer* p.133-152

Ford CE., Hamerton JL., Barnes DWH., Loutit JF. (1956) Cytological identification of radiation-chimaeras. *Nature* 177: 452– 454

Fox JG., Barthold SW., Davisson MT., Newcomer CE., Quimby FW, Smith AL. (2007) The Mouse in Biochemical Research. *Academic Press*

Francischetti IM., Saliou B., Leduc M., Carlini CR., Hatmi M., Randon J., Faili A., Bon C. (1997) Convulxin, a potent platelet-aggregating protein from Crotalus durissus terrificus venom, specifically binds to platelets. *Toxicon* 35: 1217-1228

Fruhling L., Rogers S. and Jobard P. (1949) L'hématologie normale (tissus et organs hématopoietiques sang circulant) de l'embryon, du foetus et du nouveau-he humains. *Le Sang* 20: 313

Galanello R. and Origa R. (2010) Beta-thalassemia. *Orphanet J Rare Dis* 21: 5-11

Gross J. and Lapière CM. (1962) Collagenolytic activity in amphibian tissue culture assay. *Proc.Natl. Sci.* 48: 1014-1022

Gurney AL., Carver-Moore K., de Sauvage FJ., Moore MW. (1994) Thrombocytopenia in c-mpl-deficient mice. *Science* 265: 1445–1447

Hadler-Olsen E., Kanapathippillai P., Berg E., Svineng G., Winberg JO. and Uhlin-Hansen L. (2010) Gelatin In Situ Zymography on Fixed, Paraffin-embedded Tissue: Zinc and Ethanol Fixation Preserve Enzyme Activity. J Histochem Cytochem 58: 29-39

Han P., Guo XH. and Story CJ. (2002) Enhanced expansion and maturation of megakaryocytic progenitors by fibronectin. *Cytotherapy.* 4: 277-83

Harker LA., Roskos LK., Marzec UM., Carter RA., Cherry JK., Sundell B., Cheung EN., Terry D., Sheridan W. (2000) Effects of megakaryocyte growth and development factor on platelet production, platelet life span, and platelet function in healthy human volunteers. *Blood* 95: 2514-2522

Holler E., Kolb HJ., Greinix H., Perrotin D., Campilho F., Aversa F., Gil L., Cornelissen J., Varanese L., Schacht A., Friese A. & Rustige J. (2009) Bleeding events and mortality in SCT patients: a retrospective study of hematopoietic SCT patients with organ dysfunctions du e to severe sepsis or GVHD. *Bone marrow Transplant* 43: 491–497

Holtkötter O., Nieswandt B., Smyth N., Müller W., Hafer M., Schulte V., Krieg T. and Eckes B. (2002) Integrin alpha 2-deficient mice develop normally, are fertile, but display partially defective platelet interaction with collagen. J Biol Chem. 277: 10789-10794

Hosoya A., Hoshi K., Sahara N., Ninomiya T., Akahane S., Kawamoto T. and Ozawa H (2005) Effects of fixation and decalcification on the immunohistochemical localization of bone matrix proteins in fresh-frozen bone sections. *Histochem Cell Biol* 123: 639–646

Isoyama K., Oda M., Kato K., Nagamura-Inoue T., Kai S., Kigasawa H., Kobayashi R., Mimaya J., Inoue M., Kikuchi A., Kato S. (2010) Long-term outcome of cord blood transplantation from unrelated donors as an initial transplantation procedure for children with AML in Japan. *Bone marrow Transplant.* 45: 69-77

Israels SJ., Rand ML. and Michelson AD. (2003) Neonatal Platelet Function. *Semin Thromb Hemost.* 29: 363-372

Italiano JE Jr., Lecine P., Shivdasani RA., Hartwig JH. (1999) Blood platelets are assembled principally at the ends of proplatelet processes produced by differentiated megakaryocytes. *J Cell Biol* 147: 1299-312

Ito T., Ishida Y., Kashiwagi R. and Kuriya S. (1996) Recombinant human c-Mpl ligand is not a direct stimulator of proplatelet formation in mature human megakaryocytes. *Br J Heamatol* 94: 387-390

Itoh T., Ikeda T., Gomi H., Nakao S., Suzuki T., Itohara S. (1997) Unaltered secretion of β-amyloid precursor protein in gelatinase A (matrix metalloproteinase 2)-deficient mice. *J Biol Chem.* 272: 22389 –22392

Jacobson LO., Marks EK., Robson MJ., Gaston EO., Zirkle RE. (1949) Effect of spleen protection on mortality following X-irradiation. *J Lab Clin Med* 34: 1538–43

Junt T., Schulze H., Chen Z., Massberg S., Goerge T., Krueger A., Wagner DD., Graf T., Italiano JE Jr., Shivdasani RA., von Andrian UH. (2007) Dynamic visualization of thrombopoiesis within bone marrow. *Science* 317: 1767-70

Kadler KE., Baldock C., Bella J., Boot-Handford RP. (2007) Collagens at a glance. J *Cell Sci* 120: 1955-1958

Kassim AA. and Savani BN. (2017) Hematopoietic stem cell transplantation for acute myeloid leukemia: A review. *Hematol Oncol Stem Cell Ther.* In press

Kaushansky K. & Drachmann JG. (2002) The molecular and cellular biology of thrombopoietin: the primary regulator of platelet production. *Oncogene* 13: 3359-67

Kaushansky K., Lok S., Holl RD., Broudy VC., Lin N., Bailey MC., Forstrom JW., Buddle MM., Ort PJ., Hagen FS., Roth GJ., Papayannopoulou T. & Foster DC. (1994) Promotion of megakaryocyte progenitor expansion and differentiation by the c-Mpl ligand thrombopoietin. *Nature* 369: 568-571

Kenne E., Soehnlein O., Genové G., Rotzius P., Eriksson EE., Lindbom L. (2010) Immune cell recruitment to inflammatory loci is impaired in mice deficient in basement membrane protein laminin alpha4. *J Leukoc Biol* 88: 523-8

Kielty CM. and Grant ME. (2002) The collagen family: structure, assembly, and organization in the extracellular matrix. Connective tissue and its heritable disorders. *Molecular Genetics in Medical Aspects* 2: 159 – 221

Klaihmon P., Vimonpatranon S., Noulsri E., Lertthammakiat S., Anurathapan U., Sirachainan N., Hongeng S., Pattanapanyasat K. (2017) Normalized levels of red blood cells expressing phosphatidylserine, their microparticles, and activated platelets in young patients with β-thalassemia following bone marrow transplantation. *Ann Hematol* doi: 10.1007/s00277-017-3070-2

Knight CG., Morton LF., Onley DJ., Peachey AR., Ichinohe T., Okuma M., Farndale RW., Barnes MJ. (1999) Collagen-platelet interaction: Gly-Pro-Hyp is uniquely specific for platelet Gp VI and mediates platelet activation by collagen. *Cardiovasc Res.* 41:450-457

Kondo E. (2016) Autologous Hematopoietic Stem Cell Transplantation for Diffuse Large B-Cell Lymphoma. *J Clin Exp Hematop.* 56: 100-108

Korngold, R. & Sprent, J. (1987) Variable capacity of L3T4+ T cells to cause lethal graft-versus-host disease across minor histocompatibility barriers in mice. *J. Exp. Med.* 165: 1552–1564

Kosaki G. (2008) Platelet production ba megakaryocytes: Proplatelet theory justifies cytoplasmic fragmentation model. *Int. J. Hematol.* 88: 255-267

Labrador J., López-Corral L., Vazquez L., Sánchez-Guijo F., Guerrero C., Sánchez-Barba M., Lozano FS., Alberca I., del Cañizo MC., Caballero D., González-Porras JR. (2015) Incidence and risk factors for life-threatening bleeding after allogeneic stem cell transplant. *Br J Hematol* 169: 719–725

Lagrue-Lak-Hal AH., Debili N., Kingbury G., Lecut C., Le Couedic JP., Villeval JL., Jandrot-Perrus M., Vainchenker W. (2001) Expression and function of the collagen receptor GPVI during megakaryocyte maturation. *J Biol Chem.* 276:15316-25

Lausch E., Keppler R., Hilbert K., Cormier-Daire V., Nikkel S., Nishimura G., Unger S., Spranger J., Superti-Furga A., Zabel B. (2009) Mutations in MMP9 and MMP13 determine the mode of inheritance and the clinical spectrum of metaphyseal anadysplasia. *Am J Hum Genet.* 85: 168-78

Lecine P., Italiano JE., Kim S-W., Villeval J-L. and Shivdasani RA. (2000) Hematopoietic-specific β1 tubulin participates in a pathway of platelet biogenesis dependent on the transcription factor NF-E2. *Blood* 96: 1366-1373

Lecine P., Villeval J-L., Vyas P., Swencki B., Xu Y., Shivdasani RA. (1998) Mice lacking transcription factor NF-E2 validate the proplatelet model of thrombocytopoiesis and show a platelet production defect that is intrinsic to megakaryocytes. *Blood* 92: 1608-1616

Lefrançais E., Ortiz-Muñoz G., Caudrillier A., Mallavia B., Liu F., Sayah DM., Thornton EE., Headley MB., David T., Coughlin SR., Krummel MF., Leavitt AD., Passegué E., Looney MR. (2017) The lung is a site of platelet biogenesis and a reservoir for haematopoietic progenitors. *Nature* 544: 105-109

Leitinger B. (2011) Transmembrane collagen receptors. *Annu Rev Cell Dev Biol* 27: 265-90

Lepage A., Leboeuf M., Cazenave JP., de la Salle C., Lanza F., Uzan G. (2000) The alpha(IIb)beta(3) integrin and GPIb-V-IX complex identify distinct stages in the maturation of CD34(+) cord blood cells to megakaryocytes. *Blood* 96: 4169-4177

Lok S., Kaushansky K., Holly RD., Kuijper JL., Lofton-Day CE., Oort PJ., Grant FJ., Heipel MD, Burkhead SK., Kramer JM., Bell LA., Sprecher CA., Blumberg H., Johnson R., Prunkard D., Ching AFT., Mathewes SL., Bailey MC, Forstrom JW., Buddle MM., Osborn SG., Evans SJ., Sheppard PO., Presnell SR., O'Hara PJ., Hagen FS., Roth GJ. & Foster DC. (1994) Cloning and expression of murine thrombopoietin cDNA and stimulation of platelet production in vivo. *Nature* 369: 565-8

Long MW. And Williams N. (1981) Immature megakaryocytes in the mouse. Morphology and quantification by acetylcholinesterase staining. *Blood* 58: 1032-1039

Long MW., Williams N. and McDonald TP. (1982) Immature Megakaryocytes in the Mouse: In Vitro Relationship to Megakaryocyte Progenitor Cells and Mature Megakaryocytes. *J Cell Physiol.* 112: 339-44

Makinde T. and Agrawal DK. (2008) Intra and extravascular transmembrane 99ignaling of angiopoietin-1-Tie2 receptor in health and disease. *J Cell Mol Med* 12: 810-828

Maynard DM., Heijnen HF., Horne MK., White JG., Gahl WA. (2007) Proteomic analysis of platelet alpha-granules using mass spectrometry. *J Thromb Haemost.* 5: 1945-55

Martignetti JA., Aqeel AA., Sewairi WA., Boumah CE., Kambouris M., Mayouf SA., Sheth KV., Eid WA., Dowling O., Harris J., Glucksman MJ., Bahabri S., Meyer BF., Desnick RJ. (2001) Mutation of the matrix metalloproteinase 2 gene (MMP2) causes a multicentric osteolysis and arthritis syndrome. *Nat Genet.* 28: 261–265

McDonald TP, Clift R, Cottrell M. (1989) A four-step procedure for the purification of thrombopoietin. *Exp Hematol* 17: 865

Metcalf D. (1993) Hematopoietic Regulators: Redundancy or Subtlety? *Blood* 82: 35 15-3523

Miller WP., Rothman SM., Nascene D., Kivisto T., DeFor TE., Ziegler RS., Eisengart J., Leiser K., Raymond G., Lund TC., Tolar J., Orchard PJ. (2011) Outcomes after allogeneic hematopoietic cell transplantation for childhood cerebral adrenoleukodystrophy: the largest single-institution cohort report. *Blood* 18: 1971-1978

Miner JH., Cunningham J. and Sanes JR. (1998) Roles of laminins in embryogenesis: exencephaly, syndactyly, and placentopathy in mice lacking the laminin alpha5 chain. *J Cell Biol* 143: 1713-1723

Miura N., Okada S., Zsebo KM., Miura Y., Suda T. (1993) Rat stem cell factor and IL-6 preferentially support the proliferation of c-kitpositive murine hemopoietic cells rather than their differentiation. *Exp Hematol* 21:143

Moog S., Mangin P., Lenain N., Strassel C., Ravanat C., Schuhler S., Freund M., Santer M., Kahn M., Nieswandt B., Gachet C., Cazenave JP., Lanza F. (2001) Platelet glycoprotein V binds to collagen and participates in platelet adhesion and aggregation. *Blood* 98:1038-46

Nagase H., Enghild JJ., Suzuki K., Salvesen G. (1990) Stepwise activation mechanisms of the precursor of matrix metalloproteinase 3 (stromelysin) by proteinases and (4-aminophenyl)mercuric acetate. *Biochemistry* 29: 5783– 9

Naghavi M., Wang H., …, Lopez AD. And Murray CJL. (2015) Global, regional, and national age-sex specific all-cause and cause-specific mortality for 240 causes of death, 1990-2013: a systematic analysis for the Global Burden of Disease Study 2013. *Lancet* 385: 117-171

Neel JC. And Lebrun JJ. (2013)Activin and TGFβ regulate expression of the microRNA-181 family to promote cell migration and invasion in breast cancer cells. *Cell Signal* 25: 1556-1566

Nègre E., Vogel T., Levanon A., Guy R., Walsh TJ., Roberts DD. (1994) The collagen binding domain of fibronectin contains a high affinity binding site for Candida albicans. *J Biol Chem* 269: 22039-45

Nieswandt B. & Stritt S. (2015) Megakaryocyte rupture for acute platelet needs. *J. Cell Biol.* 209: 327-328

Nieswandt B and Watson SP. (2003) Platelet-collagen interaction: is GPVI the central receptor? *Blood* 102: 449-461

Nigatu A., Sime W., Gorfu G., Geberhiwot T., Andurén I., Ingerpuu S., Doi M., Tryggvason K., Hjemdahl P. and Patarroyo M. (2006) Megakaryocytic cells synthesize and platelets secrete alpha5-laminins, and the endotheliallaminin isoform laminin 10 (alpha5beta1gamma1) strongly promotes adhesion but not activationof platelets. *Thromb Haemost.* 95: 85-93

Nilsson SK., Debatis ME., Dooner MS., Madri JA., Quesenberry PJ. And Becker PS. (1998) Immunofluorescence Characterization of Key Extracellular Matrix Proteins in Murine bone marrow In Situ. *J Histochem Cytochem* 46: 371–377

Nishikii H., Kurita N. and Chiba S. (2017) The Road Map for Megakaryopoietic Lineage from Hematopoietic Stem/Progenitor Cells. *Stem Cells Transl Med* 6: 1661-1665

O'Connor MN., Smethurst PA., Davies LW., Joutsi-Korhonen L., Onley DJ., Herr AB., Farndale RW. and Ouwehand WH. (2006) Selective blockade of glycoprotein VI clustering on collagen helices. *J Biol Chem* 281: 33505-10

Olson TS., Caselli A., Otsuru S., Hofmann TJ., Williams R., Paolucci P., Dominici M., and Horwitz EM. (2013) Megakaryocytes promote murine osteoblastic HSC niche expansion and stem cell engraftment after radioablative conditioning. *Blood* 121: 5238–5249

O'Reilly MS., Wiederschain D., Stetler-Stevenson WG., Folkman J., Moses MA. (1999) Regulation of angiostatin production by matrix metalloproteinase-2 in a model of concomitant resistance. *J Biol Chem.* 274: 29568-71

Orkin SH. And Zon LI. (2008) Hematopoiesis: An Evolving Paradigm for Stem Cell Biology. *Cell* 132: 631–644

Pallotta I., Lovett M., Kaplan DL. And Balduini A. (2011) Three-Dimensional System for the In Vitro Study of Megakaryocytes and Functional Platelet Production Using Silk-Based Vascular Tubes. *Tissue Engineering* 17: 1223-1232

Passweg JR., Baldomero H., Bader P., Bonini C., Cesaro S., Dreger P., Duarte RF., Dufour C., Falkenburg JHF., Farge-Bancel D., Gennery A., Kröger N., Lanza F., Nagler A., Sureda A. and Mohty M. for the European Society for Blood and Marrow Transplantation (EBMT). (2015) Hematopoietic SCT in Europe 2013: recent trends in the use of alternative donors showing more haploidentical donors but fewer cord blood transplants. *Bone marrow transplant.* 50: 476- 482

Patel SR., Hartwig JH., Italiano JE Jr. (2005) The biogenesis of platelets from megakaryocyte proplatelets. *J Clin Invest.* 115: 3348-54

Patterson ML., Atkinson SJ., Knäuper V., Murphy G. (2002) Specific collagenolysis by gelatinase A, MMP-2, is determined by the hemopexin domain and not the fibronectin-like domain. *FEBS Lett.* 503: 158-62

Pizzi M., Gergis U., Chaviano F. and Orazi A. (2016)The effects of hematopoietic stem cell transplant on splenic extramedullary hematopoiesis in patients with myeloproliferative neoplasm-associated myelofibrosis. *Hematol Oncol Stem Cell Ther* 9: 96-104

Rabie T., Varga-Szabo D., Bender M., Pozgaj R., Lanza F., Saito T., Watson SP., Nieswandt B. (2007) Diverging signaling events control the pathway of GPVI down-regulation in vivo. *Blood* 110: 529-535

Raslova H., Roy L., Vourc'h C., Le Couedic JP., Brison O., Metivier D., Feunteun J., Kroemer G., Debili N. and Vainchenker W. (2003) Megakaryocyte polyploidization is associated with a functional gene amplification. *Blood* 101: 541-544

Richardson JL., Shivdasani RA., Boers C., Hartwig JH., Italiano JE. Jr. (2005) Mechanisms of organelle transport and capture along proplatelets during platelet production. *Blood* 106: 4066–4075

Russell ES. (1979) Hereditary anemias of the mouse: A review for geneticists. *Adv Genet* 20: 357

Sabri S., Jandrot-Perrus M., Bertoglio J., Farndale R. W., Mas V. M., Debili N. and Vainchenker W. (2004). Differential regulation of actin stress fiber assembly and proplatelet formation by alpha2beta1 integrin and GPVI in human megakaryocytes. *Blood* 104: 3117-3125

Sarratt KL., Chen H., Zutter MM., Santoro SA., Hammer DA. And Kahn ML. (2005) GPVI and $\alpha_2\beta_1$ play independent critical roles during platelet adhesion and aggregate formation to collagen. *Blood* 106: 1268-1277

Sasaki T. and Timpl R. (2001) Domain Iva of laminin alpha5 chain is cell-adhesive and binds beta1 and alphaVbeta3 integrins through Arg-Gly-Asp. *FEBS Lett.* 509: 181-5

Sauvage de FJ., Carver-Moore K., Luoh SM., Ryan A., Dowd M., Eaton DL., Moore MW. (1996) Physiological regulation of early and late stages of megakaryocytopoiesis by thrombopoietin. *J Exp Med* 183: 651–656

Sauvage de FJ., Hass PE., Spencer SD., Malloy BE., Gurney AL., Spencer SA., Darbonne WC., Henzel WJ., Wong SC., Kuang W-J., Oles KJ., Hultgren B., Solberg LA., Goeddel DV. & Eaton DL. (1994) Stimulation of megakaryocytopoiesis and thrombopoiesis by the c-Mpl ligand. *Nature* 369: 533-539

Schaff M., Tang C., Maurer E., Bourdon C., Receveur N., Eckly A., Hechler B., Arnold C., de Arcangelis A., Nieswandt B., Denis CV., Lefebvre O., Georges-Labouesse E., Gachet C., Lanza F., Mangin PH. (2013) Integrin α6β1 is the main receptor for vascular laminins and plays a role in platelet adhesion, activation, and arterial thrombosis. *Circulation.* 128: 541-52

Schofield R., (1978) The relationship between the spleen colony-forming cell and the haemopoietic stem cell. *Blood Cells* 4: 7-25

Schulte V., Snell D., Bergmeier W., Zirngibl H., Watson SP. and Nieswandt B. (2001) Evidence for two distinct epitopes within collagen for activation of murine platelets. *J Biol Chem* 276: 364-8

Semeniak D., Kulawig R., Stegner D., Meyer I., Schwiebert S., Bösing H., Eckes B., Nieswandt B., Schulze H. (2016) Proplatelet formation is selectively inhibited by collagen type I through Syk-independent GPVI signaling. *J Cell Sci* 129: 3473-3484

Shivdasani RA., Rosenblatt MF., Zucker-Franklin D., Jackson CW., Hunt P., Saris CJ., Orkin SH. (1995) Transcription factor NF-E2 is required for platelet formation independent of the actions of thrombopoietin/MGDF in megakaryocyte development. *Cell* 81: 695-704

Smith CW., Thomas SG., Raslan Z., Patel P., Byrne M., Lordkipanidzé M., Bem D., Meyaard L., Senis YA., Watson SP., Mazharian A. (2017) Mice Lacking the Inhibitory Collagen Receptor LAIR-1 Exhibit a Mild Thrombocytosis and Hyperactive Platelets. *Arterioscler Thromb Vasc Biol* 37: 823-835

Smith AR. And Wagner JE. (2009) Alternative Hematopoietic Stem Cell Sources for Transplantation: Place of Umbilical Cord Blood. *Br J Haematol* 147: 246–261

Steevels TA., Westerlaken GH., Tijssen MR., Coffer PJ., Lenting PJ., Akkerman JW., Meyaard L. (2010) Co-expression of the collagen receptors leukocyte-associated immunoglobulin-like receptor-1 and glycoprotein VI on a subset of megakaryoblasts. *Haematologica* 95: 2005-2012

Stegner D., van Eeuwijk JMM., Angay O., Gorelashvili MG., Semeniak D., Pinnecker J., Schmithausen P., Meyer I., Friedrich M., Dütting S., Brede C., Beilhack A., Schulze H., Nieswandt B. & Heinze KG. (2017) Thrombopoiesis is spatially regulated by the bone marrow vasculature. *Nat Commun* 8; doi: 10.1038/s41467-017-00201-7

Strassel C., Eckly A., Léon C., Moog S., Cazenave J-P., Gachet C., Lanza F. (2012) Hirudin and heparin enable efficient megakaryocyte differentiation of mouse bone marrow progenitors. *Exp Cell Res.* 318: 25-32

Sureda A., Bader P., Cesaro S., Dreger P., Duarte RF., Dufour C., Falkenburg JHF., Farge-Bancel D., Gennery A., Kröger N., Lanza F., Marsh JC., Nagler A., Peters C., Velardi A., Mohty M. and Madrigal A. (2015) Indications for allo- and auto-SCT for haematological diseases, solid tumours and immune disorders: current practice in Europe. *Bone marrow Transplant* 50: 1037–1056

Takahashi C., Sheng Z., Horan TP., Kitayama H., Maki M., Hitomi K., Kitaura Y., Takai S., Sasahara RM., Horimoto A., Ikawa Y., Ratzkin BJ., Arakawa T., Noda M. (1998) Regulation of matrix metalloproteinase-9 and inhibition of tumor invasion by the membrane-anchored glycoprotein RECK. *Proc Natl Acad Sci U S A.* 95: 13221–13226

Thews, Mutschler & Vaupel (1999). Anatomie, Physiologie, Pathophysiologie des Menschen. *Academic Press*

Thomas ED., Lochte HL., Lu WC., Ferrebee JW. (1957) Intravenous infusion of bone marrow in patients receiving radiation and chemotherapy. *N Engl J Med* 257: 491–6

Thon JN. (2014) SDF-1 directs megakaryocyte relocation. *Blood* 124: 161-163

Thyboll J., Kortesmaa J., Cao R., Soininen R., Wang L., Iivanainen A., Sorokin L., Risling M., Cao Y. and Tryggvason K (2002) Deletion oft he laminin alpha4 chain leads to impaired microvessel maturation. *Mol Cell Biol* 22: 1194-1202

Vandenberg P., Kern A., Ries A., Luckenbill-Edds L., Mann K., Kuhn K. (1991) Characterization of a type IV collagen major cell binding site with affinity to the α1 β1 and the α2 β1 integrins. *J Cell Biol.* 113: 1475–1483

Van den Steen PE., Dubois B., Nelissen I., Rudd PM., Dwek RA. & Opdenakker G. (2002) Biochemistry and Molecular Biology of Gelatinase B or Matrix Metalloproteinase-9 (MMP-9). *Critical Reviews in Biochemistry and Molecular Biology* 37: 375–536

Vannucchi AM., Grossi A., Rafanelli D., Ferrini PR., Ramponi G. (1988) Partial purification and biochemical characterization of human plasma thrombopoietin. *Leukemia* 2: 236

Varga-Szabo D., Pleines I., Nieswandt B. (2008) Cell Adhesion Mechanisms in Platelets. *Arterioscler Thromb Vasc Biol.* 28: 403-12

Visse R., Nagase H. (2003) Matrix metalloproteinases and tissue inhibitors of metalloproteinases: structure, function, and biochemistry. *Circ Res* 92: 827– 39.

Watson SP. (1999) Collagen receptor signaling in platelets and megakaryocytes. *Thromb Haemost* 82: 365-376

Wendling F., Maraskovsky E., Debili N., Florindo C., Teepe M., Titeaux M., Methia N., Breton-Gorius J., Cosman D. & Vainchenker W. (1994) c-Mpl ligand is a humoal regulator of megakaryopoiesis. *Nature* 369: 571-574

Wilson, A. and Trumpp, A. (2006) Bone-marrow haematopoietic-stem-cell niches. *Nat Rev Immunol* 6: 93-106

Wright J. (1906) The origin and nature of blood platelets. *Boston Med Surg J* 154: 643-645

Wu C., Ivars F., Anderson P., Hallmann R., Vestweber D., Nilsson P., Robenek H., Tryggvason K., Song J., Korpos E., Loser K., Beissert S., Georges-Labouesse E., Sorokin LM. (2009) Endothelial basement membrane laminin alpha5 selectively inhibits T lymphocyte extravasation into the brain. *Nat Med* 15: 519-27

Yıldıran A., Çeliksoy MH., Borte S., Güner ŞN., Elli M., Fışgın T., Özyürek E., Sancak R., Oğur G. (2017) Haematopoietic stem cell transplantation in primary immunodeficiency patients in the Black Sea Region of Turkey. *Turk J Haematol.* doi: 10.4274/tjh.2016.0477

Yousif LF., Russo J. and Sorokin L. (2013) Laminin isoforms in endothelial and perivascular basement membranes. *Cell Adh Migr* 7: 101-110

Zhou BO., Ding L. and Morrison SJ. (2015) Hematopoietic stem and progenitor cells regulate the regeneration of their niche by secreting Angiopoietin-1. *Elife* 4: e05521

Zou Z., Schmaier AA., Cheng L., Mericko P., Dickeson SK., Stricker TP., Santoro SA. and Kahn ML. (2009) Negative regulation of activated alpha-2 integrins during thrombopoiesis. *Blood* 113: 6428-39

6 Appendix

6.1 Abbreviations

2D	Two-dimensional
3D	Three-dimensional
2P-IVM	Two-photon intravital microscopy
ADP	Adenosine diphosphate
APS	Ammonium persulfate
BABB	Benzylalcohol benzylbenzoate
BM	Bone marrow
BMT	Bone marrow transplantation
bp	Base pair
BSA	Bovine serum albumin
CLEC-2	C-type lectin-like receptor 2
CLSM	Confocal laser scanning microscopy
c-Mpl	Myeloproliferative leukemia virus oncogene
CRP	Collagen related peptide
CVX	Convulxin
CXCL12	CXC-chemokine ligand 12
DAG	Diacylglycerol
DAPI	4´, 6-diamidino-2-phenylindole
DMEM	Dulbecco´s Modified Eagle Media
DMS	Demarcation membrane system
DMSO	Dimethyl sulfoxide
dNTP	Deoxynucleotide triphosphates
ECL	Enhanced chemoluminescence
ECM	Extracellular matrix

ECMP	Extracellular matrix protein
EDTA	Ethylenediaminetetraacetic acid
EGTA	Ethylene glycol tetraacetic acid
ERK	Extracellular-signal-regulated kinase
FACS	Fluorescence-activated cell sorting
FcR	Fc receptor
FCS	Fetal calf serum
FITC	Fluorescein
FLC	Fetal liver cell
FSC	Forward scatter
GFOGER	Glycine-phenylalanin-hydroxyproline-glycine-glutamic acid-arginine
GP	Glyco-protein
GPCR	G protein-coupled receptor
GPO	Glycine-proline-hydroxyproline
GVHD	Graft versus host disease
GVL	Graft versus leukemia
HCT	Hematocrit
HEPES	4-(2-hydroxyethyl)-1-piperazineethanesulfonic acid
Hb	Hemoglobin
HRP	Horseradish peroxidase
HSC	Hematopoietic stem cell
HSCT	Hematopoietic stem cell transplantation
IL-3	Interleukin-3
IP_3	Inositol-1,4,5-triphosphate
ITAM	Immunoreceptor tyrosine-based activation motif
LAT	Linker for activated T cells
LSFM	Light sheet fluorescence microscopy

MCH	Mean corpuscular hemoglobin
MCHC	Mean corpuscular hemoglobin concentration
MCV	Mean corpuscular volume
MFI	Mean fluorescence intensity
MK	Megakaryocyte
MMP	Matrix metalloproteinase
MPV	Mean platelet volume
PBS	Phosphate buffered saline
PCR	Polymerase chain reaction
PE	Phycoerythrin
PFA	Paraformaldehyde
PGI$_2$	Prostacyclin
PI	Phosphatidylinositol
PIP2	Phosphatidylinositol-4,5-bisphosphate
Plt	Platelet
PRP	Platelet-rich-plasma
PVDF	Polyvinylidene difluoride
RBC	Red blood cell count
rpm	Rotations per minute
RT	Room temperature
RDW	Red blood cell distribution width
SCF	Stem cell factor
SD	Standard deviation
SDF1	Stromal-derived factor 1
SDS-PAGE	Sodium dodecyl sulfate polyacrylamide gel electrophoresis
SFKs	*Src* family kinases
SSC	Side scatter

Syk	Spleen tyrosine kinase
TAE	TRIS acetate EDTA
TBS-T	TRIS-buffered saline containing Tween
TEMED	Tetramethylethylendiamin
TPO	Thrombopoietin
TRIS	Tris(hydroxymethyl)aminomethane
TxA$_2$	Thromboxane A$_2$
U46	U46619
vWF	Von Willebrand factor
WBC	White blood cell count
WT	Wild type

6.2 Acknowledgements

The work presented in this study was conducted in the group of Prof. Harald Schulze at the Institute of Experimental Biomedicine I, University Hospital Würzburg. During the whole time as a PhD student many people helped and supported me:

- First, I would like thank my supervisor Prof. Harald Schulze who gave me the opportunity to work on this cherished project. He was a great mentor always supporting me to think outside the box. I have learned so much from him.

- Prof. Katrin Heinze, as the second supervisor, for the support in imaging techniques and the great input she gave me during the thesis committee meetings

- Prof. Thomas Dandekar for being my third supervisor, for his support and his remarks.

- Prof. Manfred Gessler who agreed to chair my thesis defence.

- Prof. Bernhard Nieswandt who gave me a warm welcome in his group and provided us with great scientific resources and input.

- Dr. David Stegner and Dr. Deya Cherpokova for their great scientific input and their patience when I needed support.

- All the other Schulze lab members, especially Dr. Georgi Manukjan who always answered stupid questions, corrected my thesis and made the time in the lab funnier.

- My *Mushrooms* Markus, Katja and Isabelle, who became more than just colleagues and always supported me during my PhD time and when I wrote my thesis. Thanks for the great fun in the lab and afterwards.

- My friends Chrissi, Dodo, Christian and Julia, who always were able to distract me from work and supported me since school time.

- And last but not least my family. Without their help I would not have come that far!

6.3 Curriculum vitae

Personal Data

Name:	Daniela Semeniak, M.Sc.
Date of birth:	30.10.1987
Place of birth:	Eberswalde, Germany
Nationality:	German

Education

03/2014 – present	PhD student, University Hospital Würzburg "Role of extracellular matrix(proteins) on platelet biogenesis"
11/12-01/13	Student employee in AG Vollmer at the TU Dresden
11/2012	Graduation Master of Science in Biology at Technical University Dresden, Thesis adviser: Prof. Dr. Günter Vollmer, Prof. Dr. Herwig Gutzeit
2010 - 2012	Biology studies (M. Sc.) at Technical University Dresden
11/2010	Graduation Bachelor of Science in Biology at Humboldt University Berlin, Thesis adviser: PD Dr. Elke Genersch and Prof. Dr. Richard Lucius.
2007 – 2010	Biology studies (Bachelor of Science) at Humboldt University, Berlin
06/2007	Abitur (German university entrance qualification)

Publications

Semeniak D. & Kulawig R., Stegner D., Meyer I., Schwiebert S., Bösing H., Eckes B., Nieswandt B. and Schulze H. (2016) Proplatelet formation is selectively inhibited by collagen type I via Syk-independent GPVI signaling. *J. Cell Sci.* 129: 3473-3484

Andres O., Wiegering V., König EM., Schneider AL., **Semeniak D**., Stritt S., Klopocki E. and Schulze H. (2016) A novel two-nucleotide deletion in HPS6 affects mepacrine uptake and platelet dense granule secretion in a family with Hermansky-Pudlak syndrome. *Pediatr. Blood. Cancer.* 64 doi: 10.1002/pbc.26320

Stegner D., Eeuwijk J., Angay O., Gorelashvili M., **Semeniak D.**, Pinnecker J., Schmithausen P., Meyer I., Friedrich M., Dütting S., Brede C., Beilhack A., Schulze H., Nieswandt B. (2017) Thrombopoiesis is spatially regulated by the bone marrow vasculature. *Nat. Commun.* doi: 10.1038/s41467-017-00201-7

Münzer P., Walker-Allgaier B., Geue S., Langhauser F., Geuss E., Stegner D., Aurbach K., **Semeniak D.,** Chatterjee M., Gonzalez-Menendez I., Märklin M., Quintanilla-Martinez L., Salih H., Litchfield D., Buchou T., Kleinschnitz C., Lang F., Nieswandt B., Pleines I., Schulze H., Gawaz M. & Borst O. (2017) CK2β is a critical regulator of thrombopoiesis, Ca^{2+}-triggered platelet activation and arterial thrombosis in vivo. *Blood.* Accepted doi: 10.1182/blood-**2017**-05-784413

6.4 Affidavit

I hereby confirm that my thesis entitled "The role of bone marrow extracellular matrix proteins on platelet biogenesis and function" is the result of my own work. I did not receive any help or support from commercial consultants. All sources and/or materials applied are listed and specified in the thesis.

Furthermore, I confirm that this thesis has not yet been submitted as part of another examination process neither in identical nor in similar form.

Würzburg, October 2017 _____

6.5 Eidesstattliche Erklärung

Hiermit erkläre ich an Eides statt, die Dissertation " Die Rolle der extrazellulären Matrixproteine des Knochenmarks auf die Thrombozytenbiogenese und -funktion" eigenständig, d.h. insbesondere selbsständig und ohne Hilfe eines kommerziellen Promotionsberaters, angefertigt und keine anderen als die von mir angegebenen Quellen und Hilfsmittel verwendet zu haben.

Ich erkläre außerdem, dass die Dissertation weder in gleicher noch in ähnlicher Form bereits in einem anderen Prüfungsverfahren vorgelegen hat.

Würzburg, Oktober 2017 _____